

Carbohydrate-Modified Microgels as a System for Extracting Naphthenic Acids from  
Tailings Pond Water

by

Kimberly D. Hyson

A thesis submitted in partial fulfillment of the requirements for the degree of

Master of Science

Department of Chemistry  
University of Alberta

© Kimberly D. Hyson, 2015

# Abstract

Northern Alberta houses massive tailings ponds, that store aqueous waste as a result of the processes employed to recover bitumen from the oil sand deposits. The aqueous waste, or tailings pond water (TPW), houses numerous toxic chemicals including naphthenic acids (NAs) - a complex group of naturally occurring hydrophobic organic acids that can have adverse and even irreversible effects on their surrounding environment. The Lowary group has shown that methyl mannose polysaccharides (MMPs) have a high binding affinity for NAs, while the Serpe group has demonstrated that poly(N-isopropylacrylamide) (pNIPAM)-based micro-particles have a high binding affinity for organic molecules in general. Our research group has been developing a unique class of microgels for the removal of NAs from TPW by utilizing pNIPAM-based porous micro-particles and incorporating unmethylated and methylated derivatives of long-chained saccharide(s)-amines. Several pNIPAM-based microgels coupled or polymerized with a series of carbohydrates have been developed and their effectiveness to treat TPW was monitored using Microtox bioassay toxicity tests and Fourier-transform infrared spectroscopy (FT-IR). According to the Microtox data the carbohydrate-modified microgels have only a marginal effect treating medium fine tailings (MFT) and the top recyclable tailings water layer. However, FT-IR analysis shows that few carbohydrate-modified poly(*N*-isopropylacrylamide)-co-acrylic acid (pNIPAM-co-Ac) microgels lower NAs concentration in MFT: pNIPAM-co-50 % Ac-di-mann-octylamine shows the best performance by decreasing the NAs concentration within a similar range as the standard sorbent: powdered activated carbon (PAC). Overall, PAC shows the best performance treating MFT according to both Microtox bioassay and FT-IR analysis.

# Acknowledgements

I would like to give a huge thanks to my supervisor, Dr. Michael Serpe, for giving me the opportunity to pursue my MSc. degree in his group. His guidance, support and patience throughout my degree is greatly appreciated. I am also thankful for the fantastic opportunities to attend various workshops, networking events and conferences while in his group, which were all insightful experiences.

I would also like to thank my committee members: Dr. Todd Lowary and Dr. Jon Veinot for providing valuable advice throughout this process and being so receptive to my questions.

I am also very appreciative for the stellar assistance and advice from a number of people within the Chemistry department who assisted me, which includes: Wayne Moffat, Jennifer Jones, Gareth Lambkin and Mark Miskolzie (a.k.a. NMRk).

The guidance I have received from my group members in the Serpe group during this process was very helpful and welcomed.

Lastly, a huge thanks goes to my friends and family for all their support during these couple of years.

# Tables of Contents

<b>Chapter 1 - The Oil Sands: Recovery &amp; Impact.....</b>	<b>1</b>
1.1 Introduction.....	1
1.2 Bitumen in the Canadian Oil Sands .....	2
1.3 The Microstructure of the Canadian Oil Sands.....	4
1.4 Recovering Bitumen .....	5
1.4.1 Hot Water Extraction Process.....	6
1.4.2 Commercial Bitumen Recovery Process .....	7
1.5 Tailing Ponds .....	9
1.5.1 Chemical Composition.....	11
1.6 Naphthenic Acids.....	12
1.6.1 Toxicological/Biological Studies.....	16
1.6.2 NAs Degradation/ Mitigation .....	18
1.6.3 Analysis of NAs.....	25
<b>Chapter 2 - Microgels &amp; Carbohydrates .....</b>	<b>30</b>
2.1 Introduction.....	30
2.2 Polymethylated Polysaccharides.....	30
2.2.1 Lipid-Interactions with Natural PMPs .....	32
2.2.2 Synthetic PMPs.....	33

2.2.3 NAs Interaction with MMPs .....	34
2.3 Hydrogel Microparticles .....	36
2.3.1 Synthesis of pNIPAM Microgels.....	38
2.3.2 pNIPAM- Based Microgels For Small Organic Molecule Removal .....	40
<b>Chapter 3 - Polymerization and Modification of Microgels .....</b>	<b>43</b>
3.1 Introduction.....	43
3.2 Materials & Methods .....	44
3.2.1 Dynamic Light Scattering & Zeta Potential Measurements .....	45
3.2.2 Nanoprobe $^1\text{H}$ Nuclear Magnetic Resonance Spectroscopy .....	46
3.2.3 General Procedures .....	46
3.3 Polymerization of Carbohydrate-Microgels .....	49
3.3.1 Preparation of pNIPAM-co-Mann-2OMe-Octylamide Microgel.....	49
3.3.2 Preparation of pNIPAM-co-Mann-3OMe-Octylamide Microgel .....	49
3.3.3 Preparation of pNIPAM-co-Penta-Mann-2,3OMe-Octylamide Microgel.....	50
3.4 Polymerization of Unmodified Microgels .....	51
3.4.1 Preparation of pNIPAM-co-10 % AAc Microgel .....	51
3.4.2 Preparation of pNIPAM-co-50 % AAc Microgel .....	52
3.4.3 Preparation of pNIPAM-co-25 % AAc Microgel .....	54
3.5 DCC Coupled Microgels.....	54

3.5.1 Attempted DCC/ DMAP Coupling of pNIPAM-co-10 % AAc Microgel & Dodecylamine .....	55
3.5.2 Preparation of DCC Coupled pNIPAM-co-10 % AAc Microgel & Dodecylamine .....	56
3.5.3 Preparation of DCC Coupled of pNIPAM-co-10 % AAc Microgel & Hexylamine .....	56
3.5.4 Preparation of DCC Coupled of pNIPAM-co-10 % AAc Microgel & Butylamine .....	57
3.5.5 Preparation of DCC Coupled of pNIPAM-co-10 % AAc Microgel & Propylamine .....	57
3.5.6 Summary of DCC Coupling DLS & Zeta Potential Data .....	58
3.6 EDC Coupling of Microgels with Aliphatic Amines and Carbohydrate-Amines .....	59
3.6.1 Preparation of pNIPAM-co-50 % AAc-Dodecylamine Microgel <i>via</i> EDC Coupling.....	60
3.6.2 Preparation of pNIPAM-co-50 % AAc-Mann-Octylamine Microgel <i>via</i> EDC Coupling.....	61
3.6.3 Preparation of pNIPAM-co-50 % AAc-Mann-3OMe-Octylamine Microgel <i>via</i> EDC Coupling.....	67
3.6.4 Preparation and Characterization of pNIPAM-co-50 % AAc-Mann-2,3OMe-Octylamine Microgel <i>via</i> EDC Coupling .....	68

3.6.5 Preparation of pNIPAM-co-50 % AAc-Glu-6OMe-Octylamine Microgel <i>via</i> EDC Coupling.....	70
3.6.6 Preparation of pNIPAM-co-50 % AAc-Di-Mann-Octylamine Microgel <i>via</i> EDC Coupling.....	72
3.6.7 Summary .....	74
<b>Chapter 4 - Remediation Performance .....</b>	<b>75</b>
4.1 Introduction.....	75
4.2 Materials & Methods .....	75
4.2.1 Microtox Bioassay .....	76
4.2.2 Fourier-Transform Infrared Spectroscopy .....	77
4.2.3 General Procedures .....	78
4.3 Microtox Bioassay Toxicity Tests .....	79
4.3.1 Microtox Data of Tailings Pond Water: MFT & Recyclable Water.....	79
4.3.2 Microtox Data of Powdered Activated Carbon Treated MFT .....	82
4.3.3 Powdered Activated Carbon Reusability for MFT Treatment.....	83
4.3.4 Microtox Data of pNIPAM-co-Mann-2OMe-Amide Microgel Treated Recyclable Water.....	84
4.3.5 Microtox Data of pNIPAM-co-Mann-3OMe-Amide Microgel Treated Recyclable Water.....	85

4.3.6 Microtox Data of pNIPAM-co-Penta-Mann-2,3OMe-Amide Microgel Treated Recyclable Water .....	87
4.3.7 Microtox Data of pNIPAM-co-10 % AAc Microgel Treated MFT .....	90
4.3.8 Microtox Data of pNIPAM-BIS Microgel Treated MFT .....	92
4.3.9 Microtox Data of pNIPAM-co-50 % AAc-Mann-Octylamine Microgel Treated MFT .....	93
4.3.10 Microtox Data of pNIPAM-co-50 % AAc-Mann-2,3OMe-Octylamine Microgel Treated MFT .....	94
4.3.11 Summary .....	96
<b>4.4 FT-IR Quantification of Naphthenic Acids .....</b>	<b>96</b>
4.4.1 Increasing pNIPAM-co-50 % AAc-Mann-2,3OMe-Octylamine Microgel for MFT Treatment .....	98
<b>Conclusion .....</b>	<b>101</b>
<b>Future Work.....</b>	<b>102</b>
<b>References .....</b>	<b>104</b>

# List of Tables

Table 1-1. Approximate elemental composition of Alberta bitumen <sup>8,14</sup> .....	3
Table 1-2. Approximate physical and chemical properties of NAs <sup>45</sup> .....	14
Table 1-3. Industrial applications of NA derivatives <sup>45,48</sup> .....	15
Table 3-1. DCC coupled microgel according to General Procedure C hydrodynamic radius by DLS and zeta potential by zeta analyzer. The averaged values (minimum of three measurements per sample) are summarized here.....	59

# List of Figures

Figure 1-1. Arrangement of oil-sand particles according to Cottrell <sup>16</sup> (a) and Mossop <sup>17</sup> (b) ...	4
Figure 1-2. Simplified flow chart of the hot water extraction process .....	9
Figure 1-3. Theoretical model of the cross-section of a tailings pond.....	10
Figure 1-4. Sample NA structures for various Z-series where R is an alkyl group and chain length is represented by x .....	12
Figure 1-5. The truncated cone-shape of cyclodextrin (A) and the cross-section of a cyclodextrin molecule showing the arrangement of glucose units (B).....	22
Figure 1-6. Structure of $\beta$ -cyclodextrin .....	23
Figure 2-1. General structure of MMP (A) from <i>Mycobacterium smegmatis</i> and MGLP (B) from <i>Mycobacterium bovis</i> BCG <sup>105</sup> .....	32
Figure 2-2. Schematic illustrating the helical structure exhibited by MMP (in blue) in the presence of a long lipid chain. Methyl groups (black circle) are pointed inwards creating a hydrophobic core suitable for organics.....	33
Figure 2-3. Structures of extracted MMP-X (A, X = 10, 11, 12, 13) and synthetic MMP-Xs (B, X = 5, 8, 11, 14) .....	35
Figure 2-4. General EDC/ NHS coupling reaction in an aqueous solution. R <sup>1</sup> and R <sup>2</sup> can be any functional group with a carboxylate and primary amine respectively (e.g., peptides, proteins, carbohydrates etc.) .....	37
Figure 2-5. General synthesis of pNIPAM-based microgels using APS as the initiator. R is any functional group that has a terminal double bond able to participate in radical polymerization in aqueous conditions. ....	39
Figure 2-6. Chemical structure of Orange II Dye .....	41

Figure 3-1. Nanoprobe $^1\text{H}$ NMR spectrum of pNIPAM-co-50 % AAc in $\text{D}_2\text{O}$ at pH 10.....	53
Figure 3-2. Nanoprobe $^1\text{H}$ NMR spectrum of pNIPAM-co-50 % AAc-Mann-Octylamine in $\text{D}_2\text{O}$ at pH 10.....	62
Figure 3-3. Nanoprobe $^1\text{H}$ NMR spectrum of pNIPAM-co-50 % AAc-Mann-Octylamine synthesized with no EDC Coupling Reagent in $\text{D}_2\text{O}$ at pH 10.....	64
Figure 3-4. Nanoprobe $^1\text{H}$ NMR spectrum of pNIPAM-co-50 % AAc-Mann-Octylamine synthesized with no EDC or NHS Coupling Reagent in $\text{D}_2\text{O}$ at pH 10.....	66
Figure 3-5. Nanoprobe $^1\text{H}$ NMR spectrum of pNIPAM-co-50 % AAc-mann-2,3OMe-octylamine in $\text{D}_2\text{O}$ at pH 10.....	69
Figure 3-6. Nanoprobe $^1\text{H}$ NMR spectrum of pNIPAM-co-50 % AAc-Glu-6OMe-Octylamine in $\text{D}_2\text{O}$ at pH 10.....	71
Figure 3-7. Nanoprobe $^1\text{H}$ NMR spectrum of pNIPAM-co-50 % AAc-Di-Mann-Octylamine in $\text{D}_2\text{O}$ at pH 10.....	73
Figure 4-1. Microtox toxicity results of recyclable TPW ( $n = 2$ ) after 5 minutes of exposure (A) and 15 minutes of exposure (B), pH $\sim 8.2$ .....	80
Figure 4-2. Microtox toxicity results of MFT ( $n = 3$ ) after 5 minutes of exposure (A) and 15 minutes of exposure (B), pH $\sim 8$ .....	80
Figure 4-3. Microtox toxicity results of MFT shaken ( $n = 3$ ) for 24 hours and centrifuged after 5 minutes of exposure (A) and 15 minutes of exposure (B), pH $\sim 8$ .....	81
Figure 4-4. Microtox toxicity results of PAC treated MFT ( $n = 3$ ) compared to untreated MFT ( $n = 3$ ) and MFT further centrifuged and shaken ( $n = 3$ )after 5 minutes of exposure (A) and 15 minutes of exposure (B), pH 8.....	82

Figure 4-5. Microtox toxicity results of the reusability of PAC treated MFT at a sample concentration of 45 % (n = 1). MFT toxicity after 14 treatments is shown at 5 minutes (A) and 15 minutes (B) exposure at pH 8.....	83
Figure 4-6. Microtox toxicity results of pNIPAM-co-Mann-2O-Me-Amide Microgel treated recyclable water and untreated recyclable water (n = 3) after 5 minutes (A) and 15 minutes (B) of exposure. pH was unmeasured and unaltered. ....	85
Figure 4-7. Microtox toxicity results of pNIPAM-co-Mann-3OMe-Amide Microgel treated recyclable water and untreated recyclable water after 5 minutes (A) and 15 minutes (B) of exposure. pH was unmeasured and unaltered. ....	86
Figure 4-8. Microtox toxicity results of pNIPAM-co-Penta-Mann-2,3OMe-Amide Microgel treated recyclable water and untreated recyclable water (n = 3) after 5 minutes (A) and 15 minutes (B) of exposure. pH was unmeasured and unaltered. ....	88
Figure 4-9. Microtox toxicity results of pNIPAM-co-Penta-Mann-2,3OMe-Amide Microgel (n = 1) treated MFT compared to untreated MFT (n = 3) and MFT (centrifuged and shaken, n = 3) after 5 minutes (A) and 15 minutes (B) of exposure, pH = 8.....	89
Figure 4-10. Microtox toxicity results of pNIPAM-co-10 % AAc Microgel and PAC treated MFT compared to untreated MFT and MFT (centrifuged and shaken) after 5 minutes (A) and 15 minutes (B) of exposure, pH = 8.....	90
Figure 4-11 Microtox toxicity results of pNIPAM-co-10 % AAc (1 $\times$ , 2 $\times$ , 3 $\times$ ) and PAC treated MFT compared to untreated MFT and MFT further centrifuged and shaken after 5 minutes (A) and 15 minutes (B) of exposure, pH 8.....	91

Figure 4-12. Microtox toxicity results of pNIPAM-BIS microgel (n = 1) treated MFT compared to untreated MFT (n = 3) and MFT further centrifuged and shaken (n = 3) after 5 minutes (A) and 15 minutes (B) of exposure, pH 8.....	92
Figure 4-13. Microtox toxicity results of pNIPAM-co-50 % AAc-Mann-Octylamine Microgel and PAC (n = 3) treated MFT compared to untreated MFT (n = 3) and MFT further centrifuged and shaken (n = 3) after 5 minutes of exposure (A) and 15 minutes of exposure (B), pH 8.....	94
Figure 4-14. Microtox toxicity results of pNIPAM-co-50 % AAc-mann-2,3OMe-octylamine microgel (n = 1) and PAC (n = 3) treated MFT compared to untreated MFT (n = 3) and MFT further centrifuged and shaken (n = 3) after 5 minutes (A) and 15 minutes of exposure (B), pH 8.....	96
Figure 4-15. Data from FT-IR analyses of NAs concentration (average) in MFT (n = 3), PAC (n = 3), pNIPAM-co-50 % AAc (n = 3), pNIPAM-co-50 % AAc-mann-octylamine (n = 2), pNIPAM-co-50 % AAc-mann-2,3OMe-octylamine (n = 2), pNIPAM-co-50 % AAc-glu-6-OMe-octylamine (n = 2), pNIPAM-co-50 % AAc-Di-Mann-Octylamine (n = 2). The numbers shown above each bar are the high and low values measured.....	97
Figure 4-16. Data from FT-IR analyses of NAs concentration (average) in MFT (n = 3), PAC (n = 3), pNIPAM-co-50 % AAc (n = 3), pNIPAM-co-50 % AAc-mann-2,3OMe-octylamine (1×, n = 2), pNIPAM-co-50 % AAc-mann-2,3OMe-octylamine (2×, n = 2). The numbers shown above each bar are the high and low measured values.....	99

# List of Abbreviations and Symbols

Orange II	4-(2-hydroxy-1-naphthylazo) benzenesulfonic acid sodium salt
PDI	1,4-phenylene diisocynate
V50	2,2'-azobis(amidinopropane)dihydrochloride
APBA	3-aminophenylboronic acid
MMP	3- <i>O</i> -methyl-mannose polysaccharides
MGLP	6- <i>O</i> -methyl-glucose lipopolysaccharides
K <sub>a</sub>	acid dissociation constant
AOF	acid extractable organic fraction
AAc	acrylic acid
AC	activated carbon
acyl-CoA	acyl-coenzyme A
API, °	American Petroleum Institute gravity
APS	ammonium persulfate
amu	atomic mass unit
β-CDs	beta-cyclodextrin
n	carbon number
cP	centipoise
cm	centimeter
c-NAs	classical-naphthenic acids
CTL	coal-to-liquid
co	cross-link
cyroSEM	cyro-scanning electron microscopy

°C	degrees in Celsius
DI	deionized
DCM	dichloromethane
DCC	dicyclohexylcarbodiimide
DLS	dynamic light scattering
ESI-MS	electrospray ionization-mass spectroscopy
EP	epichlorohydrin
eq.	equivalent
FAs	fatty acids
FFT	fluid fine tailings
FT-IR	Fourier-transform infrared spectroscopy
GTL	gas-to-liquid
r <sup>2</sup>	goodness of fit
g	grams
GAC	granular activated carbon
HS-MS	high resolution mass spectroscopy
HWE	hot water extraction
Z	hydrogen deficiency
IC	inhibitory concentration
kDa	kiloDalton
kg	kilograms
L	litre
LC	lower concentration

LCST	lower critical solution temperature
m/z	mass-to-charge ratio
MFT	mature fine tailings
MHz	megahertz
$\mu\text{g}$	micrograms
$\mu\text{CT}$	microtomograph
mg	milligram
mL	milliliter
mmol	millimole
mV	millivolts
M	molar concentration
mol	mole
EDC	<i>N</i> -(3-dimethylaminopropyl)- <i>N'</i> -ethyl-carbodiimide hydrochloride
BIS	<i>N,N'</i> -methylenebis(acrylamide)
nm	nanometers
NAs	naphthenic acids
NHS	<i>N</i> -hydroxysuccinimide
sulfo-NHS	<i>N</i> -hydroxysulfosuccinimide
NIS	<i>N</i> -iodosuccinimide
NMR	nuclear magnetic resonance
$\Omega$	ohm
OSPW	oil sand-process affected water
oxy-NAs	oxidized-naphthenic acids

ppm	Parts per million
%	percentage
pNIPAM	poly(N-isopropylacrylamide)
PMPs	polymethylated mannose polysaccharides
pH	potential hydrogen
PAC	powdered activated carbon
PSV	primary separation vessel
PA	process-affect
<sup>1</sup> H	proton
rbf	round bottom flask
SSU	secondary separation unit
Kd	sorption distribution coefficient
TOR	tailings oil recovery
TPW	tailings pond water
3D	three-dimensional
TAN	total acid number
TDS	total dissolved solids
UV	ultraviolet
v/v	volume/volume
wt. %	weight %

# **Chapter 1 - The Oil Sands: Recovery & Impact**

## **1.1 Introduction**

The global push toward fossil fuels as the dominant source of energy was initiated during the industrial revolution. During this time, coal became the primary energy source and replaced biomass, water and wood energies.<sup>1</sup> Since then our energy dependence on fossil fuels has continued and other forms have emerged, such as natural gas and, in particular, oil – crucial in global energy demands and economies worldwide.

Oil products (also referred to as petroleum products) are produced from the refinement of crude oil. Crude oil is a naturally occurring black/dark brown free-flowing viscous liquid mainly composed of a complex mixture of hydrocarbons along with some nitrogen, oxygen and sulphur containing compounds and trace metals.<sup>2</sup> Crude oil is commonly obtained by conventional methods, which encompasses well-established oil well drilling and production techniques to recover crude oil that is located in reservoirs hundreds to tens of thousands of feet underground.<sup>3</sup> By contrast, unconventional oil reserves are found in accumulations where permeability is low and, therefore, require advanced technologies for recovery, which are generally time consuming and expensive.<sup>4</sup> However, with conventional oil reserves depleting, unconventional oil production has been increasing with projected production to be 2.6 – 5.5 billion barrels of oil by 2030.<sup>5,6</sup> Unconventional oil resources includes extra-heavy oil, shale oil, gas-to-liquids (GTL), coal-to-liquids (CTL) and the largest contributor: oil sands (also referred to as tar sands or bituminous sands).<sup>7</sup>

Canada's oil sands are located in Peace River, Cold Lake and Athabasca in Alberta and Saskatchewan and comprise the third largest oil reserve in the world.<sup>8</sup> According to the Canadian Energy Research Institute it was estimated that Canadian oil and oil equivalent production averaged 3.5 million barrels per day in 2013, while oil sands related production accounted for 56 percent of this total or 1.98 million barrels per day.<sup>9</sup> The revenues generated that year from existing and new projects from the oil sands were estimated to be \$2.484 trillion with oil sand related taxes directed to the Canadian Federal Government totalling \$574 billion.<sup>9</sup>

Overall, the economic benefits from the Canadian Oil Sands are staggering; however, the negative environmental consequences as a result of the processes employed to recover oil from the oil sands continue to generate toxic pollutants affecting the surrounding environment, particularly nearby water systems.<sup>10,11</sup> Common processes employed to extract bitumen, the generation and identification of some of these pollutants as well as possible remediation methods will be discussed further.

## **1.2 Bitumen in the Canadian Oil Sands**

The oil sands in Canada is composed of a natural mix of sand/quartz, water, clay and, in particular, bitumen.<sup>8</sup> The bitumen content in Canada's oil sands can vary between ~ 0–10 weight % (wt. %) depending on the location.<sup>8</sup> Oil sands are classified as either rich (> 10 wt. %), medium-grade (8–10 wt. %) or low-grade (6–8 wt. %) depending on their bitumen content.<sup>8,12</sup> On average the bitumen content of Canada's oil sands is > 10 wt. % and, therefore, classified as bitumen rich.<sup>8,12,13</sup>

Bitumen is a natural form of heavy oil composed of a complex mixture of hydrocarbons containing carbon, hydrogen, nitrogen, and sulphur (CHNS).<sup>8</sup> Nickel and vanadium constituents have also been shown to be a major component in bitumen.<sup>14</sup> The elemental composition of bitumen exists as a range (Table 1-1) due to the variability between oil sand deposits in Canada, which also adds to the complexity of characterizing bitumen samples.<sup>8,14</sup>

**Table 1-1.** Approximate elemental composition of Alberta bitumen<sup>8,14</sup>

Element	Abundance Range
Carbon	82.0–83.0 wt. %
Hydrogen	10.1–10.2 wt. %
Nitrogen	0.2–0.4 wt. %
Sulfur	4.5–6.0 wt. %
Oxygen	0.2–1.0 wt. %
Vanadium	180–250 ppm
Nickel	60–90 ppm

Bitumen in Canada's oil sands has on average an API gravity (American Petroleum Institute gravity, °) of 6 °–10 °, which is within the range of heavy oil, while conventional oil can have an API gravity of > 25 °.<sup>15</sup> Bitumen also has a relatively high viscosity (~ 500,000 cP at 38 °C) compared to conventional crude oil (~ 10 cP at 38 °C), low volatility and high acid content with an approximate TAN value (total acid number) of 2.5 mg KOH per gram of sample.<sup>8,13</sup>

### 1.3 The Microstructure of the Canadian Oil Sands

In 1963 Cottrell proposed the first model structure of the oil sands in terms of the mutual arrangement of sand, clay, water and bitumen, which was postulated based on his earlier experimental work on the anhydrous approach to extraction of bitumen from Athabasca oil.<sup>16</sup> His model proposed that individual grains of sand were surrounded by a film of water containing a suspension of clay minerals. Surrounding the water layer is bitumen, which also filled the gaps between individual grains of sand (Figure 1-1a).<sup>16</sup>

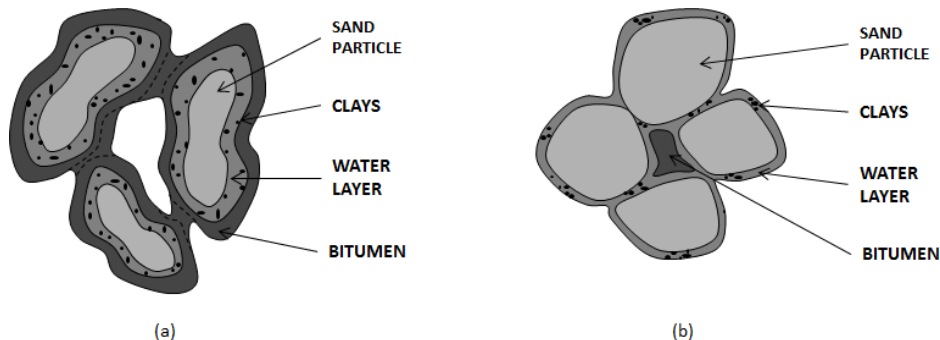


**Figure 1-1.** Arrangement of oil-sand particles according to Cottrell<sup>16</sup> (a) and Mossop<sup>17</sup> (b)

Cottrell's model has been discussed, refined and supported by many authors including: Dusseault and Morgenstern;<sup>18</sup> Takamura;<sup>19</sup> Mossop and Czarnecki *et al.*<sup>20</sup> The refined microstructure of the oil sands represented by Mossop's<sup>17</sup> model shown in Figure 1-1b generally illustrates the refined models proposed by the authors mentioned. Although the water-layer oil sand microstructure has been frequently mentioned in literature there has

been no experimental evidence that clearly illustrates this phenomenon. Recently, extensive characterization of the microstructure of the Canadian oil sands was investigated by Doan *et al.*<sup>21</sup> Images of the microstructure of the oil sands were obtained by high resolution three-dimensional (3D) X-ray microtomography ( $\mu$ CT) and cyro-scanning electron microscopy (cyroSEM), which showed no evidence of a water layer surrounding the quartz grains as mentioned in previous literature.<sup>21</sup> Instead, bitumen strongly adhering to the quartz grains was observed as well as the concave shape of the bitumen suggestive of a hydrophobic nature of the grain-bitumen.<sup>21</sup>

There are many variations of the microstructure of the Canadian oil sands in literature, which is noted by both Dusseault<sup>22</sup> and Doan *et al.*<sup>21</sup> as being due to pressure release and gas expansion as a result of inadequate sampling techniques disrupting the microstructure of the *in situ* oil sands. In the end, understanding the composition and mutual arrangement of the oil sands is important as it provides valuable information regarding the physical characteristics, which leads to proper processing and treatment methodologies avoiding costly mistakes.

## 1.4 Recovering Bitumen

The recovery of the oil sands and the extraction and refinement of bitumen relies on many intricate processes compared to conventional crude oil. Recovering oil sands through open-pit surface mining accounts for 60 % of bitumen production and is used when overburden (*i.e.*, rock or other deposits on top of the sands to be extracted) is less than 75 m; however, 80 % of known bitumen reserves are at depths greater than 75 m, which requires

the use of *in situ* mining methods (e.g., steam-assisted gravity drainage, cyclic steam simulation and vapour extraction process).<sup>23</sup> Currently, *in situ* mining is a relatively new process compared to surface mining; it is – inefficient and very costly due to the intensive energy and the water input needed. Surface mining is one of the first technologies developed for the recovery of bitumen along with one of the most employed extraction process, which was first developed by Karl Clark: the hot water extraction process.<sup>23</sup> Years of these methods being augmented has improved the bitumen recovery of up to 90 %, while *in situ* processes recover less than 80 % of bitumen.<sup>23</sup> Although *in situ* processes are currently less efficient and relatively high cost, the amount of waste generated is estimated to be less than that of surface mining, making it an attractive alternative for future mining efforts. Therefore, surface mining is the preferred method for the foreseeable future. While effective, this method (which relies on hot water extraction), generates a lot of toxic by-products, which are stored in tailing ponds. These tailings ponds, their environmental impact, and an investigation into utilizing polymer-based materials to reduce the environmental impact are the focus of this dissertation.

#### **1.4.1 Hot Water Extraction Process**

In the early 1920s Dr. Karl Clark was employed by the Alberta Research Council to determine a way to utilize the bitumen found in oil sands as a road paving material.<sup>24,25</sup> During his experiments he discovered that the addition of hot water (80–90 °C) to the oil sands caused the heavy oil trapped in the oil sands to froth and float to the top of the mixture.<sup>24</sup> This unexpected behaviour led to the first experimental separation plant to be developed and the implementation of hot water extraction (HWE) process was underway.<sup>24</sup>

In 1930, Clark and Pasternick continued research on a pilot plant scale and noted that the separation of the oil sands and bitumen using hot water was comparable to previous results; however, the bitumen was described as being highly dispersed in the plant water and not easily recovered.<sup>26</sup> Bituminous sand presumed to be free of salts and clay was acquired and controlled amounts of acid, salts and clay were added to the sand and the effect on separation was monitored.<sup>26</sup> Overall, the addition of an alkaline material and surface-active agent were deemed necessary to improve separation.<sup>24,26</sup>

Since the 1990's, significant efforts have been made to improve the HWE process pioneered by Clark and Pasternick. Most notably is the work of Cyberman whose efforts are responsible for the introduction of hydrotransport technology reducing the processing temperature from 80–90 °C to 35–40 °C.<sup>27</sup> Hydrotransport works by transporting a mixture of water and the oil sands from the mining sites through a pipeline, which cools and mixes the slurry breaking down the oil sands and causing the bitumen to separate in the form of small oil droplets.<sup>28</sup> The benefits from this new technology is lower operation temperature, lower energy consumption and flexibility of transportation.<sup>27,28</sup>

#### **1.4.2 Commercial Bitumen Recovery Process**

Open-pit surface mining is a massive operation used to recover oil sands from surface bitumen reserves, which accounts for a small percentage of known bitumen reserves. First, 400-ton trucks transport millions of tons of excavated oil sands (average daily amount) to a crushing facility, crushing any recovered ore to inches in size, which is then mixed with hot water (35–40 °C) in a conditioning tank.<sup>23</sup> Next, a caustic solution of sodium hydroxide is

added to neutralize any acidity in the bitumen producing surface-active surfactants that are able to separate the bitumen from the water; therefore, separating the bitumen from the clay and sand overall improving the bitumen extraction process.<sup>23,29</sup> The hot mixture is transferred via pipeline (hydrotransport) to a primary separation vessel (PSV) that transforms the bitumen into a froth by air injection.<sup>23</sup> The froth at this point is lighter than water in the presence of bubbles attached to the bitumen forming a bitumen-rich froth layer.<sup>23,29</sup>

Inside the PSV is a bottom sludge layer that mainly consists of water-saturated sand, clay and fines with some bound bitumen, which is commonly referred to as tailings.<sup>29</sup> The tailings is further processed by being transported to the tailings oil recovery (TOR) unit to recover residual bitumen, while the remaining waste mixture is transferred to large storage ponds also known as tailing ponds.<sup>23,29</sup> The intermediate layer (referred to as middlings in Figure 1-2) is transferred to the secondary separation unit (SSU) for further bitumen extraction generating a bitumen-rich froth, which is mixed with froth generated in the PSV followed by heating and deaerating in the froth treater.<sup>29</sup> Naphtha (hydrocarbon liquid from petroleum distillates) is added to the treated froth to reduce the viscosity of the bitumen to allow it to flow to the centrifuge separating any water and sand, which is directed to the tailings ponds (Figure 1-2).<sup>23,29</sup>

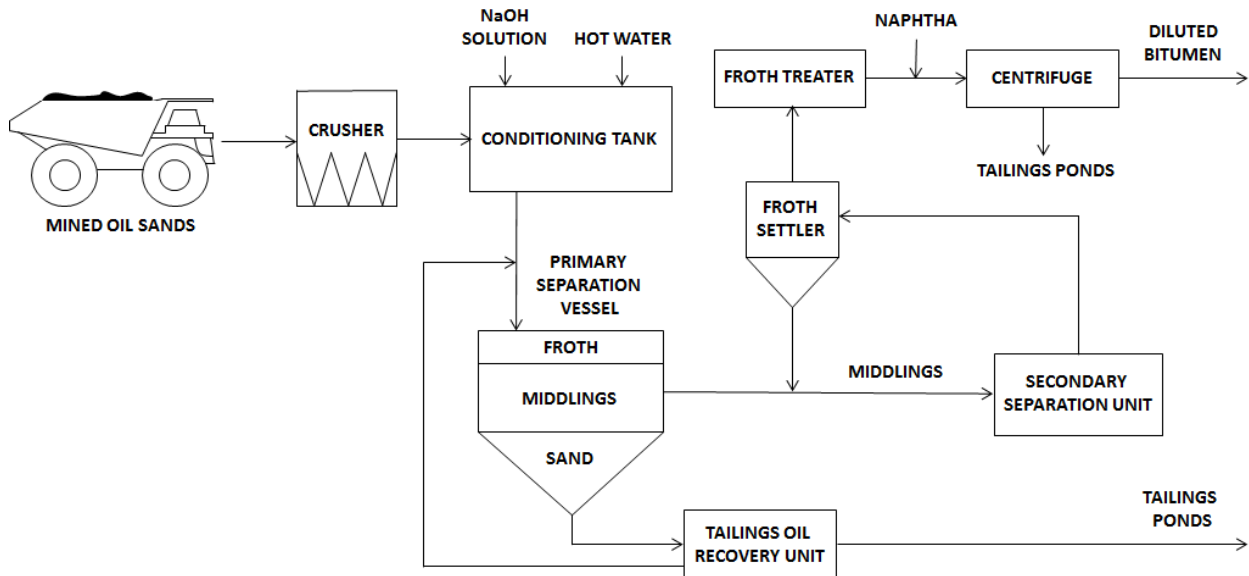


**Figure 1-2.** Simplified flow chart of the hot water extraction process

The mining process coupled with the HWE process is able to recover greater than 90 % of the bitumen and can recycle more than 90% of the water.<sup>29</sup> However, the main issue with these processes is the generation of tailing ponds, which are saturated with toxic chemicals that are detrimental to the environment.

## 1.5 Tailing Ponds

Tailings ponds house toxic process-affected (PA) water and sand waste generated by the HWE process. In 2013, it was estimated that there was approximately 976 Mm<sup>3</sup> of fluid tailings contained within the tailings ponds in Canada, with an overall net cumulative footprint (including dykes, berms, beaches and in-pit ponds) of approximately 220 km<sup>2</sup>.<sup>30,31</sup>

The Canadian tailing facilities in 2009 were reported as 130 km<sup>2</sup> an increase of 60 % between 2009 and 2013.<sup>32</sup>

The PA water in the tailings pond is recycled and re-used during the extraction process, causing it to become enriched with various inorganic and organic contaminants from the mined ore, processing additives and unrecovered bitumen.<sup>33</sup> Over time the tailings settle into four main fractions in the pond: a bottom layer of rapidly-settling coarse sand (> 44 µm); a thick suspension of tailings referred to mature fine tailings (MFT); an aqueous suspension of fine particles (20–80 weight % clays) referred to as fluid fine tailings (FFT); and a top water layer with residual bitumen that is recyclable (Figure 1-3).<sup>32-34</sup>

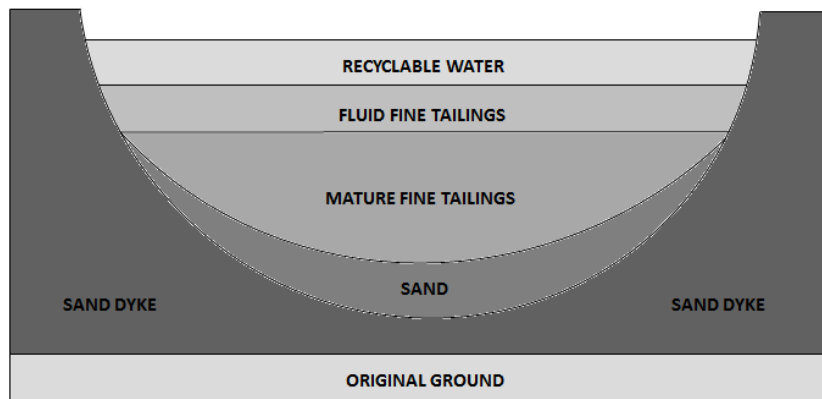


**Figure 1-3.** Theoretical model of the cross-section of a tailings pond

The tailings ponds are generally constructed from an array of excavated materials (e.g., rock, sand and clay) from nearby quarries, which gives little control over the grain size and compaction characteristics resulting in leakage.<sup>35</sup> According to a Toronto-based

company Environmental Defense the ponds in Alberta are leaking over 11 million litres a day of contaminated water into the surrounding environment, which was based on industry's own estimates (non-participating industries were estimated based on acquired averages from participating industries).<sup>36,37</sup> Overall, the identification and remediation methods are required to protect the surrounding environment, which is discussed further.

### **1.5.1 Chemical Composition**

The chemical composition of the tailings ponds is complicated and depended on the mineralogy, mining techniques, extraction processes and the additives used.<sup>32,33</sup> This composition is also prone to change as the tailings age, improvements made to tailings production technology as well as biogenic activity.<sup>33</sup> On average the tailings pond PA water has been determined as being moderately hard ( $\sim 15\text{--}25 \text{ mg L}^{-1} \text{ Ca}^{2+}$ ,  $\sim 5\text{--}10 \text{ mg L}^{-1} \text{ Mg}^{2+}$ ) with a pH of  $\sim 8\text{--}8.4$  and an alkalinity of  $\sim 800\text{--}1000 \text{ mg L}^{-1} \text{ HCO}_3^{-1}$ .<sup>34</sup> Although the composition of the tailings ponds can vary significantly, it has been reported that the tailings PA water in Alberta have trace amounts of metals such as: arsenic, molybdenum, copper, chromium, lead, nickel, iron and vanadium with iron being the most abundant metal constituting  $\sim 4\text{--}9 \%$  of the solid phase.<sup>33,34</sup> Numerous organic contaminates are contained in the oil sands as well, which has been reported as: asphaltenes, humic and fulvic acids, phthalates, benzene, toluene, ethylbenzene, xylene, and polycyclic aromatic hydrocarbons.<sup>33,38</sup> The actual total dissolved solids (TDS) in the tailings pond PA water has been reported with varying ranges in literature:  $\sim 2000\text{--}2500 \text{ mg L}^{-1}$ <sup>34,39</sup> and  $1,000\text{--}100,000 \text{ mg L}^{-1}$ ,<sup>40,41</sup> which could be primarily due to differing sampling techniques, sample acquisition location as well as tailings type. However, the solids in tailings pond PA water

has been reported as being primarily sodium, bicarbonate, chloride, sulphate and, in particular, naphthenate salts.<sup>34</sup> Although the tailings pond water (TPW) is alkaline, the acid content in the tailings pond is increasing due to the TPW being recycled numerous times saturating the tailings pond. Naphthenic acids (NAs) comprise the organic acid content in the TPW at an increasing concentration of 40–120 mg L<sup>-1</sup> and are primarily responsible for the acute toxicity of the TPW.<sup>42</sup>

## 1.6 Naphthenic Acids

Naphthenic acids (NAs) are naturally occurring organic acids found in oil sand deposits that are released from bitumen during oil sand processing.<sup>43</sup> NAs are classically defined as a complex mixture of alkyl-substituted acyclic, cyclic and polycyclic saturated carboxylic acids (Figure 1-4) represented by the general formula C<sub>n</sub>H<sub>2n+z</sub>O<sub>2</sub>, where n represents the carbon number and Z is a negative, even integer that specifies the hydrogen deficiency due to carbon rings within the structure.<sup>44</sup>

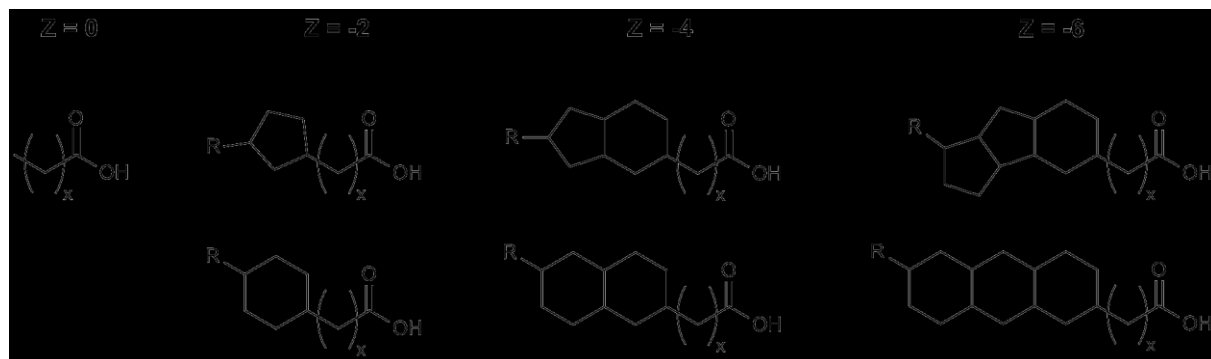


**Figure 1-4.** Sample NA structures for various Z-series where R is an alkyl group and chain length is represented by x.

As shown in Figure 1-4, the Z value is 0 for saturated linear or branched alkyl chains, -2 for monocyclic NAs, -4 for bicyclic NAs, -6 for tricyclic NAs and so on. Between Z series the molecular weight changes between 2 mass units ( $H_2$ ) and by 14 mass units ( $CH_2$ ) between n series.<sup>44</sup>

The  $Z = -4$  series constitutes ~ 90 % of the carboxylic acid fraction in unrefined bitumen, while the  $Z = -4$  series predominates in tailings pond water in Alberta.<sup>42,45</sup> Although NAs defined by the classical definition (c-NAs) constitute a large portion of the acid-extractable organic fraction (AOF), other NAs that fall outside the classical definition have also been found. Oxidized NAs (oxy-NAs, containing three or more oxygen atoms) and c-NAs with/ without sulphur and/ or nitrogen atoms as impurities have been measured in TPW; however, they exist in smaller quantities compared to c-NAs.<sup>42,46,47</sup>

The polarity and nonvolatility of NAs increases with molecular weight giving individual compounds varying physical, chemical and toxicological properties.<sup>45</sup> There are, however, physical and chemical properties that can generally explain a mixture of NAs, which is summarized in Table 1-2.

**Table 1-2.** Approximate physical and chemical properties of NAs<sup>45</sup>

Property	General Characteristic
Colour	Pale yellow, dark amber, yellowish brown, black
Odour	Musty petroleum/ hydrocarbon scent
State	Viscous liquid
Molecular Weight	~ 140–450 amu
Solubility	< 50 mg L <sup>-1</sup> at pH 7 in water Completely soluble in organic solvents
Density	0.97–0.99 g cm <sup>-3</sup>
Refractive Index	~ 1.5
pK <sub>a</sub>	5–6
Boiling Point	250–350 °C

A range of industrial applications also exist for naphthenic acid derivatives including: metal naphthenate salts, naphthenate esters and amides (Table 1-3). Two-thirds of NAs produced are converted to metal salts with copper naphthenate being the largest derivative produced.<sup>45</sup>

**Table 1-3.** Industrial applications of NA derivatives<sup>45,48</sup>

Naphthenic Acid Derivative	Industrial Applications
Na Salt	Emulsifying agent agricultural insecticides Demulsifier in oil industry
Ca napthenate	Additive for oil lubricator
Fe and Mn napthenate	Fuel additives for improved combustion and reduced corrosion
Pb and Ba salts	Catalysts in oil-based paints
Cu and Zn napthenate	Wood preservatives
Co napthenate	Curing agent in rubbers and resins
Mn, Pb, Co and Ca soaps	Oxidative catalysts
Alkyl and glycol naphthenate esters	Improve the flexibility and workability of resins
Amides and imidazolines of NAs	Corrosion inhibitors, emulsifiers and bactericides

During bitumen processing NAs are transferred to tailings ponds water and stored in TPW. The NAs are able to enter surrounding water systems primarily through effluent discharge, but also through groundwater mixing and erosion of riverbank oil deposits, which can have detrimental effects on biological organisms and systems.<sup>45</sup> Ross *et al.* determined that surface water samples near the Lower Athabasca Region had NAs concentrations range from < 2–80.7 µg L<sup>-1</sup> and samples from the Athabasca River ranged from < 2–19.5 µg L<sup>-1</sup>.<sup>10</sup> Further investigation by Frank *et al.* determined that various ground water samples obtained from wells near the Athabasca River had NAs concentrations ranging from 39–55 mg L<sup>-1</sup> similar to what is found in TPW (54–60 mg L<sup>-1</sup>).<sup>49</sup>

The storage of TPW has been shown to be leaking into its surroundings according to several studies discussed earlier. Overall, major repercussions and even irreversible alterations in the environment can occur. In particular, plants, animals, micro-organisms and even humans are at risk making the remediation of TPW imperative.

### **1.6.1 Toxicological/Biological Studies**

NAs and naphthenates are considered to be the most toxic components in oil sands tailings pond water and refinery effluent. Clemente and Fedorak deemed that the acute toxicity of NAs may be related to their surfactant properties whereby NAs are able to penetrate through the membrane lipid bilayer due to their hydrophobic character affecting membrane fluidity, thickness, and surface tension.<sup>44,50</sup> Clemente and Fedorak<sup>50</sup> also determined that lower molecular weight NAs were contributing to most of the toxicity in a mixture of NAs. Although this trend has been noted by other researchers, the mechanism explaining this phenomenon is not well understood. Frank *et al.*, however, believed the toxicity was a result of the higher molecular weight NAs due to having higher carboxylic acid content and therefore lower hydrophobicity that could become more bioavailable and bioaccumulate in cells.<sup>51</sup> Although the toxicity of NAs is not completely understood numerous investigations have shown that the NAs are acutely and chronically toxic to a variety of plants, zooplankton, bacteria, phytoplankton and in particular mammals and aquatic organisms.<sup>52</sup>

### **1.6.1.1 Aquatic Toxicity**

NAs and derivatives of NAs found in oil sand process-affected water (OSPW) have significant and detrimental effects in aquatic environments. McKinnon and Boerger<sup>53</sup> determined the LC<sub>50</sub> (lethal concentration that will kill 50 % of test subjects) value by bioassays of 7 % for rainbow trout (*Salmo gairdneri*) and 2 % for water fleas (*Daphnia magna*) when exposed to Athabasca OSPW.<sup>42</sup> Dokholyan and Magomedov<sup>54</sup> studied the acute toxicity of NAs by exposing freshwater roach (*Rutilus rutilus*) to 12–100 mg L<sup>-1</sup> of commercial NAs (com-NAs), which determined the tolerance varied with age amongst the fish: 50 % of 2-month-old roach died with exposure to 50 mg L<sup>-1</sup> com-NAs, while 75 mg L<sup>-1</sup> of com-NAs was needed to kill 50 % of the 2-year-old roach.<sup>42</sup> Peters and co-workers exposed both com-NAs and OSPW to both Japanese medaka (*Orizias latipes*) and yellow perch (*Perca flavescens*) and both species showed an increase in deformity and a decrease in larval length at hatch as NA-com/OSPW concentrations increased.<sup>55</sup>

Research by Warith and Young<sup>56</sup> exposed fresh water green algae (*Selenastrum capricornutum*) to NAs containing sludge-like fluids obtained from Athabasca tailings ponds to be toxic with an average LC<sub>50</sub> of 25.8 % v/v (volume/volume), which affected growth rates.<sup>42</sup> Similarly, tadpoles of Canadian toads (*Bufo boreas*) and Wood frogs (*Rana sylvatica*), were exposed to OSPW (NAs < 3 mg L<sup>-1</sup>), which adversely affected their growth and development.<sup>57</sup>

### **1.6.1.2 Mammal Toxicity**

The toxicity data of NAs for mammals is limited compared to aquatic organisms; however, the lethal dosage of NAs for humans was determined to be  $\sim 1$  L or  $11 \text{ g kg}^{-1}$  bodyweight.<sup>42,45</sup> The LD<sub>50</sub> of NAs for Wistar rats (*Rattus norvegicus*) was determined to be  $3.0\text{--}5.2 \text{ g kg}^{-1}$  of bodyweight.<sup>42</sup> Further tests with Wistar rats by Rogers *et al.* found that the high dose effect was hepatotoxicity (*i.e.* chemical-driven liver damage) suggestive that the liver is a potential target organ.<sup>58</sup> Non-lethal effects were also observed including: decreased blood glucose levels, reduced leukocyte count as well as increased muscle glycogen.<sup>58</sup>

### **1.6.2 NAs Degradation/ Mitigation**

With NAs being the most toxic component in TPW various approaches to reduce NAs in TPW has been considered, which includes oxidation, adsorption/sorption, biodegradation and phytodegradation, photolysis, and hydrolysis.<sup>42</sup> Among the possible pathways for TPW remediation aerobic microbial biodegradation has received considerable attention due to its economical sustainability and believed to be the more viable option for NAs degradation.<sup>42</sup> Adsorption/sorption are among some of the earliest approaches for process water treatment; however, few studies have outlined the mechanisms governing these processes.<sup>45</sup> Degradation of NAs by advanced oxidation, in particular by ozonolysis, which has also been considered due to its ability to enhance the degradability of NAs when coupled with biodegradation and can be enhanced by UV (ultraviolet) light. Finally, phytodegradation through the use of natural wetlands has been proposed, but limited results outlining the effectiveness of this method has been reported due to the possible leaching of contaminants in a large-scale set-up.<sup>42</sup>

### **1.6.2.1 Biodegradation**

In general NAs have a high water solubility and not easily adsorbed by soil and sediment, which is described by its low sorption distribution coefficient ( $K_d$ ) of  $\sim 0.5$  in sand/clay; ideal for something with high bioavailability.<sup>59</sup> NAs, however, are weakly biodegradable, which is reflected in their high toxicity in aquatic environments as mentioned previously.

Herman and co-workers<sup>60</sup> utilized a mixture of bacterial cultures enriched from oil sands tailings and exposed them to com-NAs and oil sands tailings containing NAs. Two distinctive cultures: *Pseudomonas stutzeri* and *Alcaligenes denitrificans* were responsible for the degradation of com-NAs converting  $\sim 50\%$  of organic carbon into  $\text{CO}_2$ .<sup>60</sup> Three colony types were identified to degrade the tailings pond extraction: *Acinetobacter calcoaceticus*, *Kilrthia sp.* and finally a member of the *Pseudomonas fluorescens* group, which converted  $\sim 20\%$  of the organic carbon in the tailings extraction in  $\text{CO}_2$ .<sup>60</sup> Clemente and co-workers<sup>61</sup> used aerobic cultures from oil sands process-affected waters and exposed them to com-NAs, which degraded by  $\sim 60\%$  and was released as  $\text{CO}_2$ , also lowering the overall toxicity.

The biodegradation of NAs for the remediation of TPW shows to be a promising area, but requires a diverse and robust mixture of cultures to be successful in such a complex and toxic environment.<sup>45</sup> Further investigation of enriched cultures recovered from PA water by Clemente *et al.* treating com-NAs determined the naphthenic acids with lower molecular weights and fewer rings are most susceptible to biodegradation.<sup>62</sup> Appropriate conditions

including control of nutrients, salinity and pH is required for the microbial cultures to thrive, which is difficult to control in tailings pond.<sup>45</sup>

### 1.6.2.2 Adsorption/ Sorption

The use of adsorbents has yielded promising results removing an array of pollutants including soluble organic compounds<sup>63</sup>, oil and grease<sup>64</sup> and even heavy metals.<sup>65,38</sup> Adsorbent materials are widely used to treat PA water with the most common being activated carbon, zeolites, clays, and oligosaccharides.

Activated carbon (AC) is an amorphous form of carbon that has an intricate porosity and high specific area allowing it to have a high adsorption capacity for various organic contaminants.<sup>66</sup> The treatment of PA water with activated carbon has been shown to significantly reduce the concentration of NAs and, as a result, reduce the overall toxicity.<sup>67</sup> The adsorption capacity for AC can range from 35–160 mg NAs per g of material depending on the source of AC.<sup>68,69</sup> However, activated carbon is expensive and has demonstrated poor removal rates for other pollutants such as emulsified oils, aliphatic hydrocarbons, and other volatile organic compounds (BTEX: benzene, toluene, ethylbenzene and xylene).<sup>38,70</sup> Despite these shortcomings, various forms of activated carbon continues to play a major role in water remediation in the oil sand industry.<sup>38,71</sup>

Clays have also been shown to lower the concentration of NAs and therefore the toxicity with the main adsorbent–adsorbate interaction believed to be due to hydrogen bonding between the carboxylic acid group and water molecules on the clay mineral surface.<sup>45,72</sup> Further investigation by Zou *et al.* showed that several clays saturated with

sodium: Na-montmorillonite, Na-illite and Na-kaolinite was able to absorb 49.3, 19.1, 5.92 g com-NAs per kg of clay respectively.<sup>72</sup> According to Zou *et al.* the adsorbent–adsorbate interaction is believed to be due not only to hydrogen bonding, but electrostatic charge–dipole interaction between the clays and naphthenic acids, which is influenced based on surface charge as well as surface area.<sup>72</sup>

Similar to clay, zeolites are naturally occurring and have also been shown to remove not only naphthenic acids, but BTEX as well.<sup>38</sup> Zeolites modified through dealumination increased adsorption of organic compounds by increasing hydrophobicity allowing for the removal of 60–70 % of BTEX.<sup>70</sup> Gaiker and Maiti determined Na-X zeolites (molecular sieves) showed a very low adsorption capacity for naphthenic acid due to small pore size; however, the affinity towards naphthenic acids determined by the equilibrium constant is high with a value of  $105.5 \times 10^{-3} \text{ cm}^3 \text{ mole}^{-1}$  compared to other adsorbents including: polyvinylpyridine ( $44.7 \times 10^{-3} \text{ cm}^3 \text{ mole}^{-1}$ ), bentonite ( $54.74 \times 10^{-3} \text{ cm}^3 \text{ mole}^{-1}$ ), Indion FFIP ( $63.92 \times 10^{-3} \text{ cm}^3 \text{ mole}^{-1}$ ) and amongst others.<sup>73</sup>

Cyclodextrins (CDs) are oligosaccharides consisting of glucose units that are a by-product of the digestion of cellulose and have been shown to form stable complexes with aliphatic and alicyclic carboxylic acids.<sup>74,75</sup> These stable complexes are owed to their truncated cone-shape with a hollow hydrophobic core, an ideal cavity for organic compounds featuring long alkyl chains and aromatic groups (Figure 1-5).<sup>74,76</sup>

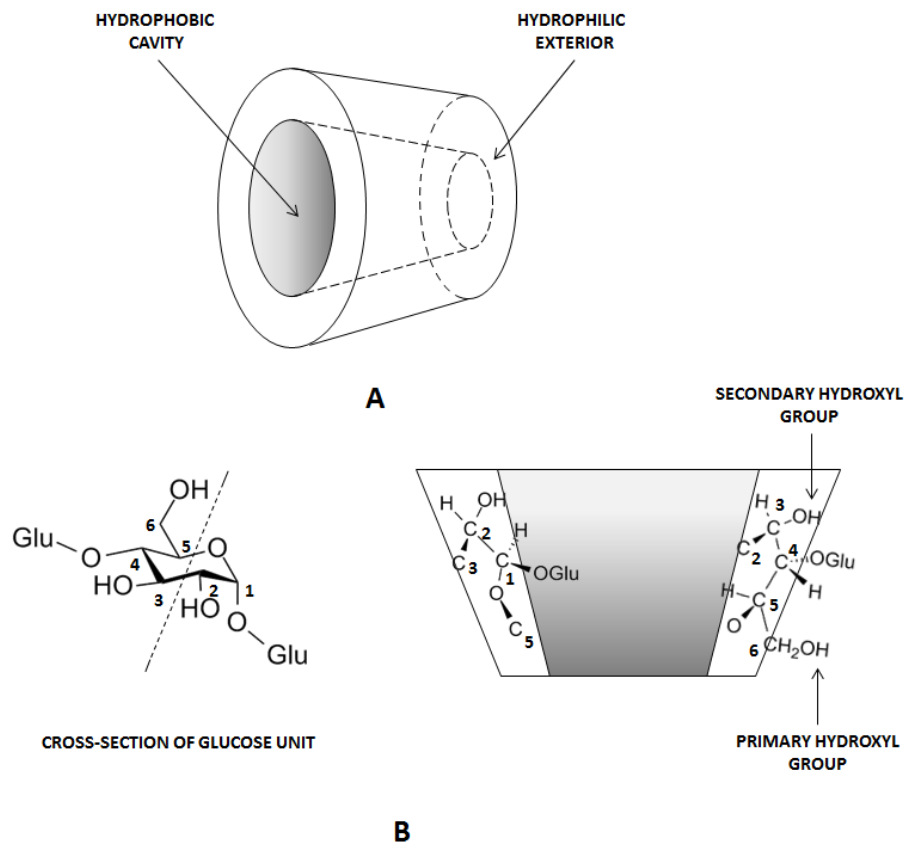


**Figure 1-5.** The truncated cone-shape of cyclodextrin (A) and the cross-section of a cyclodextrin molecule showing the arrangement of glucose units (B)

The adsorption properties of  $\beta$ -cyclodextrin ( $\beta$ -CDs, Figure 1-6) towards com-NAs and NAs from extracted from Syncrude tailings pond water was explored by Muhamed *et al.* through the use of spectral displacement techniques.<sup>77</sup> Strong binding constants were measured for both Fluka NAs ( $23.4 \times 10^4 \text{ M}^{-1}$ ) and Syncrude NAs ( $12.7 \times 10^4 \text{ M}^{-1}$ ) with varying values due to differences between types and size of naphthenic acids available in commercially purchased NAs versus tailings pond water.<sup>77</sup> The effects of  $\beta$ -CD in polymeric material was also been explored by Muhamed *et al.*, which showed  $\beta$ -CD-modified polymeric materials to have sorption capacities ranging from 20 to 30 mg NAs g<sup>-1</sup> compared

to granular activated carbon (GAC) with a range of 100 to 160 mg NAs g<sup>-1</sup> of material.<sup>68</sup> The polymeric materials included:  $\beta$ -CD cross linked with 1,4-phenylene diisocyanate ( $\beta$ -CD-PDI) and epichlorohydrin ( $\beta$ -CD-EP). Significant differences in the sorption capacities between GAC and the sorbents were related to the differing accessible surface areas and pore structure.<sup>68,78</sup>

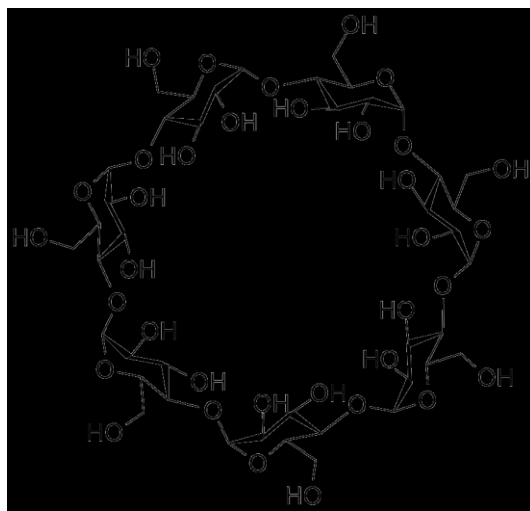


**Figure 1-6.** Structure of  $\beta$ -cyclodextrin

### 1.6.2.3 Ozone

Oxidation of NAs by ozone is an advanced oxidation technique that has been explored extensively to treat OSPW. Scott *et al.* was among the first to treat OSPW with ozone by filtering OSPW into a Seair gas/liquid diffusion system.<sup>79</sup> The concentration of NAs in OSPW acquired from Syncrude tailings ponds dropped from 59 mg L<sup>-1</sup> to 2 mg L<sup>-1</sup> with an ozone concentration of 150 mg L<sup>-1</sup> and a significant drop in the toxicity.<sup>79</sup> Gamal El-Din *et al.* conducted a similar experiment and noted a shift in NAs profiles before and after ozonation.<sup>80</sup> Overall, the total NAs concentrations decreased by 90 % after ozonation with

NAs with  $Z = -2$ ,  $-4$ , and  $-8$  decreased by 74, 94, and 99 %, respectively, which shows preferential reactivity towards NAs with higher cyclicity (*i.e.* more negative  $Z$ ).<sup>80,81</sup> In addition, an increase for some  $Z = 0$  and  $Z = -2$  NAs (low molecular weight and low cyclicity) was observed, which was also noted by Pereira *et al.*<sup>82</sup> and Scott *et al.*<sup>79</sup> and possibly due to ring opening during the oxidation of more cyclic NAs.<sup>80</sup> A decrease in other organic compounds in OSPW was also noted again when measured, including the AOF fraction of OSPW.<sup>80</sup>

The use of ozone as a method to reduce NAs shows to be a promising treatment method; however, the by-products of ozonolysis of NAs need to be explored further in order for it to be considered a viable method for water remediation. Although the overall toxicity of TPW and concentration of NAs has been shown to decrease once treated with ozone, aquatic organisms and mammals still showed adverse side effects, but to a lesser extent compared to untreated TPW. He *et al.* showed that ozone treated TPW exposed to early life stage of fathead minnow (*Pimephales promelas*) still exhibited haemorrhaging, pericardial effusion (*i.e.* fluid build-up around the heart) and spinal malformation.<sup>83</sup> Garcia-Garcia *et al.* exposed mice to ozone treated TPW, which showed inflammation of the mesenteric lymph nodes due to the residual toxic substrates remaining.<sup>84</sup>

Despite these shortcomings mentioned, a method to enhance the oxidation of NAs using an oxidant is to incorporate UV light. UV light is capable of breaking covalent bonds in organics through hemolysis generating reactive hydroxyl radicals<sup>85</sup>, which facilitates in the oxidation of toxic organic complexes present in tailings pond water. Liang *et al.* did an extensive comparison of several oxidants ( $\text{TiO}_2$ ,  $\text{H}_5\text{IO}_6$ ,  $\text{Na}_2\text{S}_2\text{O}_8$ ,  $\text{H}_2\text{O}_2$ ) with and without UV light as a method to remove NAs from samples of model oil sands process water, which

was made.<sup>86</sup> Based on the study, when no UV light was used there was no significant degradation of NAs, indicating none of these oxidants can directly oxidize NAs.<sup>86</sup> Overall, the reactive radicals generated by the illumination of UV light in the presence of the oxidants are responsible for the oxidation of NAs.

### **1.6.3 Analysis of NAs**

Naphthenic acids, as mentioned earlier, are a complex mixture of many different types of acids. The effects of NAs in terms of corrosiveness and toxicity greatly depend on the concentrations and types of acids. Currently, there are no analytical methods that identify or quantify individual acids and their toxicity.<sup>50</sup> Presently, analytical methods treat these acids as a group, or as sub-groups based on carbon and Z numbers.<sup>50</sup> Although extensive studies using high-end methodologies and instruments are not exact and sometimes not comparable due to how complex TPW is, the results should be viewed as at least semi-quantitative.<sup>71,81</sup>

#### **1.6.3.1 Toxicity Analysis: Microtox Bacterial Bioassay**

A common method for the determination of the overall toxicity of oil sand PA water is the use of the Microtox toxicity assay, which uses a luminescent bacterium (*Vibrio fischeri*) as the test organism.<sup>50</sup> Although this method is not selective for determining toxicity contributed strictly from NAs, the Microtox bioassay is easy to use, inexpensive and quick, which was investigated in an extensive study by Kaiser *et al.*<sup>87</sup>

The Microtox toxicity test exposes the luminescent bacterium to aqueous samples and measures the increase or decrease in light output. The toxicity value determined by the Microtox instrument is expressed as the inhibitory concentration of the sample that is responsible for x decrease in luminescence  $IC_x$ , (where x is the percent decrease in *V. fischeri* luminescence).<sup>50</sup> For example: a 50 % decrease in luminescence is referred to as the  $IC_{50}$ , which means 50 % of the bacteria exposed to the aqueous sample are dead.<sup>50</sup>

### **1.6.3.2 Fourier-Transform Infrared Spectroscopy**

Fourier-transform infrared spectroscopy (FT-IR) is an industry standard method first developed by Syncrude Canada Ltd. to quantify NAs in TPW.<sup>50</sup> In short, aqueous samples are acidified and the NAs are extracted with dicholormethane (DCM). The extractions are concentrated and analyzed by FT-IR by measuring the absorbances of the monomeric (1743  $\text{cm}^{-1}$ ) and dimeric (1706  $\text{cm}^{-1}$ ) form of the carboxylic groups.<sup>50</sup> The minimum detection limit for this method is within a few tenths of a milligram per litre; however, this is subject to change depending on the extract volume and the extent the DCM extraction is concentrated.<sup>50</sup> The FT-IR method, however, does not just detect compounds that strictly adhere to the chemical formula for NAs; instead, the data obtained from FT-IR measures the total AOF.<sup>81</sup> The lack of selectivity using FT-IR also results in the over estimation of NAs according to Scott *et al.* when compared to the measured acids concentrations from gas chromatography-mass spectroscopy (GC-MS).<sup>79</sup>

### **1.6.3.3 Gas Chromatography**

For analysis using gas chromatography (GC) with flame ionization detection (FID), NAs are first derivatized to form methyl esters, which elute as an unresolved “hump”; when integrated and compared to an internal standard, a total NA concentration may be deduced.<sup>43</sup> Commonly, GC is paired with low resolution MS to improve resolution and the limit of detection (LOD) to 0.01 mg L<sup>-1</sup>.<sup>79</sup> GC-MS compared to FT-IR is a sensitive method of detection for NAs and also suffers few matrix effects.<sup>79</sup> The method, however, is time-consuming, and other moieties originating from the volatile derivatives complicate mass spectral interpretation and, therefore, misclassifications of compounds are a results as well as false high concentrations.<sup>79,88</sup>

### **1.6.3.4 Mass Spectroscopy**

Mass spectroscopy is currently the most common method for the analysis of NAs in TPW, which begins with the establishment of a profile of individual NA isomers by plotting the relative response of each mass (*i.e.* m/z value) corresponding to a particular n and Z combination.<sup>71,81</sup>

Negative ion electrospray ionization-mass spectroscopy (ESI-MS) has been used to determine NAs concentration in com-NAs as well as PA water from Syncrude. Headley *et al.* was able to develop a method for ESI-MS that first preconcentrates samples using a solid-phase extraction procedure utilizing a cross-linked polystyrene-based polymer containing divinyl benzene support sorbent.<sup>89</sup> The acids were eluted from the sorbent with acetonitrile

and analyzed by ESI-MS with a detection limit based on a 500 ml water sample of 0.01 mg naphthenic acids L<sup>-1</sup>.<sup>50,89</sup>

### 1.6.3.5 High Performance Liquid Chromatography

High performance liquid chromatograph (HPLC) has also been explored by Clemente *et al.* to not only quantify the amount of NAs, but monitor the biodegradation of naphthenic acids.<sup>90</sup> Prior to analysis, aqueous solutions of NAs were derivatized with 2-nitrophenylhydrazine (NPH) in the presence of 1-ethyl-3-(3-dimethylaminopropyl) carbodiimide (EDC) and separated and analyzed by HPLC.<sup>90</sup> The naphthenic acids eluted as an unresolved “hump” similar to GC analyses and had a detection limit of ~ 15 mg NAs L<sup>-1</sup>, which was later improved by Yen *et al.* to ~ 5 mg NAs L<sup>-1</sup>.<sup>50</sup>

The development and optimization of this method was compared to the industry standard FT-IR method, which showed the FT-IR method had on average higher predicted concentrations of ~ 11 %; however, it is difficult to say which values are more accurate.<sup>91</sup> HPLC, however, compared to other methods is less time intensive and does not require harsh chlorinated solvents.<sup>50</sup>

The benefits of both HPLC and MS was explored by Martin *et al.*<sup>71</sup> and Han *et al.*<sup>92</sup> with HPLC coupled with high resolution mass spectroscopy (HRMS) as a method to determine NAs concentrations. The method was found to be comparable to FT-IR measurements ( $r^2 = 0.82$ ); however, it was postulated that both methods were experiencing similar interferences from other compounds such as natural fatty acids (FAs) present in the water.<sup>81</sup> Ross *et al.* conducted a study investigating the contribution of natural FAs effects on

the measurement of bitumen-derived NAs, which showed to contribute to the over estimation of NAs concentrations in TPW.<sup>93</sup> The corrected method using HPLC/HRMS resulted in NAs measurements to be orders of magnitude lower than measured values of PA water compared to other measurements using HPLC/HRMS.<sup>81,93</sup>

# Chapter 2 - Microgels & Carbohydrates

## 2.1 Introduction

The oil sands processing facilities in Canada are required to operate under a zero water discharge policy and, therefore, no PA water is allowed to be released into the environment. Overall, this results in the accumulation and storage of numerous toxic chemicals, which was discussed in detail in Chapter 1. The development of a method to remediate the tailings ponds, and in particular NAs, has been the subject of great interest by the research community. The focus of this chapter is to provide an overview of two existing technologies and their use in water remediation: a class of carbohydrates referred to as polymethylated polysaccharides that exhibit a high affinity towards organics as well as NAs and specialized polymeric microparticles capable of absorbing organics.

## 2.2 Polymethylated Polysaccharides

Polymethylated polysaccharides (PMPs) are cytoplasmic (lipo)polysaccharides produced by Mycobacteria, which are composed of 10–20 carbohydrate residues (mannose or glucose), some of which are *O*-methylated.<sup>94</sup> Two known classes of PMPs are 3-*O*-methylmannose polysaccharides (MMPs) and 6-*O*-methyl-glucose lipopolysaccharides (MGLPs). A property associated with PMPs is their ability to form stable complexes with long-chained FAs and acyl-coenzyme A (acyl-CoA) derivatives, which suggests that they may play a role in regulating lipid metabolism in mycobacteria.<sup>95,96</sup> MGLPs can be isolated from a variety of

fast and slow growing *Mycobacterium* species (e.g., *M. phlei*<sup>97</sup>, *M. smegmatis*<sup>98</sup>, *M. bovis* BCG<sup>99</sup>, *M. tuberculosis*<sup>97,100</sup>, *M. leprae*<sup>100</sup>, *M. xenopi*<sup>101</sup> and others<sup>102</sup>) and even several *Nocardia* species.<sup>103</sup> Unlike MGLPs, MMPs have only been found in various fast growing mycobacteria, which could be a conditional requirement for the production of MMPs.<sup>98</sup>

Generally, MMPs consist of 11–14 linear  $\alpha$ -(1→4)-linked 3-*O*-methyl-D-mannose residues terminated at the non-reducing end by a single unmethylated D-mannose and at the reducing end by a methyl aglycon (Figure 2-1a).<sup>104</sup> MMPs in the cells of *Mycobacterium smegmatis* exist as a mixture of at least four isomers due to differences in size ( $\sim$  2.0–2.5 kDa<sup>102,104</sup>) and degree of *O*-methylation.<sup>98</sup> In general, MGLPs are composed of a mixture of  $\alpha$ -(1→4)-linked glucose and 6-*O*-methylglucose units terminated with a 3-*O*-methylglucose at the reducing end.<sup>96</sup> In addition, there are two  $\beta$ -(1→3)-linked branching glucose monosaccharides at residues 1 and 3 of the MGLPs backbone (Figure 2-1).<sup>96</sup> MGLPs from *Mycobacterium bovis* BCG contain 12 methyl groups and have an average molecular weight of 3.5 kDa.<sup>102</sup>

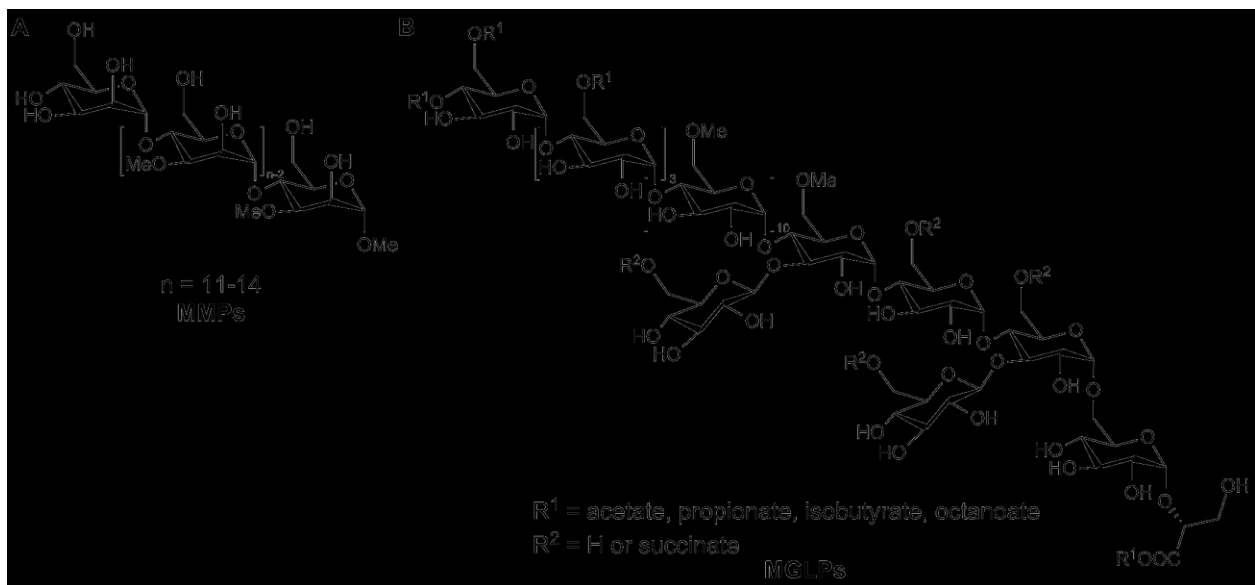


**Figure 2-1.** General structure of MMP (A) from *Mycobacterium smegmatis* and MGLP (B) from *Mycobacterium bovis* BCG<sup>105</sup>

### 2.2.1 Lipid-Interactions with Natural PMPs

As mentioned earlier, PMPs are able to form stable complexes with lipids and enzymes involved in lipid metabolism. Similar to amylose (polysaccharide composed of  $\alpha$ -D-glucose units), both MGLPs and MMPs are comprised of hexose units predominantly  $\alpha$ -(1→4) linked, suggesting that the conformation and interaction with lipids may be similar to the helical structure with a hydrophobic core exhibited by amylose.<sup>94</sup> Studies conducted using nuclear magnetic resonance (NMR) spectroscopy were able to monitor MMPs (from *M. smegmatis*) undergoing a conformational transition from a random coil in its free form, to an ordered helical structure.<sup>106,107</sup> The helical structure had a nonpolar cavity with methyl groups point inwards suited to binding to long-chain acyl-CoAs and FAs, which is illustrated in Figure 2-2.<sup>106,107</sup>

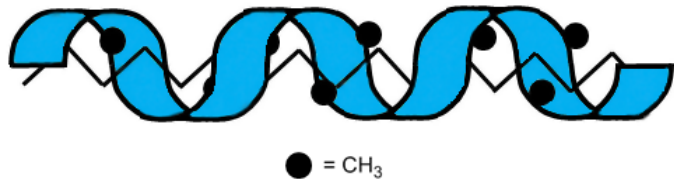


**Figure 2-2.** Schematic illustrating the helical structure exhibited by MMP (in blue) in the presence of a long lipid chain. Methyl groups (black circle) are pointed inwards creating a hydrophobic core suitable for organics.

Unlike MMPs, MGLPs were determined to exist in a coil conformation even in the absence of a long-chain lipid chain due to the presence of acyl groups on the backbone of the polysaccharide stabilizing the helical structure in its free form.<sup>94</sup>

The formation of these mycobacterial PMP-lipid complexes was investigated by Kiho *et al.* using fluorometric titration techniques and was determined to be largely entropically driven.<sup>108</sup> The chain length of the polysaccharide has also been shown to play a role in complexation with lipids.<sup>106</sup> The interaction of MMPs with palmitic and stearic acid was determined to be most optimal with 12  $\alpha$ -(1 $\rightarrow$ 4)-linked hexoses, while the homologue with one less hexose showed a 5-fold weaker interaction.<sup>108</sup>

## 2.2.2 Synthetic PMPs

The natural abundance of PMPs is low and exists as a mixture of homologs, which are difficult to separate and, therefore, challenging to conduct detailed structure-function studies.<sup>102</sup> Previous synthetic work reported the preparation of MMPs analogues in which all of the mannopyranose residues are methylated, unlike natural MMPs with an unmethylated residue at the non-reducing end.<sup>105,109,110</sup> In short, synthetic PMPs have been prepared from

an iterative reaction sequence, with a glycosyl donor containing a non-participating protecting group, which allowed careful control of reaction conditions to ensure good glycosylation stereoselectivities.<sup>105,109,110</sup>

The Lowary group developed a synthetic approach and produced a series of MMP derivatives with donors that contained ester moieties adjacent to the glycosylation site, which act as a temporary protecting group needed to facilitate chain extension.<sup>105</sup> An iterative approach was used to assemble the MMP derivatives by glycosylation using *N*-iodosuccinimide (NIS)–silver triflate (AgOTf/ CF<sub>3</sub>SO<sub>3</sub>Ag) or NIS–trimethylsilyl triflate (TMSOTf/ CF<sub>3</sub>SO<sub>3</sub>Si(CH<sub>3</sub>)<sub>3</sub>) activating conditions.<sup>102,105</sup>

### 2.2.3 NAs Interaction with MMPs

The high lipid affinities exhibited by MMPs was explored further by Liu *et al.* by using these polysaccharides as sorbents to remove hydrophobic contaminants from aqueous solutions.<sup>105</sup> In the study, MMPs extracted from *Mycobacterium smegmatis* (a mixture of MMP-10, -11, -12 and -13, Figure 2-3a) and synthetic MMPs (MMP-5<sub>s</sub>, -8<sub>s</sub>, -11<sub>s</sub> and -14<sub>s</sub>, Figure 2-3b) were exposed to various linear, saturated and unsaturated FAs and, in particular, a commercial mixture of NAs in aqueous solution.<sup>105</sup>

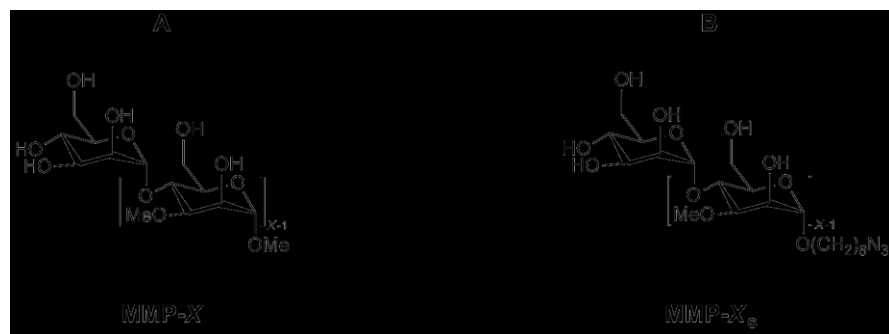


**Figure 2-3.** Structures of extracted MMP-X (A,  $X = 10, 11, 12, 13$ ) and synthetic MMP-X<sub>s</sub> (B,  $X = 5, 8, 11, 14$ )

A commercially produced NAs mixture was used in this work, which was composed of alkyl-substituted cyclic and acyclic aliphatic carboxylic acids and was characterized by electrospray ionisation mass spectrometry (ESI-MS) revealing species belonging to the  $C_nH_{2n+Z}O_2$  series with  $n = 12$  ( $Z = 2$ ), 13 ( $Z = 2$ ), 14 ( $Z = 4$ ), 15 ( $Z = 4$ ) and 16 ( $Z = 4$ ).<sup>105</sup> The association constants ( $K_a$ ) for MMPs binding to com-NAs was measured by direct ESI-MS as well as “proxy protein/proxy ligand” ESI-MS method, which is a competitive binding assay – a method used to determine whether MMPs bind specifically to NAs in an aqueous solution.<sup>105</sup> For a mixture of extracted NAs the apparent  $K_a$  values was determined to be  $(1.1 \pm 0.3) \times 10^3 M^{-1}$  by direct ESI-MS and an average  $(4.6 \pm 0.5) \times 10^4 M^{-1}$  by “proxy protein” ESI-MS assay.<sup>105</sup> The affinities of the individual synthetic MMPs for com-NAs were measured by proxy protein/proxy ligand ESI-MS, which showed increasing affinities  $(1.8 \pm 0.5) \times 10^4 M^{-1}$  (MMP-5<sub>s</sub>) to  $(8.8 \pm 0.3) \times 10^4 M^{-1}$  (MMP-14<sub>s</sub>).<sup>105</sup> The affinities measured for synthetic MMPs and extracted MMPs are comparable; however, natural MMPs are isolated in low yields making synthetic glycans an attractive alternative.<sup>105</sup>

Following this study, preliminary studies lead by the Lowary group further demonstrated that polystyrene resin functionalized with a synthetic MMP pentasaccharide derivative could detoxify TPW, as determined by Microtox analysis.<sup>105</sup> Further unpublished work showed that the pentasaccharide was stable in TPW for one month suggestive long-term field use of these materials may be possible.

## 2.3 Hydrogel Microparticles

Hydrogel particles (also known as nano- or microgels depending on their size) are three-dimensional polymeric gel networks that range in diameter from  $\sim 100$  nm to microns in size.<sup>111,112</sup> The particles can be made responsive to a variety of external stimuli, which can cause them to transition from a solvent swollen to a de-swollen state in response to an external stimulus such as changes in the material's environment (variations in temperature<sup>113</sup>, pH<sup>114</sup>, or presence/absence of chemical compounds<sup>115,116</sup>) or the application of an external field (light<sup>117</sup>, electrical<sup>118</sup> or magnetic fields<sup>119,120</sup>), which is much faster compared to their macroscopic hydrogel counterparts.<sup>111,121</sup>

Poly(*N*-isopropylacrylamide) (pNIPAM)-based microgels (and hydrogels) are among some of the most well-known and well-studied responsive polymers.<sup>112,122</sup> pNIPAM is fully water soluble at temperatures  $\lesssim 32$  °C existing as a random coil; however, as temperatures exceed  $\gtrsim 32$  °C pNIPAM undergoes a random coil-to-globule transition expelling its solvating water.<sup>112</sup> This temperature is referred to as the lower critical solution temperature (LCST) for pNIPAM, which was first observed by Wu *et al.* with homopolymer NIPAM chains in water.<sup>123,124</sup>

The LCST of pNIPAM based microgels, as well as their functionality, is easily tuneable by the addition of a co-monomer into the polymeric network. Comonomers that have been incorporated into pNIPAM microgel systems include: acrylic acid (AAc)<sup>125-127</sup>, vinyl acetic acid<sup>127,128</sup>, allyl acetic acid<sup>129</sup>, aminoethyl methacrylate hydrochloride<sup>130</sup> and others.<sup>121</sup> Of the co-monomers mentioned, AAc is widely used and can be easily copolymerized into the microgel system.<sup>112</sup> The AAc co-monomer renders the microgel pH responsive<sup>127</sup> and the carboxylic group serves as a reactive site for further

functionalization.<sup>112</sup> Zhang *et al.* functionalized pNIPAM microgels containing AAc with 3-aminophenylboronic acid (APBA) *via* carbodiimide coupling using *N*-(3-dimethylaminopropyl)-*N'*-ethyl-carbodiimide hydrochloride (EDC).<sup>131</sup> EDC is a water-soluble carbodiimide that reacts with carboxylic acid groups to form an *O*-acylisourea intermediate, which can be displaced by nucleophilic attack from primary amino groups.<sup>132</sup> The *O*-acylisourea intermediate is unstable in aqueous solutions and regeneration of the carboxyl groups is a result due to hydrolysis and generation of *N*-unsubstituted urea (Figure 2-4).<sup>132,133</sup> *N*-hydroxysuccinimide (NHS) or its water soluble analog *N*-hydroxysulfosuccinimide (sulfo-NHS) is sometimes included to create a more stable intermediate in aqueous solutions, which allows for efficient conjugation and better yield.<sup>132,133</sup>

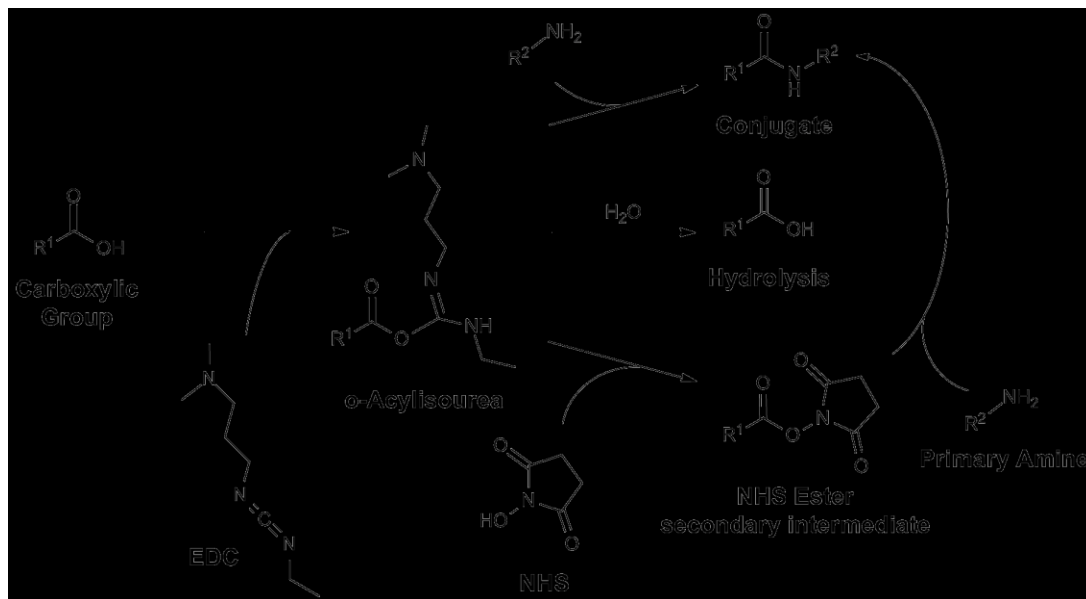


**Figure 2-4.** General EDC/ NHS coupling reaction in an aqueous solution.  $\text{R}^1$  and  $\text{R}^2$  can be any functional group with a carboxylate and primary amine respectively (e.g., peptides, proteins, carbohydrates *etc.*)

Dicyclohexylcarbodiimide (DCC) is another carbodiimide coupling reagent that is typically used; however, DCC is only soluble in aprotic solvents and does not work as efficiently in aqueous solutions compared to EDC.<sup>134</sup>

### 2.3.1 Synthesis of pNIPAM Microgels

There are several methods of synthesizing microgels including: precipitation polymerization<sup>135</sup>, emulsion polymerization<sup>113,136</sup>, anionic copolymerization<sup>137</sup> and cross-linking of neighbouring polymer chains<sup>138,122</sup>. Precipitation polymerization was first utilized by Philip Chibante in 1978 for the preparation of pNIPAM microgels and has been widely adopted since then.<sup>139</sup> Free radical precipitation polymerization is a standard approach for the polymerization of pNIPAM-based hydrogel particles driven by homogenous nucleation<sup>140</sup> and is the method used to synthesize pNIPAM-based microgels discussed in this dissertation.

The synthesis of pNIPAM-based microgels has NIPAM as the major monomer and the cross-linker is *N,N'*-methylenebis(acrylamide) (BIS), which are both dissolved in water and added to the same vessel. The vessel is heated to 60–70 °C and also purged with N<sub>2</sub>, which helps remove any dissolved O<sub>2</sub> that could intercept radicals and disrupt the polymerization.<sup>141</sup> The initiator, which is commonly ammonium persulfate (APS) or 2,2'-azobis(amidinopropane) dihydrochloride (V50), is added to the vessel and dissociates to give free radicals due to the energy in the system (Figure 2-5).<sup>135</sup> Another comonomer can be introduced into the free radical polymerization to add additional functionality to the particles.

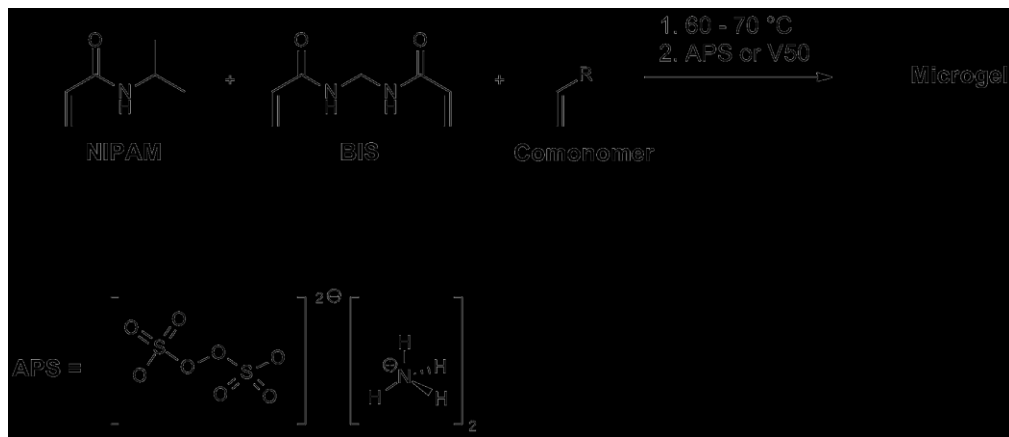


**Figure 2-5.** General synthesis of pNIPAM-based microgels using APS as the initiator.  
R is any functional group that has a terminal double bond able to participate in radical polymerization in aqueous conditions.

During the polymerization NIPAM plays a critical role in particle synthesis. At a critical chain length of NIPAM polymer the growing chain collapses and becomes a colloidally unstable ‘precursor particle’.<sup>140</sup> The ‘precursor particle’ acts as a nucleus for further polymerization, which collapse on the nuclei surface due to the polymerization temperature being well above the LCST of NIPAM.<sup>140,142</sup> The growing pNIPAM microgel particles are colloidally stabilized by steric mechanisms and electrostatic stabilization originating from the initiator’s charged groups.<sup>140,142</sup> The distribution of monomers within the particles has been investigated by Hoare *et al.* by comparing radial distribution profiles acquired from kinetic model predictions and monomer distribution profiles determined by image analysis of the dry-state transmission electron microscopy (TEM) image in which functional groups are selectively stained with uranyl acetate.<sup>143</sup> Several different types of microgels were synthesized; in particular, pNIPAM-co-AAc with BIS as the cross-linker was investigated. Overall, it was determined that the AAc and BIS was more concentrated in the core of the microgel particles according to both the experimental data as well as the models.<sup>143</sup> Overall,

data from previous polymerization studies have outlined many advantages of using this synthetic approach including the production of particles with very low polydispersity and control over parameters including: particle size, charge, and crosslink (co) density.<sup>135,144</sup>

### 2.3.2 pNIPAM- Based Microgels For Small Organic Molecule Removal

The applications for pNIPAM-based microgels are quite widespread including: biosensing<sup>145</sup>, drug release/delivery vehicles<sup>146</sup>, catalysis<sup>147</sup> and many others.<sup>148-150</sup> Water remediation is another application that has been gaining interest and was investigated by Morris *et al.* as a possible sorbent for Pb(II) using poly(N-isopropylacrylamide)-co-acrylic acid (pNIPAm-co-AAc).<sup>151</sup> Morris and co-workers were able to determine that as the AAc and/or the pH increases the amount of lead adsorbed increases.<sup>151,152</sup> Similarly, Snowden *et al.* also investigated the sorbent properties of pNIPAM-based microgels to remove lead nitrate as well as cadmium nitrate, which were absorbed in a larger capacity by the cationic microgels compared to its anionic analogue indicative that charge plays a crucial role in remediation.<sup>153</sup>

Recently, the Serpe group was able to show that pNIPAM-based microgels show potential for removing small organic contaminants by using azo dye 4-(2-hydroxy-1-naphthylazo) benzenesulfonic acid sodium salt (Orange II, Figure 2-6) as a model water contaminant, which has been found in industrial effluents.<sup>152,154-156</sup>

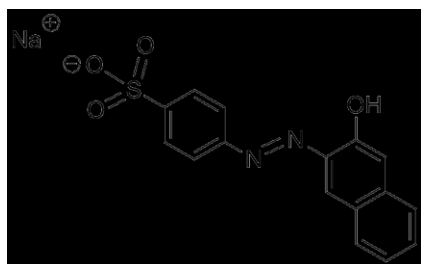


**Figure 2-6.** Chemical structure of Orange II Dye

A series of pNIPAm-co-AAc microgels were developed with 0 %, 5 %, 10 % and 15 % AAc by mmol. The 10 % AAc pNIPAM-based microgel showed the most promising results by removing 29.5 % Orange II at room temperature, which was increased to 56.6 % by heating for 90 minutes exploiting the thermoresponsive nature of the microgels.<sup>154</sup> Of the Orange II absorbed after heating 74.4 % of the Orange II was retained.<sup>154</sup> This work was expanded on by synthesizing pNIPAm-co-AAc microgel aggregates by polymerizing BIS in the presence of pNIPAm-co-AAc microgel.<sup>155</sup> The maximum removal efficiency reached by the microgel aggregates at elevated temperatures was 73.1 %; however, 75.6 % of the dye leaked, which was not comparable to the performance of the unaggregated microgels.<sup>155</sup> The enhancement in uptake of Orange II, however, is believed to be due to the increased volume of the aggregated microgels compared to the unaggregated microgels providing a larger reservoir for Orange II.<sup>155</sup> Also, the aggregates are more hydrophobic than the unaggregated microgels increasing their affinity for organics as well as the BIS itself is interacting with the Orange II.<sup>155,156</sup> The reusability of these microgels and microgel-based aggregates was investigated by methanol extractions to remove the dye, which showed a 34.6 % recovery of dye from microgel particles, while its aggregated-based microgel counterpart showed recovery of up

84.6 % of dye.<sup>156</sup> Overall, these microgels and microgel-based aggregates are not only effective for water remediation, but show promise in their reusability.

The water remediation abilities exhibited by microgels to remove small organics in aqueous solutions makes it an ideal sorbent. The development of a novel water remediation sorbent for TPW by combining microgels and sugars that mimic PMPs to reduce the concentration of NAs and other toxic organics is the focus of this dissertation and is discussed in greater detail in Chapter 3.

# **Chapter 3 - Polymerization and Modification of Microgels**

## **3.1 Introduction**

As detailed in Chapter 1 the processes to extract bitumen from the oil sands located in northern Alberta generates large volumes of liquid waste that are stored in tailings ponds. Based on the existing technology outlined in Chapter 2, this dissertation focuses on the development of pNIPAM-based microgels modified with carbohydrates as a method to create a sorbent that mimics the interactions exhibited by PMPs in the presence of lipids, but with NAs found in tailings pond water. In Chapter 3 the development and characterization of the sorbent is discussed, while in Chapter 4 the performance of the sorbent treating tailings pond water was monitored.

The purpose of this chapter is to discuss the synthesis, modification and characterization of pNIPAM-based microgels. In particular, the incorporation of carbohydrates into the microgel particles is one of the main focuses in this chapter. Several different types of sugars were synthesized by the Lowary group. The first class of carbohydrates were several monosaccharides and a pentasaccharide, which all have an octyl amide chain with a terminal double bound capable of participating in radical polymerization. Another class of simpler carbohydrates used in this dissertation are a series of monosaccharides and a disaccharide, which all have an octylamine chain capable of being coupled onto pNIPAM-co-AAc microgel. Coupling the carbohydrates to pNIPAM-co-AAc

through either EDC or DCC coupling was investigated and optimized, which was discovered that EDC/ NHS coupling was the best approach. The carbohydrate-modified microgels were characterized using nanoprobe NMR spectroscopy to confirm the carbohydrates were successfully coupled to the microgel.

### 3.2 Materials & Methods

*N*-isopropylacrylamide was purchased from TCI (Portland, OR) and purified by recrystallization from hexanes (ACS reagent grade, purchased from EMD, Gibbstown, OR). *N,N'*-Methylenebisacrylamide (99 %), acrylic acid (99 %), ammonium persulfate (98 %), dodecylamine (98 %), hexylamine (99 %), butylamine (99.5 %), propylamine (98 %), *N*-hydroxysuccinimide (98 %), *N,N'*-dicyclohexylcarbodiimide, 4-(dimethylamino)pyridine (99 %) sodium hydroxide (97 %) and deuterium oxide (99.9 %) were purchased from Sigma-Aldrich (Oakville, ON) and were used as received. 1-Ethyl-3-(3-dimethylaminopropyl)carbodiimide hydrochloride was purchased from Thermo Scientific (Burlington, ON). Chloroform and hydrochloric acid (ACS reagent, 37 %) was purchased from Caledon Laboratories Ltd. (Georgetown, ON). Carbohydrate-octylamides (mann-2OMe-octylamide, mann-3OMe-octylamide, penta-mann-2,3OMe-octylamide) were synthesized by Anushka Jayasuriya (Dr. Todd Lowary Group, University of Alberta), while carbohydrate-octylamines (mann-octylamine, mann-3OMe-octylamine, mann-2,3OMe-octylamine, glu-6OMe-octylamine, di-mann-octylamine) were synthesized by Kamar Sahloul (Dr. Todd Lowary Group, University of Alberta). Microgel samples were lyophilized using a VirTis bench-top K-manifold freeze dryer (Stone Ridge, New York). Deionized (DI) water with a resistivity of 18.2 MΩ·cm was obtained from a Milli-Q Plus system (located in the

Biological Laboratory in the Department of Chemistry, University of Alberta) purchased from Millipore (Billerica, MA), and filtered through a 0.2 m filter prior to use.

Stock solutions of NaOH (0.0274 M) and HCl (0.0329 M) were prepared in DI water and used further to prepare stock solutions of pH 3 and pH 7 in DI water with ionic strengths of 1 mM.

### **3.2.1 Dynamic Light Scattering & Zeta Potential Measurements**

Dynamic light scattering (DLS) and zeta potential (or electrokinetic potential) measurements were performed using a Malvern Zetasizer Nano S. The material measured was assumed to have similar optical properties as polystyrene latex. The temperature was set to 25 °C and the dispersant was set to water. The refractive index was set to 1.330 and the dielectric constant was 78.5. An equilibrium time of 120 seconds was set between measurements and the amount of measurements was set to automatic. Measurements (both zeta potential and DLS) were done in triplicate per sample. For DLS measurements, low volume disposable sizing cuvettes were used, while for zeta potential measurements standard polystyrene cuvettes were used as well as a zeta dip cell.

The zeta potential and particle size of modified pNIPAM-co-AAc microgels was measured at pH 3 and pH 7 to determine the success of coupling reactions by measuring the hydrodynamic radius (or solvated/hydrated radius) using dynamic light scattering (DLS) at pH = 3 and pH = 7. At pH = 3, the pH is lower than the pK<sub>a</sub> of AAc (~ 4.2) in pNIPAM-co-AAc microgel; therefore, the carboxylic group will be protonated resulting in potential intramolecular hydrogen bonding and a smaller particle size. However, at pH = 7, the AAc

( $pK_a$  is  $\sim 4.2$ ) moiety will be deprotonated resulting in the particle to become larger due to electrostatic repulsion. Theoretically, if the coupling reaction is successful there should be no change in the size of the particle at pH = 3 to pH = 7 due to the formation of an amide.

The zeta potential of the particles was also measured to determine the stability of the particles and charge of the particles after modification by DCC coupling. In short, the zeta potential is the potential difference between ions in the dispersant (*e.g.*, solvent) and the layer of ions attached to the dispersed particle surface.<sup>157,158</sup> Zeta potential values between -10 mV–+10 mV are considered neutral, while values greater than +30 mV or less than -30 mV are considered strongly cationic and strongly anionic respectively.<sup>158</sup> Overall, if the particles were successfully coupled they should be neutral due to amide formation.

### **3.2.2 Nanoprobe $^1\text{H}$ Nuclear Magnetic Resonance Spectroscopy**

Microgel particles were characterized with nanoprobe  $^1\text{H}$  Nuclear Magnetic Resonance spectroscopy in  $\text{D}_2\text{O}$  at pH 10, which was adjusted using NaOD. Spectra were recorded on a Varian three-channel i600 MHz spectrometer. Characterization of microgels was done by the NMR Spectroscopy Laboratory (Department of Chemistry, University of Alberta).

### **3.2.3 General Procedures**

### **3.2.3.1 General Procedure 1: Preparation of Carbohydrate-pNIPAM Microgels**

NIPAM (17 eq.) and BIS (1 eq.) was added to a 500 mL beaker along with 300 mL of MilliQ water, which was allowed to stir until a solution of NIPAM and BIS was established. The solution was filtered through a 0.2  $\mu\text{m}$  filter into a 500 mL 3-neck round bottom flask and was heated to 70 °C and degassed with N<sub>2</sub> and stirred for ~ 1 hour. The flask was purged with N<sub>2</sub> gas and the appropriate saccharide monomer (0.046–0.30 eq.) was added to the solution and initiated with APS (0.3 eq.). The reaction was allowed to stir for 1 hour resulting in the formation of a mixture due to polymerization of particles, which was filtered through cotton wool. The mixture was centrifuged at 8000 RPM for 1 hour and the supernatant was decanted and the resulting polymer was washed with MilliQ water. The particles were purified using this process, which was repeated 6 times. Finally, the sample was lyophilized for 24 hours.

### **3.2.3.2 General Procedure 2: Preparation of pNIPAM Microgels**

NIPAM (17 eq.) and BIS (1 eq.) was added to a 250 mL beaker along with 200 mL of MilliQ water, which was allowed to stir until a solution of NIPAM and BIS monomers was established. The solution was filtered through a 0.2  $\mu\text{m}$  filter into a 500 mL 3-neck round bottom flask and was heated to 70 °C and degassed with N<sub>2</sub> gas and allowed to stir for ~ 1 hour. The flask was purged with N<sub>2</sub> gas and another co-monomer (1–10 eq.) was added to the solution along with APS (0.3 eq.). The reaction was allowed to stir for 5–24 hour resulting in the formation of a mixture, which was filtered through cotton wool. The mixture was centrifuged at 10000 RPM for 1 hour and the supernatant was decanted and the resulting

polymer was washed MilliQ water. The particles were purified using this process, which was repeated 6 times. Finally, the sample was lyophilized for 24 hours.

### **3.2.3.3 General Procedure 3: DCC Coupling of pNIPAM-co-10 % AAc Microgels and Aliphatic Amines<sup>159</sup>**

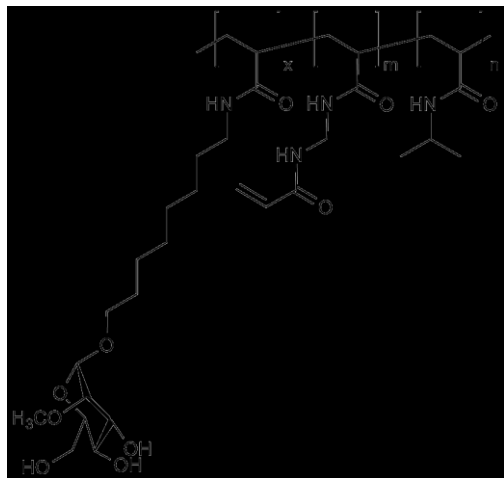
pNIPAM-co-10 % AAc (1 eq.) was added to a 25 mL vial along with 10 mL of chloroform, which was allowed to stir until a uniform colourless mixture was established. An aliphatic amine (1 eq.) was added to the vial followed by DCC (1.1 eq.), which was purged with N<sub>2</sub> and allowed to stir overnight. The filtrate was removed under reduced-pressure evaporation to recover the product.

### **3.2.3.4 General Procedure 4: EDC/NHS Coupling of pNIPAM-co-AAc Microgels**

pNIPAM-co- AAc (1 eq. of AAc) was added to a 50 mL round bottom flask (rbf) along with 25 mL of MilliQ H<sub>2</sub>O and allowed to stir for 2 hours until a uniform mixture was established. Next, NHS (5 eq.) and EDC (5 eq.) were added to the flask and allowed to stir for 30 minutes. A primary amine (5 eq.) was added to the flask and allowed to stir overnight. The resulting mixture was washed with MilliQ water (10 mL × 6) and centrifuged at 10,000 rpm followed by lyophilisation for 24 hours.

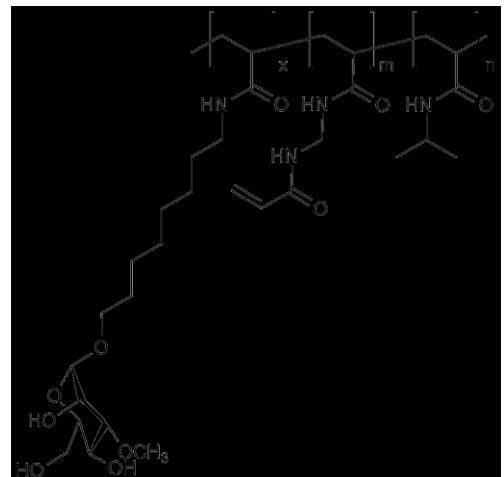
### 3.3 Polymerization of Carbohydrate-Microgels

#### 3.3.1 Preparation of pNIPAM-co-Mann-2OMe-Octylamide Microgel



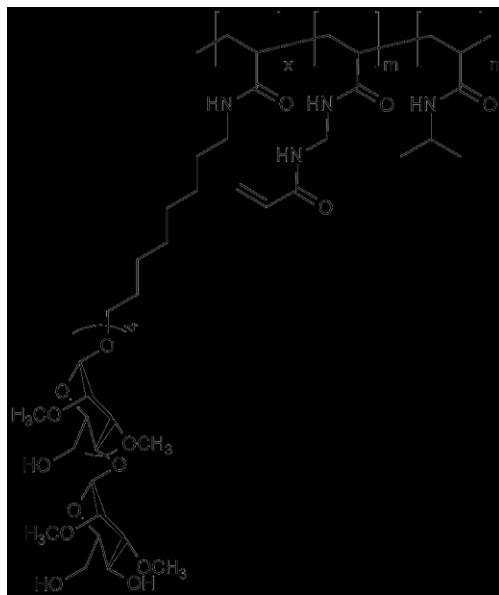
The polymerization of NIPAM (1.342 g, 11.8 mmol, 16.4 eq.), BIS (0.104 g, 0.719 mmol, 1.00 eq.) and mann-2OMe-octylamide (0.070 g, 0.19 mmol, 0.26 eq.) was initiated with APS (0.045 g, 0.20 mmol, 0.28 eq.) according to General Procedure 1 recovering a colourless solid (yield: 0.052 g).

#### 3.3.2 Preparation of pNIPAM-co-Mann-3OMe-Octylamide Microgel



The polymerization of NIPAM (1.342 g, 11.8 mmol, 17.3 eq.), BIS (0.105 g, 0.684 mmol, 1.00 eq.), Mann-3OMe-Octylamide (0.070 g, 0.19 mmol, 0.27 eq.) was initiated with APS (0.043 g, 0.187 mmol, 0.27 eq.) according to General Procedure 1 recovering a colourless solid (yield: 0.054 g).

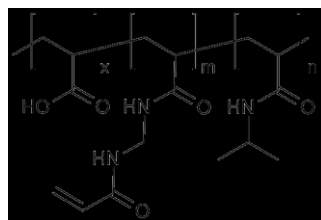
### 3.3.3 Preparation of pNIPAM-co-Penta-Mann-2,3OMe-Octylamide Microgel



The polymerization of NIPAM (1.3460 g, 11.8 mmol, 17.0 eq.), BIS (0.1073 g, 0.696 mmol, 1.00 eq.), penta-mann-2,3OMe-octylamide (0.035 g, 0.032 mmol, 0.046 eq.) was initiated with APS (0.045 g, 0.20 mmol, 0.29 eq.) according to General Procedure 1 recovering a colourless solid (yield: 0.103 g)

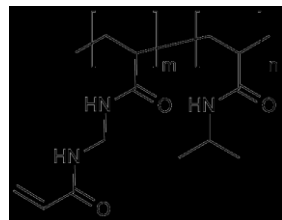
## 3.4 Polymerization of Unmodified Microgels

### 3.4.1 Preparation of pNIPAM-co-10 % AAc Microgel



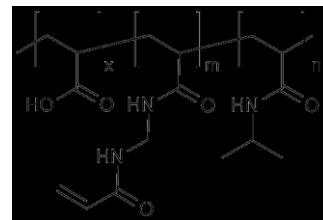
The polymerization of NIPAM (1.340 g, 11.8 mmol, 16.9 eq.), BIS (0.108 g, 0.697 mmol, 1.00 eq.), AAc (0.098 mL, 1.4 mmol, 2.0 eq.) was initiated with APS (0.045 g, 0.20 mmol, 0.28 eq.) and allowed to stir overnight according to procedure B recovering a colourless solid (yield: 1.511 g).

### 3.1.6 Preparation of pNIPAM-BIS Microgel



The polymerization of NIPAM (1.349 g, 11.87 mmol, 16.8 eq.) and BIS (0.109 g, 0.708 mmol, 1.00 eq.) was initiated with APS (0.0453 g, 0.198 mmol, 0.279 eq.) and allowed to stir overnight according to General Procedure 2 recovering a solid (yield: 1.433 g).

### 3.4.2 Preparation of pNIPAM-co-50 % AAc Microgel



The polymerization of NIPAM (0.7183 g, 6.313 mmol, 8.98 eq.), BIS (0.1082 g, 0.703 mmol, 1 eq.) and AAc (0.481 mL, 7.02 mmol, 9.98 eq.) was initiated with APS (0.0453 g, 0.1985 mmol, 0.28 eq.) and allowed to stir for 5 hours according to General Procedure 2 recovering a colourless solid (yield: 1.006 g).

### 3.4.2.1 Nanoprobe $^1\text{H}$ NMR Characterization of pNIPAM-co-50 % AAc Microgel

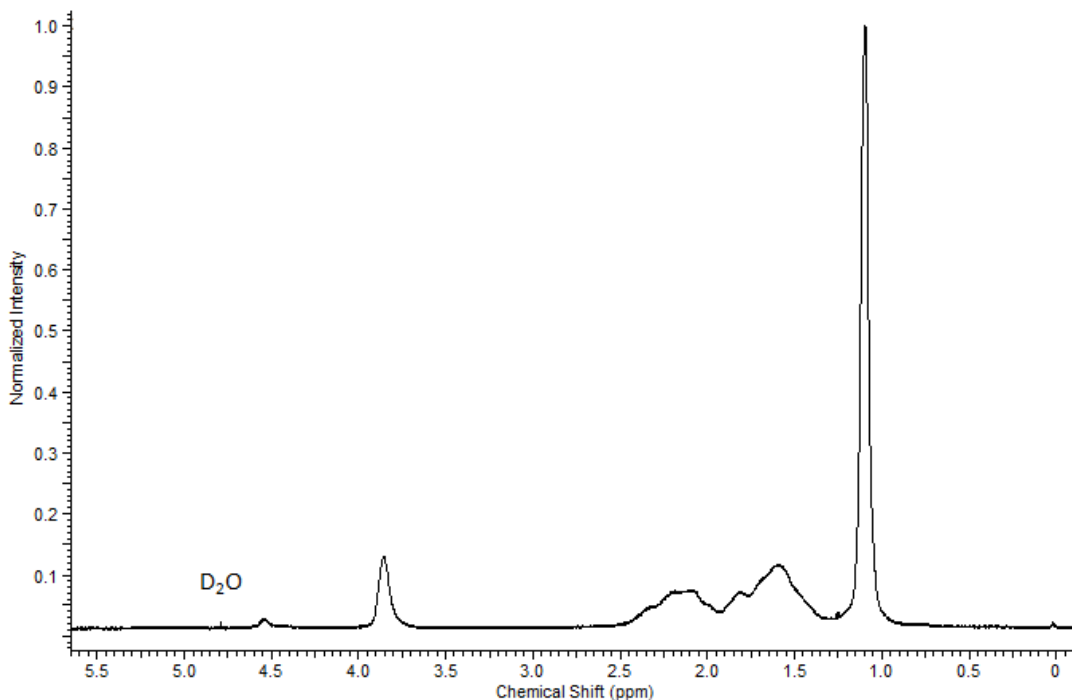
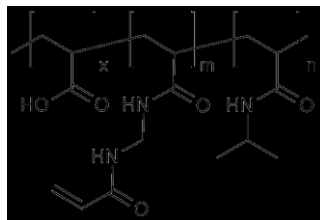


**Figure 3-1.** Nanoprobe  $^1\text{H}$  NMR spectrum of pNIPAM-co-50 % AAc in D<sub>2</sub>O at pH 10.

The nanoprobe  $^1\text{H}$  NMR spectrum of pNIPAM-co-50 % AAc in D<sub>2</sub>O at pH 10 (Figure 3-1) shows a broad singlet at 1.10 ppm, which corresponds to methyl  $^1\text{H}$ 's on the isopropyl group (NIPAM: isopropyl group), while broad multiplets between 1.30–2.50 ppm corresponds to methylene  $^1\text{H}$ 's (polymerized backbone and BIS) finally with a broad signal at 3.85 ppm which is methine  $^1\text{H}$ 's from NIPAM.

### 3.4.3 Preparation of pNIPAM-co-25 % AAc Microgel



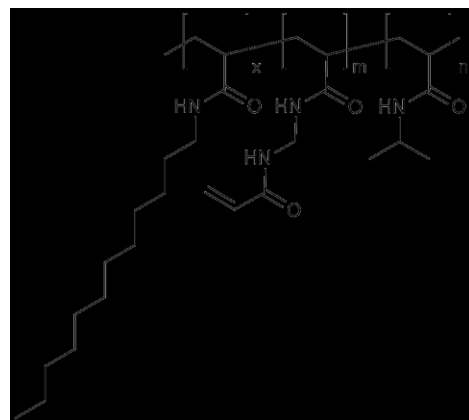
The polymerization of NIPAM (1.124 g, 9.894 mmol, 16.4 eq.), BIS (0.111 g, 0.601 mmol, 1.00 eq.) and AAc (0.239 mL, 3.48 mmol, 5.82 eq.) was initiated with APS (0.045 g, 0.199 mmol, 0.331 eq.) and allowed to stir overnight according to General Procedure 2 recovering a fibrous colourless solid (yield: 0.512 g).

## 3.5 DCC Coupled Microgels

Based on the progress made with the carbohydrate-microgels and the extensive amount of time needed to synthesize the carbohydrate-octylamides shown above, a simpler, but similar class of carbohydrates with primary octylamines were synthesized. DCC coupling was investigated as possible a method to couple the sugars to our pNIPAM-co-AAc microgels.

pNIPAM-co-AAc microgels were used to be coupled to the alkyl amines as well as carbohydrate octylamines. Based on the monomer distribution of pNIPAM-co-AAc discussed in Chapter 1, the carbohydrates and simple alkyl amines were believed to be concentrated in the core of the microgel due to the AAc moieties being concentrated in the core of the microgels according to Hoare *et al.*<sup>143</sup>

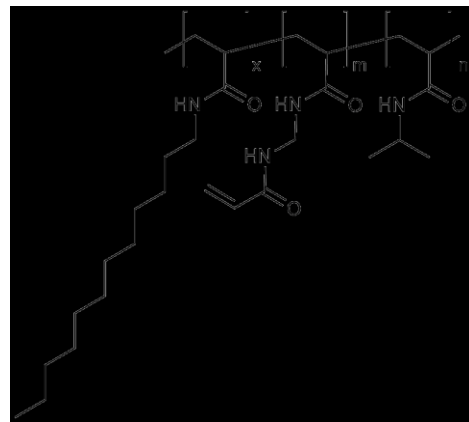
### **3.5.1 Attempted DCC/ DMAP Coupling of pNIPAM-co-10 % AAc Microgel & Dodecylamine**



pNIPAM-co-10 % AAc (0.052 g, 0.048 mmol of AAc, 1.0 eq. of AAc) was added to a 100 mL rbf along with 50 mL of MilliQ water, which was allowed to stir until a uniform colourless mixture was established. DMAP (0.106 g, 0.865 mmol, 18 eq.), DCC (0.106 g, 0.514 mmol, 11 eq.) and dodecylamine (0.157 g, 0.847 mmol, 18 eq.) were added to the flask, which were semi-soluble and allowed to stir overnight. The contents were centrifuged for 1 hour at 10,000 rpm followed by decantation and rinsing with MilliQ water and remixed by vortexing. This process was repeated six times followed by lyophilisation overnight recovering a colourless solid.

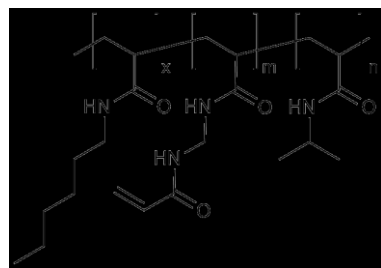
The sample was measured by DLS as described earlier, which showed a large change between pH 7 ( $639 \pm 5$  nm) and 3 ( $561 \pm 4$  nm). The large difference between pH 7 and pH 3 is suggestive that the coupling reaction was unsuccessful using this DCC/ DMAP approach since amide formation was not successful and, therefore, the AAc moiety can be protonated or deprotonated based on the pH. Overall, the changes in the particle size due to electrostatic repulsion in the particle occur at different pH's.

### 3.5.2 Preparation of DCC Coupled pNIPAM-co-10 % AAc Microgel & Dodecylamine



pNIPAM-co-10 % AAc (0.511 g, 0.455 mmol of AAc, 1.00 eq. of AAc) was added to a vial along with DCC (0.116 g, 0.564 mmol, 1.24 eq.) and dodecylamine (0.090 g, 0.49 mmol, 1.1 eq.) in chloroform according to General Procedure 3 recovering a colourless solid. The hydrodynamic radius and zeta potential at pH 3 and 7 measured (Table 3-1).

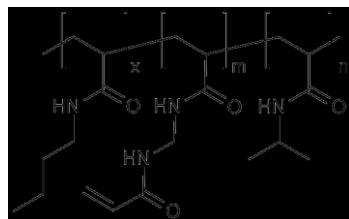
### 3.5.3 Preparation of DCC Coupled of pNIPAM-co-10 % AAc Microgel & Hexylamine



pNIPAM-co-10 % AAc (0.504 g, 0.452 mmol of AAc, 1.00 eq. of AAc) was added to a vial along with DCC (0.115 g, 0.542 mmol, 1.20 eq.) and hexylamine (0.065 mL, 0.50

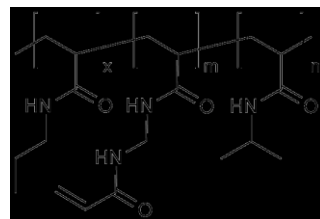
mmol, 1.1 eq.) according to General Procedure 3. A colourless solid was recovered. The hydrodynamic radius and zeta potential at pH 3 and 7 measured (Table 3-1).

### 3.5.4 Preparation of DCC Coupled of pNIPAM-co-10 % AAc Microgel & Butylamine



pNIPAM-co-10 % AAc (0.500 g, 0.449 mmol of AAc, 1.00 eq. of AAc) was added to a vial along with DCC (0.119 g, 0.577 mmol, 1.2 eq.) and butylamine (0.049 mL, 0.50 mmol, 1.1 eq.) according to General Procedure 3. A colourless solid was recovered. The hydrodynamic radius and zeta potential at pH 3 and 7 measured (Table 3-1).

### 3.5.5 Preparation of DCC Coupled of pNIPAM-co-10 % AAc Microgel & Propylamine



pNIPAM-co-10 % AAc (0.500 g, 0.449 mmol of AAc, 1.00 eq. of AAc) was added to a vial along with DCC (0.1153 g, 0.542 mmol, 1.2 eq.) and butylamine (0.0694 mL, 0.497 mmol, 1.09 eq.) according to General Procedure 3. A colourless solid was recovered. The hydrodynamic radius and zeta potential at pH 3 and 7 measured (Table 3-1).

### **3.5.6 Summary of DCC Coupling DLS & Zeta Potential Data**

As mentioned earlier unsuccessful amide formation results in the AAc ( $pK_a$  is  $\sim 4.2$ ) moiety to be protonated or deprotonated based on the pH resulting in changes in the particle size due to electrostatic repulsion in the particle. The change between particle size at pH = 3 and pH = 7 for pNIPAM-co-10 % AAc DCC coupled to dodecylamine (35 nm) is less compared to the uncoupled pNIPAM-co-10 % AAc control (71 nm) as well as the other amines ( $\sim 121$  nm) suggestive that a larger portion of the carboxylic group coupling sites have been successfully coupled to dodecylamine compared to the other aliphatic amines. The zeta potential values of the uncoupled control are weakly anionic at both pH = 3 and 7, unlike the dodecylamine coupled microgel, which is predominately neutral at both pH's and expected for a coupled microgel. Unlike dodecylamine, the other amines (hexyl-, butyl- and propylamine) DCC coupled to pNIPAM-co-10% AAc showed a small increase in negative charge from pH = 3 to pH = 7 possibly due to deprotonation of unsuccessfully coupled carboxylic groups.

**Table 3-1.** DCC coupled microgel according to General Procedure 3 hydrodynamic radius by DLS and zeta potential by zeta analyzer. The averaged values (minimum of three measurements per sample) are summarized here.

Sample	<u>Zeta Potential (mV)</u>		<u>Particle Size (nm)</u>	
	pH = 3	pH = 7	pH = 3	pH = 7
pNIPAM-co-10 % AAc*	553 ± 3	624 ± 6	-14.6 ± 0.3	-16.0 ± 0.2
pNIPAM-co-10% AAc-Dodecylamine	568 ± 5	604 ± 8	10.0 ± 0.2	0.8 ± .4
pNIPAM-co-10% AAc-Hexylamine	596 ± 7	699 ± 6	-9.2 ± 0.3	-19 ± 1
pNIPAM-co-10% AAc-Butylamine	590 ± 10	750 ± 10	-5.2 ± 0.4	-15.1 ± 0.2
pNIPAM-co-10% AAc-Propylamine	580. ± 1	680 ± 20	-7.6 ± 0.7	-16.4 ± 0.5

\*pNIPAM-co-10 % AAc control not DCC coupled to aliphatic amine

Overall, DCC coupling of large aliphatic amines shows to be a viable option for pNIPAM-co-AAc microgels; however, pNIPAM-co-10 % AAc has solubility issues, which could affect the yield and coupling success. Also, DCC coupling requires the use of the harsh chlorinated solvents, which generates more toxic waste and not ideal for the development of a sorbent for water remediation.

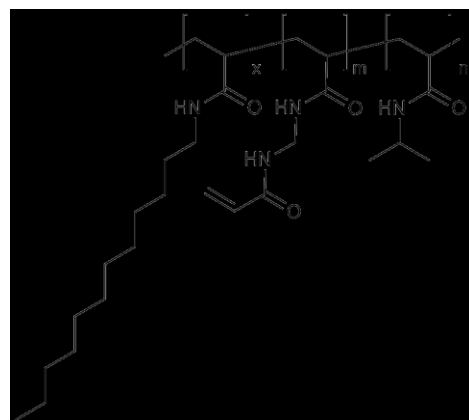
### **3.6 EDC Coupling of Microgels with Aliphatic Amines and Carbohydrate-Amines**

Based on the results and difficulties faced with DCC coupling, EDC coupling was considered as a viable alternative. As mentioned earlier, EDC coupling can be done in an

aqueous solution, which is ideal working conditions for both microgels and the synthetic carbohydrates mentioned in this dissertation.

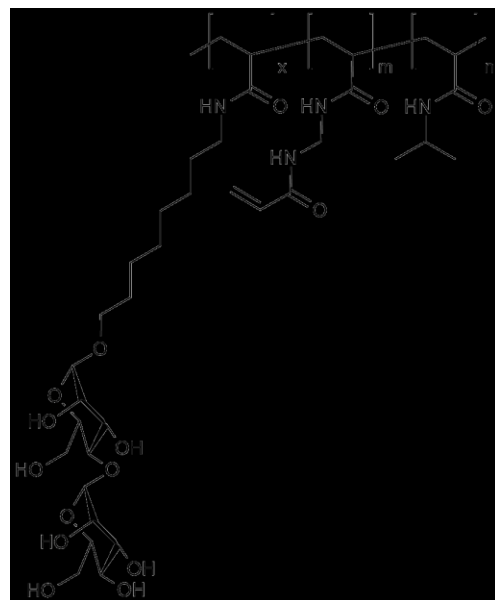
Similar to the DCC coupling experiments conducted, pNIPAM-co-AAc microgels were used in the EDC experiments with alkyl amines as well as carbohydrate octylamines and believed to be concentrated in the core of the microgel due to the AAc moieties being concentrated in the core of the microgels.<sup>143</sup>

### 3.6.1 Preparation of pNIPAM-co-50 % AAc-Dodecylamine Microgel *via* EDC Coupling



pNIPAM-co-50 % AAc (0.096 g, 5.0 mmol of AAc, 1.0 eq. of AAc) was added to a 50 mL rbf flask along with NHS (0.581 g, 5.05 mmol, 1.0 eq.), EDC (0.951 g, 4.96 mmol, 1.0 eq.) and dodecylamine (0.947 g, 0.744 mmol, 0.15 eq.) according to General Procedure D. Microgel was not characterized by nanoprobe <sup>1</sup>H NMR spectroscopy due to solubility issues, which could be due to increase hydrophobicity coming from the long aliphatic chain.

### 3.6.2 Preparation of pNIPAM-co-50 % AAc-Mann-Octylamine Microgel *via* EDC Coupling



pNIPAM-co-50 % AAc (0.029 g, 0.15 mmol of AAc, 1.0 eq. of AAc) was added to a 50 mL rbf flask along with NHS (0.031 g, 0.69 mmol, 4.6 eq.), EDC (0.142 g, 0.741 mmol, 4.9 eq.) and Mann-Octylamine (0.229 g, 0.744 mmol, 4.9 eq.) according to General Procedure 4.

### 3.6.2.1 Nanoprobe $^1\text{H}$ NMR Characterization of pNIPAM-co-50 % AAc-Mann-Octylamine Microgel

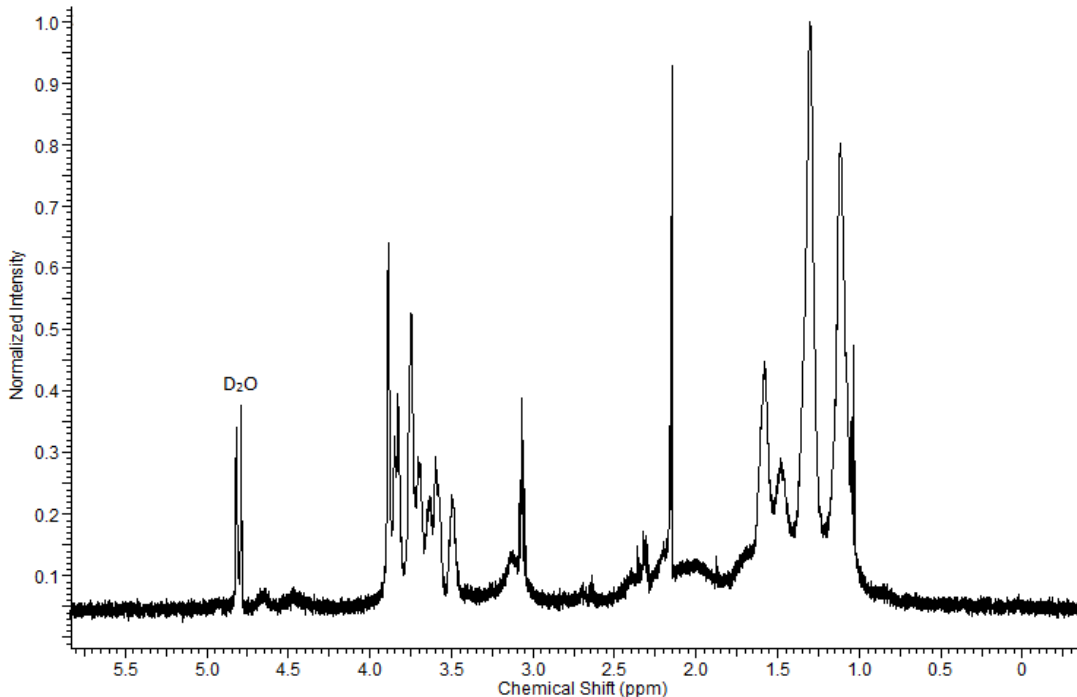


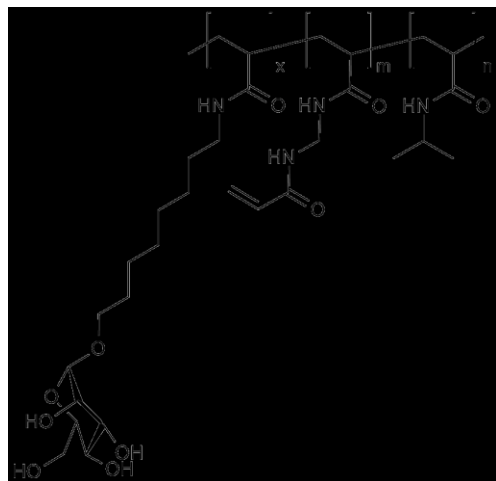
**Figure 3-2.** Nanoprobe  $^1\text{H}$  NMR spectrum of pNIPAM-co-50 % AAc-Mann-Octylamine in  $\text{D}_2\text{O}$  at pH 10.

The nanoprobe  $^1\text{H}$  NMR spectrum of pNIPAM-co-50 % AAc-mann-octylamine in  $\text{D}_2\text{O}$  at pH 10 (Figure 3-2) shows broad multiplets between 3.00–4.00 ppm, which corresponds to the methine  $^1\text{H}$ 's on the sugar ring, while the broad multiplets between 1.00–2.00 ppm corresponds to the methyl  $^1\text{H}$ 's (NIPAM: isopropyl group) and  $^1\text{H}$ 's methylene

(polymerized backbone, octylamine and BIS). A sharp broad signal at 3.04 ppm corresponds to methylene  $^1\text{H}$ 's next to the amide functional group.

The synthesis of pNIPAM-co-50 % AAc-Mann-Octylamine without EDC and/ or NHS coupling reagents was investigated to ensure the microgels synthesized *via* EDC/ NHS were only showing signals corresponding to the carbohydrate coupled to the microgel.

### 3.6.2.2 Preparation of pNIPAM-co-50 % AAc- pNIPAM-co-50 % AAc-Mann-Octylamine Microgel *via* NHS Coupling (No EDC Coupling Reagent)



pNIPAM-co-50 % AAc (0.026 g, 0.14 mmol of AAc, 1.0 eq. of AAc) was added to a 50 mL rbf flask along with NHS (0.030 g, 0.66 mmol, 4.7 eq.) and Mann-Octylamine (0.218 g, 0.678 mmol, 4.8 eq.) according to General Procedure D, except with no EDC coupling reagent.

### **3.6.2.2.1 Nanoprobe $^1\text{H}$ NMR Characterization of pNIPAM-co-50 % AAc-Mann-Octylamine Microgel *via* NHS Coupling (No EDC Coupling Reagent)**

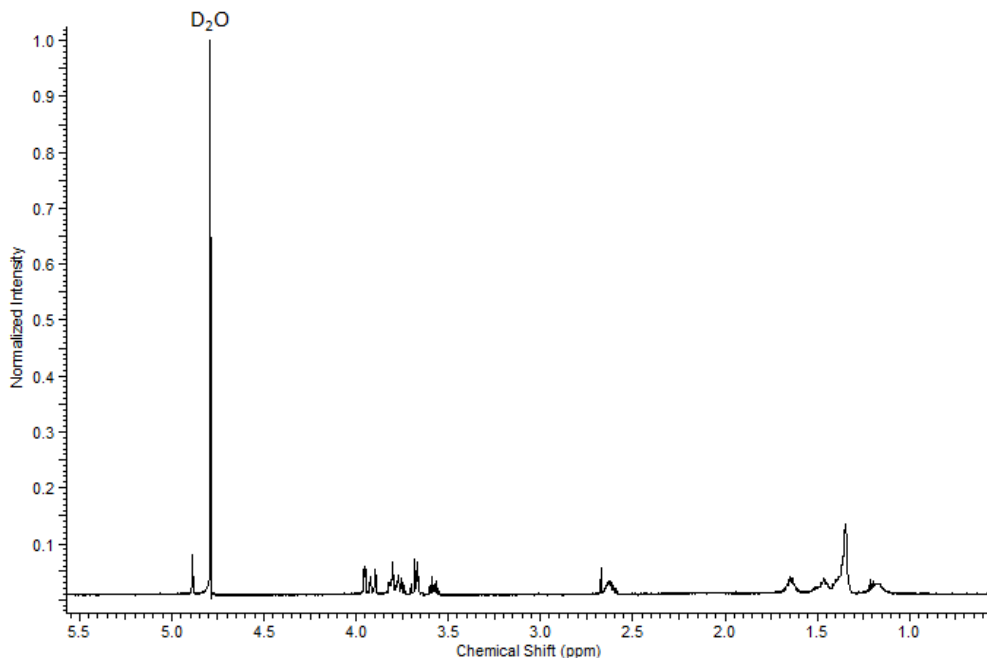
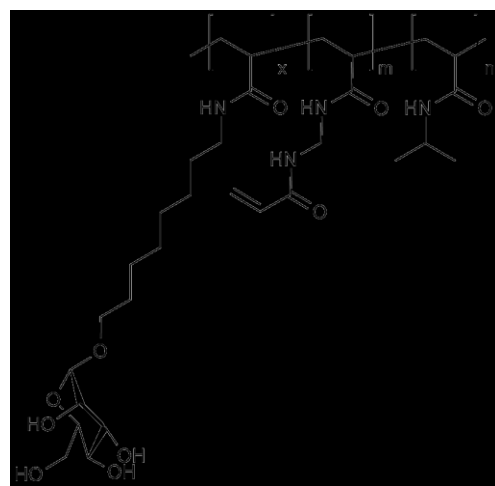


**Figure 3-3.** Nanoprobe  $^1\text{H}$  NMR spectrum of pNIPAM-co-50 % AAc-Mann-Octylamine synthesized with no EDC Coupling Reagent in  $\text{D}_2\text{O}$  at pH 10.

The nanoprobe  $^1\text{H}$  NMR spectrum of pNIPAM-co-50 % AAc- mann-octylamine in  $\text{D}_2\text{O}$  at pH 10 (Figure 3-3) small broad signals between 3.00–4.00 ppm, which corresponds to the methine 1H's on the sugar ring, while the broad multiplets between 1.00–2.00 ppm corresponds to the methyl 1H's (NIPAM: isopropyl group) and 1H's methylene (polymerized backbone, octylamine and BIS). Overall, the spectrum is in low concentration; therefore, the signals are smaller compared to previous spectra.

Based on the  $^1\text{H}$  NMR spectrum above, the synthesis of pNIPAM-co-50 % AAC-mann-octylamine is still able to generate the carbohydrate-modified microgel without the EDC coupling reagent, which is due to NHS facilitating the coupling reaction.

### **3.6.2.3 Preparation of pNIPAM-co-50 % AAc- pNIPAM-co-50 % AAc-Mann-Octylamine Microgel with no NHS or EDC Coupling Reagent**



pNIPAM-co-50 % AAc (0.029 g, 0.13 mmol of AAc, 1.0 eq. of AAc) was added to a 50 mL rbf flask along with Mann-Octylamine (0.286 g, 0.890 mmol, 6.8 eq.) according to General Procedure D, except with no EDC or NHS coupling reagent.

### **3.6.2.3.1 Nanoprobe $^1\text{H}$ NMR Characterization of pNIPAM-co-50 % AAc-Mann-Octylamine Microgel with no NHS or EDC Coupling Reagent**

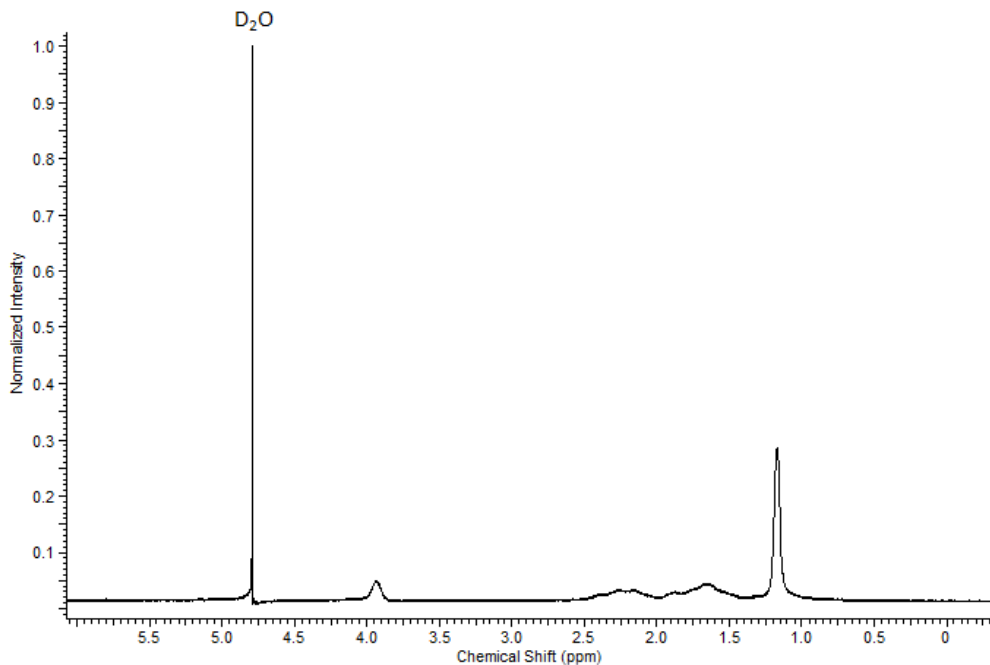


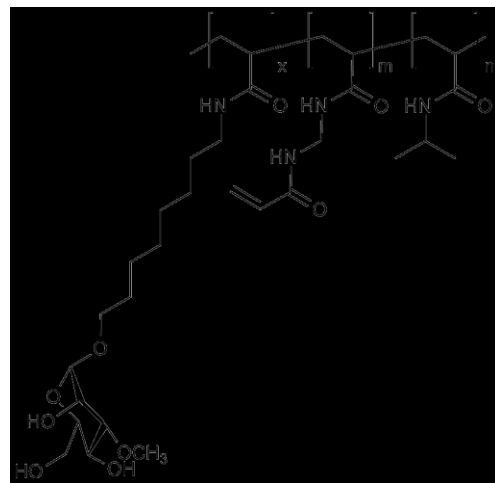
**Figure 3-4.** Nanoprobe  $^1\text{H}$  NMR spectrum of pNIPAM-co-50 % AAc-Mann-Octylamine synthesized with no EDC or NHS Coupling Reagent in D<sub>2</sub>O at pH 10.

The nanoprobe  $^1\text{H}$  NMR spectrum of pNIPAM-co-50 % AAc- mann-octylamine in D<sub>2</sub>O at pH 10 (Figure 3-4) has broad multiplets between 1.00–2.50 ppm corresponds to the methyl  $^1\text{H}$ 's (NIPAM: isopropyl group) and  $^1\text{H}$ 's methylene (polymerized backbone, octylamine and BIS) and finally with a broad signal at 3.9 ppm which is methine  $^1\text{H}$ 's from NIPAM.

Overall, the spectrum is similar to pNIPAM-co-50 % AAc suggestive without both EDC and NHS coupling reagents the carbohydrate-modified cannot be successfully synthesized. Also, uncoupled carbohydrate octylamine used in these experiments are being

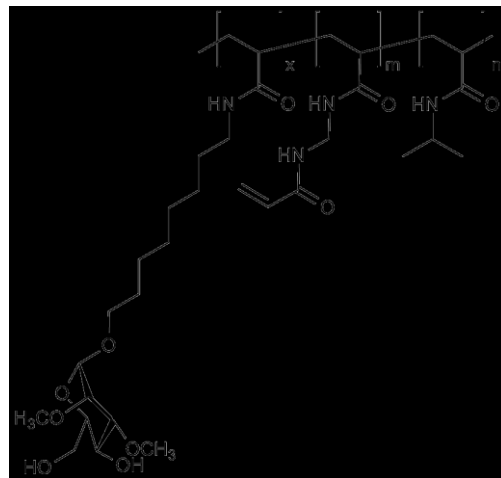
successfully removed from being washed with MilliQ water ( $10\text{ mL} \times 6$ ) and centrifuged at 10,000 rpm between each wash.

### 3.6.3 Preparation of pNIPAM-co-50 % AAc-Mann-3OMe-Octylamine Microgel *via* EDC Coupling



pNIPAM-co-50 % AAc (0.026 g, 0.14 mmol of AAc, 1.0 eq. of AAc) was added to a 50 mL rbf flask along with NHS (0.035 g, 0.78 mmol, 5.5 eq.), EDC (0.143 g, 0.745 mmol, 5.3 eq.) and mann-3OMe-octylamine (0.109 g, 0.339 mmol, 2.4 eq.) according to General Procedure 4. Yield was  $\leq 0.010\text{ g}$  due to solubility issues and was not characterized with  $^1\text{H}$  NMR spectroscopy.

**3.6.4 Preparation and Characterization of pNIPAM-co-50 % AAc-Mann-2,3OMe-Octylamine Microgel *via* EDC Coupling**



pNIPAM-co-50 % AAc (0.026 g, 0.14 mmol of AAc, 1.0 eq. of AAc) was added to a 50 mL rbf flask along with NHS (0.031 g, 0.70 mmol, 5.0 eq.), EDC (0.130 g, 0.676 mmol, 4.8 eq.) and mann-2,3O-octylamine (0.227 g, 0.678 mmol, 4.8 eq.) according to General Procedure 4 (yield: 0.041 g).

### 3.6.4.1 Nanoprobe $^1\text{H}$ NMR Characterization of pNIPAM-co-50 % AAc-Mann-2,3OMe-Octylamine Microgel

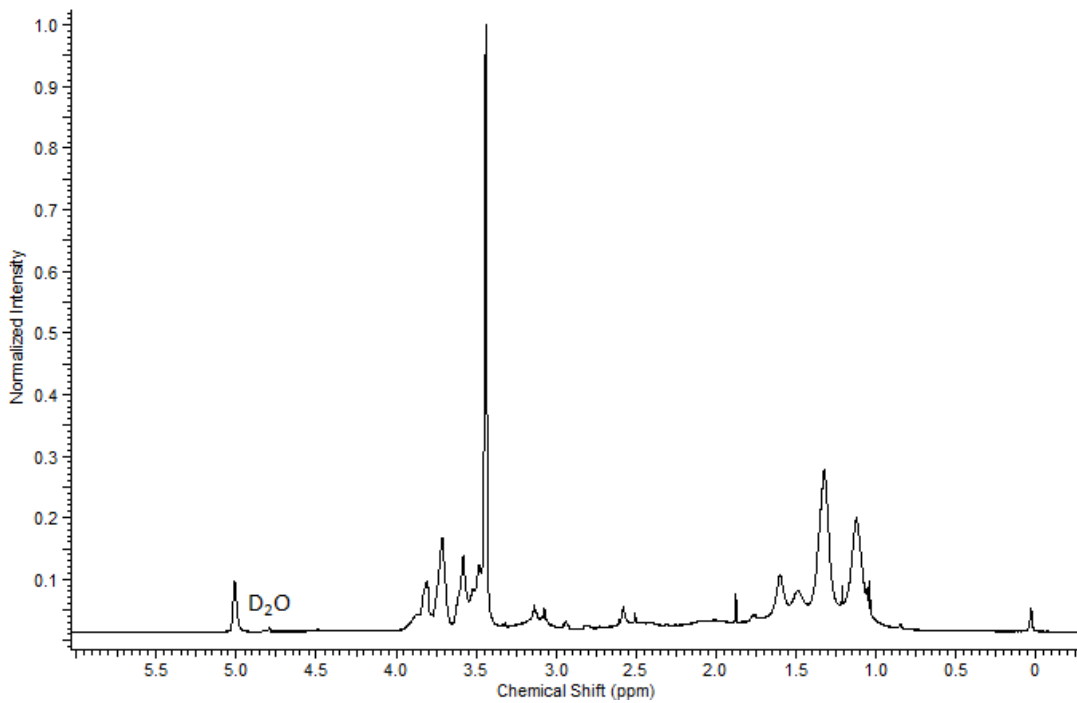
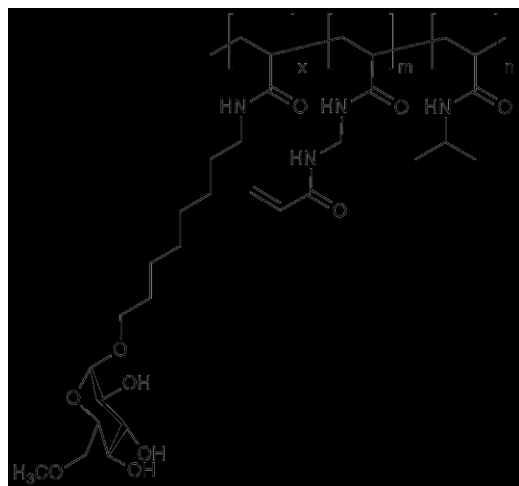


**Figure 3-5.** Nanoprobe  $^1\text{H}$  NMR spectrum of pNIPAM-co-50 % AAc-mann-2,3OMe-octylamine in  $\text{D}_2\text{O}$  at pH 10.

The  $^1\text{H}$  NMR spectrum of pNIPAM-co-50 % AAc-mann-2,3OMe-octylamine in  $\text{D}_2\text{O}$  at pH 10 (Figure 3-5) shows broad multiplets between 3.00–4.00 ppm, which corresponds to methine  $^1\text{H}$ 's on the sugar ring, while the broad multiplets between 1.00–2.00 ppm corresponds to the methyl  $^1\text{H}$ 's (NIPAM: isopropyl group) and methylene  $^1\text{H}$ 's (polymerized backbone, octylamine and BIS). A sharp broad signal at 3.41 ppm corresponds to methyl  $^1\text{H}$ 's at the 2 and 3 position on the sugar ring.

### **3.6.5 Preparation of pNIPAM-co-50 % AAc-Glu-6OMe-Octylamine Microgel via EDC Coupling**



pNIPAM-co-50 % AAc (0.050 g, 0.25 mmol of AAc, 1.0 eq. of AAc) was added to a 50 mL rbf flask along with NHS (0.054 g, 1.2 mmol, 4.7 eq.), EDC (0.246 g, 1.28 mmol, 5.1 eq.) and glu-6OMe-octylamine (0.227 g, 0.678 mmol, 4.8 eq.) according to General Procedure 4 producing a colourless fibrous solid (yield: 0.042 g).

### 3.6.5.1 Nanoprobe $^1\text{H}$ NMR Characterization of pNIPAM-co-50 % AAc-Glu-6OMe-Octylamine Microgel

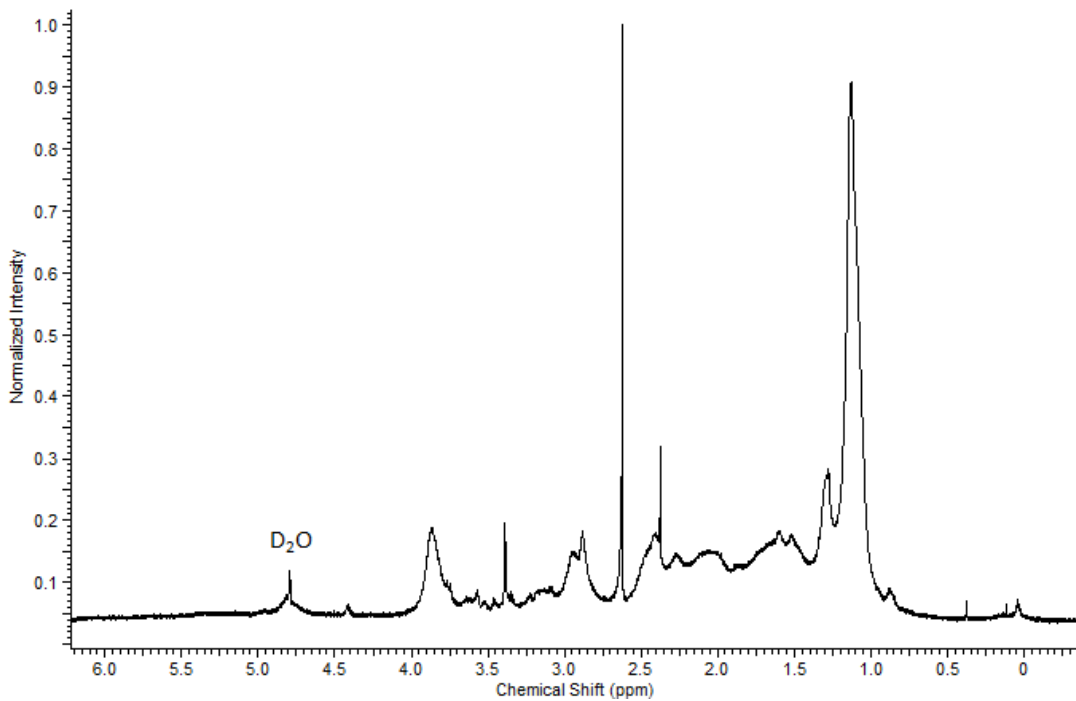
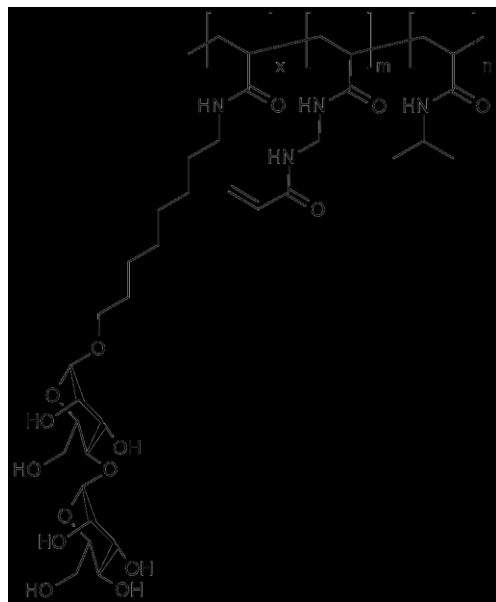


**Figure 3-6.** Nanoprobe  $^1\text{H}$  NMR spectrum of pNIPAM-co-50 % AAc-Glu-6OMe-Octylamine in D<sub>2</sub>O at pH 10.

The  $^1\text{H}$  NMR spectrum of pNIPAM-co-50 % AAc-glu-6OMe-octylamine in D<sub>2</sub>O at pH 10 (Figure 3-6) shows a range of indiscernible broad multiplets 1.00–4.00 ppm. Broad multiplet between 3.00–4.00 ppm are weak compared to previous spectra, which corresponds to  $^1\text{H}$ 's on the sugar ring are, while the broad multiplets between 1.00–2.00 ppm corresponds to the methyl (NIPAM: isopropyl group), methylene (polymerized backbone, octylamine and BIS) present on the octylamine methyl finally with a broad signal at 2.70–3.20 ppm which is the methyl  $^1\text{H}$ 's at position 6 on the sugar ring.

### 3.6.6 Preparation of pNIPAM-co-50 % AAc-Di-Mann-Octylamine Microgel *via* EDC Coupling



pNIPAM-co-50 % AAc (0.0503 g, 0.2519 mmol of AAc, 1 eq. of AAc) was added to a 50 mL rbf flask along with NHS (0.0311 g, 0.689 mmol, 2.7 eq.), EDC (0.1367 g, 0.713 mmol, 2.8 eq.) and glu-6OMe-octylamine (0.0968 g, 0.2062 mmol, 0.818 eq.) according to General Procedure F (yield: 0.0456 g).

### 3.6.6.1 Nanoprobe $^1\text{H}$ NMR of pNIPAM-co-50 % AAc-Di-Mann-Octylamine Microgel Characterization

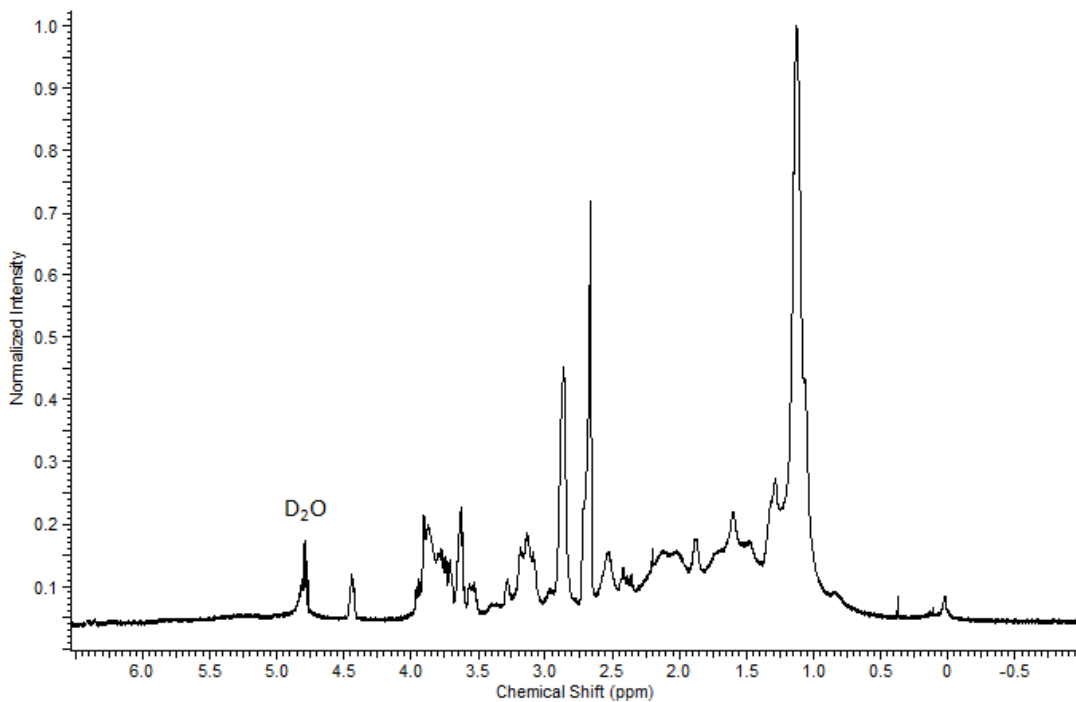


**Figure 3-7.** Nanoprobe  $^1\text{H}$  NMR spectrum of pNIPAM-co-50 % AAc-Di-Mann-Octylamine in D<sub>2</sub>O at pH 10.

The  $^1\text{H}$  NMR spectrum of pNIPAM-co-50 % AAc-glu-6OMe-octylamine in D<sub>2</sub>O at pH 10 (Figure 3-6) shows a range of broad multiplets between 1.00–4.00 ppm. Broad multiplet between 3.00–4.00 ppm corresponds to  $^1\text{H}$ 's on the sugar rings, while the broad multiplets between 1.00–2.00 ppm corresponds to the methyl  $^1\text{H}$ 's (NIPAM: isopropyl group) and methylene  $^1\text{H}$ 's (polymerized backbone, octylamine and BIS) present on the octylamine.

### **3.6.7 Summary**

The polymerization of pNIPAM cross-linked with long-chained carbohydrates is a plausible option to synthesize carbohydrate-microgels; however, long-chained carbohydrate monomers are expensive and time-consuming to synthesize. The modification of pNIPAM-co-AAc microgels *via* EDC or DCC coupling is a viable method to tune the microgel's properties. In particular, EDC/ NHS coupling of carbohydrate(s)-octylamines to pNIPAM-co-AAc microgels is a much better option compared to the direct polymerization based on cost, time and the qualitative characterization with nanoprobe  $^1\text{H}$  NMR spectroscopy. Also, the absence of the EDC coupling reagent in the EDC/ NHS coupling reactions still generates the carbohydrate-modified microgels; however, in the absence of both NHS and EDC coupling reagents the desired carbohydrate-modified microgel is not synthesized and excess carbohydrate is removed during the washes.

# **Chapter 4 - Remediation Performance**

## **4.1 Introduction**

The purpose of this chapter is to discuss the performance of the carbohydrate-modified microgels treating tailings pond water. Waste water was acquired from the Canada's Oil Sands Innovation Alliance, which was tailings pond water from the recyclable water layer and the mature fine tailings layer. The performance of the carbohydrate-modified microgels ability to treat tailings pond water was monitored by Microtox bioassay to monitor the change in the overall toxicity. In conjunction with Microtox bioassay, FT-IR was used to monitor the total amount of acid extractable organic acids before and after treatment with the carbohydrate microgels.

## **4.2 Materials & Methods**

The tailings waste water: recyclable water and medium fine tailings water was provided by Canada's Oil Sands Innovation Alliance (COSIA, Calgary, AB) from Canadian tailings ponds. Powdered activated carbon was purchased from Caledon Laboratories Ltd. (Georgetown, ON). Modern Water Microtox solutions including Microtox® acute toxicity test reagent (*Vibrio fischeri*), Modern Water Microtox® Reconstitution Solution, Modern Water Microtox Diluent as well as the disposable borosilicate cuvettes were purchased from Osprey Scientific Inc. (Edmonton, AB). Dicholormethane was purchased from Sigma Aldrich (Oakville, ON) and was dried using Grubbs-type solvent purification system<sup>160</sup>

manufactured by Innovative Technology, Inc. Deionized water with a resistivity of 18.2 MΩ·cm was obtained from a Milli-Q Plus system (located in the Biological Laboratory in the Department of Chemistry, University of Alberta) purchased from Millipore (Billerica, MA), and filtered through a 0.2 m filter prior to use.

#### **4.2.1 Microtox Bioassay**

Toxicity tests were performed by using a Modern Water Microtox® Model 500 (M500) Toxicity Analyzer. The instrument includes a temperature-controlled incubator block that has 30 incubator wells, read well and a pre-cooling well. Vials used were disposable borosilicate cuvettes (3-mL capacity, 50 mm length × 12 mm diameter, flat bottom). The incubator wells and read well were both at  $15 \pm 0.5$  °C, while the pre-cooling well was held at  $5.5 \pm 1$  °C to maintain the luminescent bacteria during the assays. A digital display indicates the light levels of the measured samples exposed to the luminescent bacteria. The luminescent bacteria used was *Vibrio fischeri*, which was obtained a freeze dried reagent (Microtox® acute toxicity test reagent). The reagent was stored at  $\sim -20\text{--}25$  °C (freezer) and reconstituted before each analysis by the addition of 1 mL of Modern Water Microtox® Reconstitution Solution (purchased non-toxic solution of 0.01 % NaCl in ultrapure water). Samples were prepared according to the Microtox® Basic Test, which is used to measure the toxicity (inhibition concentrations) in influent streams and in-plant process streams. Solutions used to prepare samples include: Modern Water Microtox Diluent (2 % NaCl provide osmotic protection for the marine luminescent bacteria) and Modern Water Microtox Osmotic Adjusting Solution (OSA, 22% NaCl solution in purified water, used to osmotically adjust samples to 2% NaCl).

#### **4.2.2 Fourier-Transform Infrared Spectroscopy**

The method used for sample analysis by FT-IR was originally developed by Jivraj *et al.*<sup>161</sup> at the Syncrude Canada Ltd. Research Department and adopted by Scott *et al.*<sup>79</sup> The instrument used for Fourier-transform infrared spectroscopy quantification NAs was a Thermo Nicolet Magna 760 FT-IR (located in Analytical and Instrumentation Laboratory in the Department of Chemistry, University of Alberta) operated in transmission mode and Omnic Software (version 7.1) was used to acquire and process spectra. The baseline used for peak height measurements was  $\sim 1800\text{--}1900\text{ cm}^{-1}$  and the absorbances at 1743 and  $1705\text{ cm}^{-1}$  were summed for each spectrum. Each spectrum was acquired with 64 co-added scans. The solvent used was dry DCM and the background solvent was acquired using 64 scans and used for all spectra. The spectral resolution was  $4\text{ cm}^{-1}$  and the spectral range was  $4000\text{--}400\text{ cm}^{-1}$ . The liquid cell had a pathlength of 3.0 mm and used polished KCl transmission windows purchased from International Crystal Laboratories (Garfield, NJ). The bench was purged continuously with dry  $\text{N}_2$ .

The concentration of NAs in samples was quantified by a calibration plot, which was developed by preparing a standard stock solution ( $1000\text{ mg NAs kg DCM}^{-1}$ ) by dissolving Aldrich naphthenic acids (0.200 g) in DCM (200.5 g). Aldrich naphthenic acids were purchased from Sigma-Aldrich (Oakville, Ontario) and used as received. Aliquots of the stock solution were taken and diluted accordingly to prepare a series of calibration standards ( $1\text{--}175\text{ mg NAs kg DCM}^{-1}$ ), which were analyzed in a similar manner described above. The sum of the peak heights were graphed versus the naphthenic acids concentrations in the standards.

Treated waste water samples were prepared by first filtering (0.45 µm) then adjusting the pH of the samples to pH 2 with HCl followed by the addition of 0.15 g of NaCl (0.15 g per 1 ml of sample) to prevent an emulsion forming during extraction. The NAs were extracted with dry-DCM (15 mL) in a 30 mL separatory funnel, which transfers all the NAs and hydrocarbons to the non-polar phase (DCM layer). The DCM layer was recovered and this process was repeated two more times. The NAs were separated from the other hydrocarbons with 15 mL of a Na<sub>2</sub>CO<sub>3</sub> stock solution (4% w v<sup>-1</sup> Na<sub>2</sub>CO<sub>3</sub> adjusted to pH 11.6 with NaOH) in a 30 mL separatory funnel. The alkaline layer was collected and this process was repeated two more times. The collected alkaline extraction was acidified with HCl to pH 2 to separate the naphthenic acids (or free carboxylics), extracted with DCM in triplicates as described earlier. The DCM extract was allowed to evaporate overnight followed by reconstitution with dry DCM (~ 5 mL) and analysis.

#### **4.2.3 General Procedures**

##### **4.2.3.1 General Procedure 5: Waste Water Preparation**

A 45 mL sample of waste water (medium fine tailings or recyclable water) was collected with a 50 mL syringe and transferred to a 50 mL centrifuged tube. The sample was centrifuged at 10,000 RPM for 1 hour.

##### **4.2.3.2 General Procedure 6: Waste Water Treatment**

Prepared microgel (~ 0.0260 g) was added to a 10 mL centrifuge tube along with waste water (5–10 mL, see: General Procedure 5), which was shaken at moderate speed for ~

24 hours. After shaking, the mixture was centrifuged at 10,000 RPM for 1 hour and the aqueous liquid was removed.

## **4.3 Microtox Bioassay Toxicity Tests**

### **4.3.1 Microtox Data of Tailings Pond Water: MFT & Recyclable Water**

Two types of tailings pond water (provided by COSIA) used to in this dissertation, which included recyclable tailings water (top layer) and mature fine tailings water (Figure 4-1) stored in containers. The large tailings pond water samples were stirred vigorously to ensure homogeneity followed by 45 mL aliquots recovered and centrifuged at 10,000 RPM for 1 hour. The toxicity of both types of tailings was assessed by Microtox bioassay which showed that the recyclable tailings pond water (Figure 4-1) was significantly less toxic, compared to the MFT water (Figure 4-2). Overall, this is suggestive that the components primarily responsible for the acute toxicity (believed to be NAs) exists in higher concentration in the MFT layer compared to the recyclable top water layer in the tailings pond.

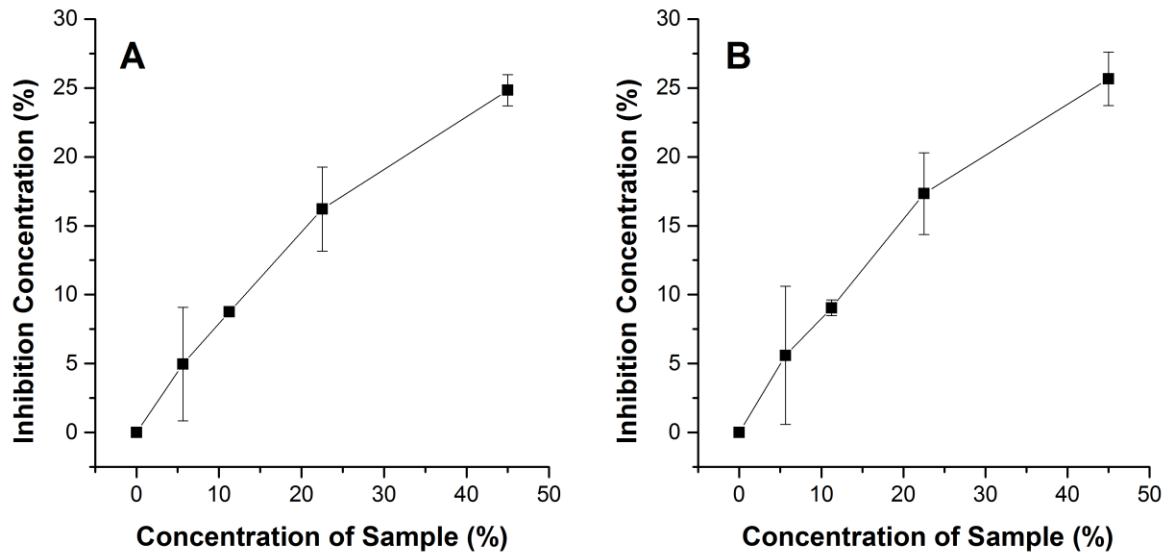


**Figure 4-1.** Microtox toxicity results of recyclable TPW ( $n = 2$ ) after 5 minutes of exposure (A) and 15 minutes of exposure (B), pH  $\sim 8.2$ .

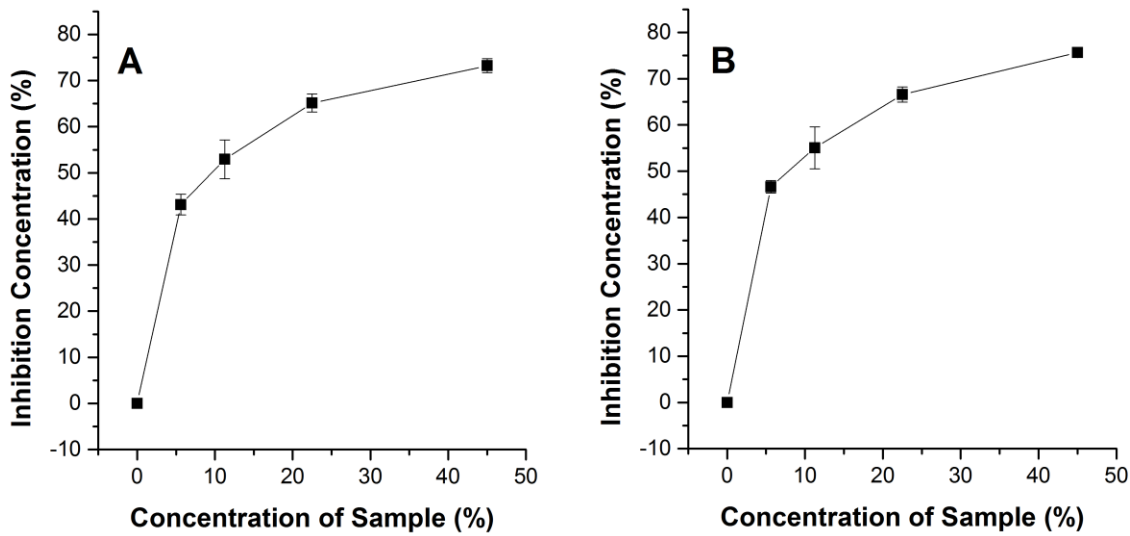


**Figure 4-2.** Microtox toxicity results of MFT ( $n = 3$ ) after 5 minutes of exposure (A) and 15 minutes of exposure (B), pH  $\sim 8$ .

Due to the large disparity between the MFT and recyclable water samples, MFT was primarily used in this dissertation as it is believed to have a higher concentration of NAs based on the overall toxicity. However, untreated MFT samples prepared for Microtox bioassay toxicity tests according to General Procedure E showed a decrease in overall toxicity (Figure 4-3) compared to the direct analysis of the untreated MFT as described earlier (Figure 4-2). A 45 % concentrated sample of untreated MFT shaken and further centrifuged after 5 minutes and 15 minutes of exposure had an IC of  $50 \pm 10\%$  and  $50 \pm 10\%$  respectively, while untreated MFT had an IC of  $73 \pm 1\%$  and  $76 \pm 1\%$  respectively. It is possible that further centrifugation results in residual bitumen in the water sample extracted dissolved toxic contaminants, and in particular, NAs.

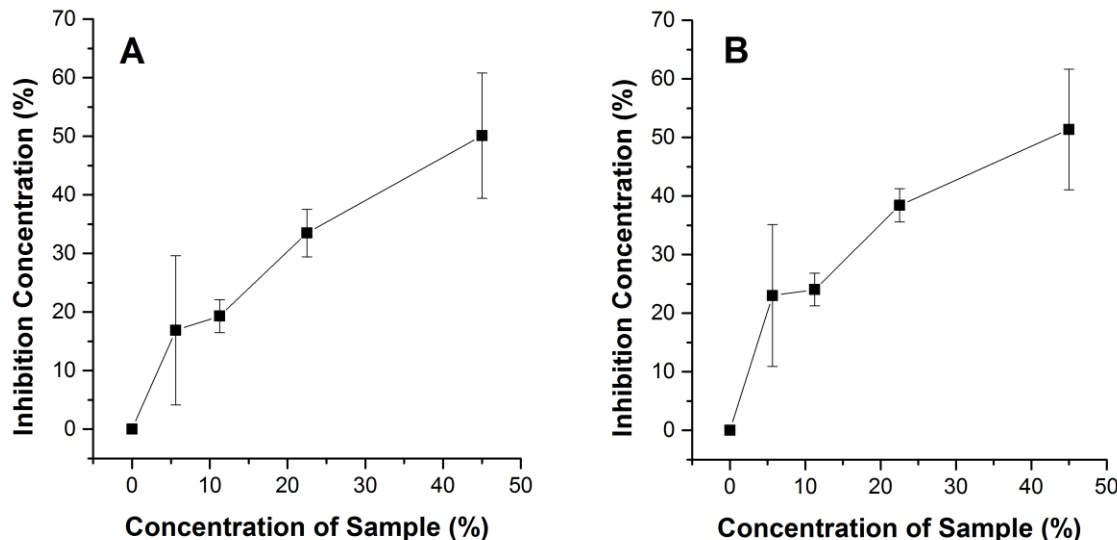


**Figure 4-3.** Microtox toxicity results of MFT shaken ( $n = 3$ ) for 24 hours and centrifuged after 5 minutes of exposure (A) and 15 minutes of exposure (B), pH  $\sim 8$

#### 4.3.2 Microtox Data of Powdered Activated Carbon Treated MFT

As mentioned earlier activated carbon is currently being used in numerous water treatment plants; therefore, powdered activated carbon (PAC) was used as the benchmark for TPW remediation in this dissertation. Roughly 5 mL samples of the MFT water was treated with  $\sim 0.0260$  g of powdered activated carbon according to General Procedure E and was monitored by Microtox bioassays (Figure 4-4).

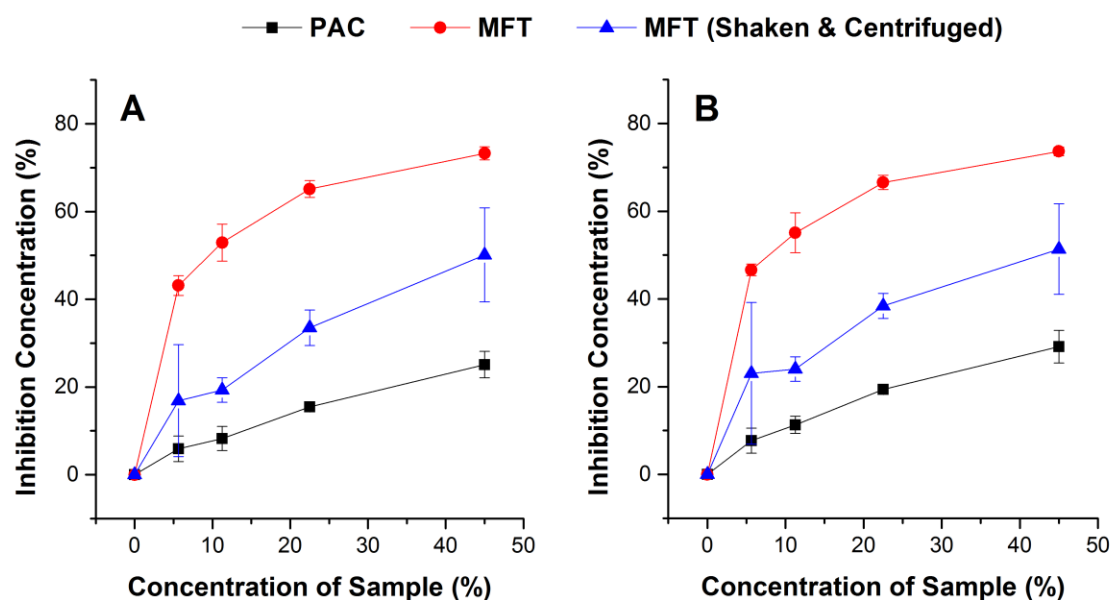
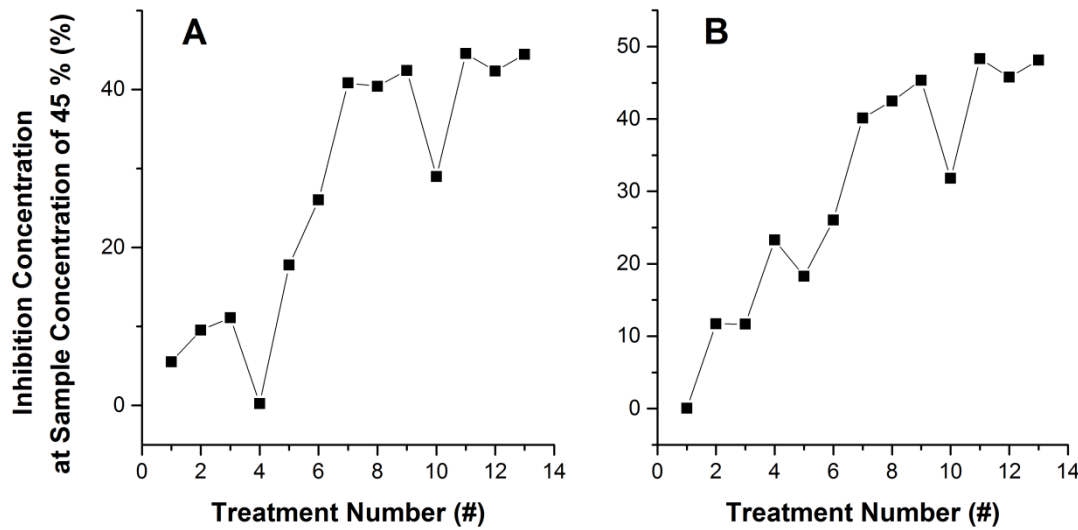


**Figure 4-4.** Microtox toxicity results of PAC treated MFT ( $n = 3$ ) compared to untreated MFT ( $n = 3$ ) and MFT further centrifuged and shaken ( $n = 3$ ) after 5 minutes of exposure (A) and 15 minutes of exposure (B), pH 8.

A 45 % concentrated sample of PAC treated MFT after 5 minutes and 15 minutes exposure showed a large decrease in toxicity with an IC of  $25 \pm 3\%$  and  $29 \pm 4\%$  respectively compared to untreated MFT with an IC of  $73 \pm 1\%$  and  $76 \pm 1\%$  respectively.

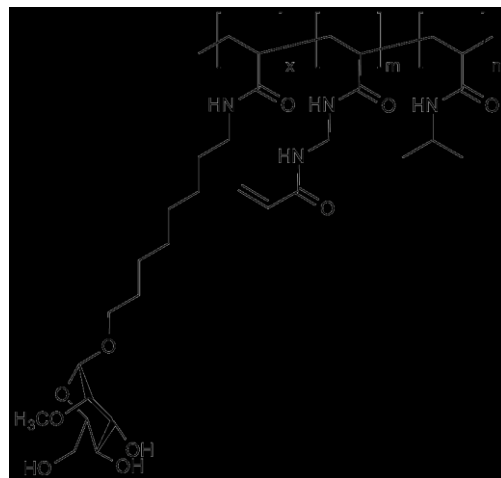
#### 4.3.3 Powdered Activated Carbon Reusability for MFT Treatment

The resuability of PAC was investigated by treating a 10 mL sample of MFT with 0.0255 g of PAC according to General Procedure E. This treatment process was repeated 17 times with the same sample of PAC and measured by Microtox bioassay between each reuse, which shows after approximately the 7th treatment PAC no longer functions optimally. In Figure 4-5 the inhibition concentration at a sample concentration of 45 % for reusability after 12 treatments is shown.



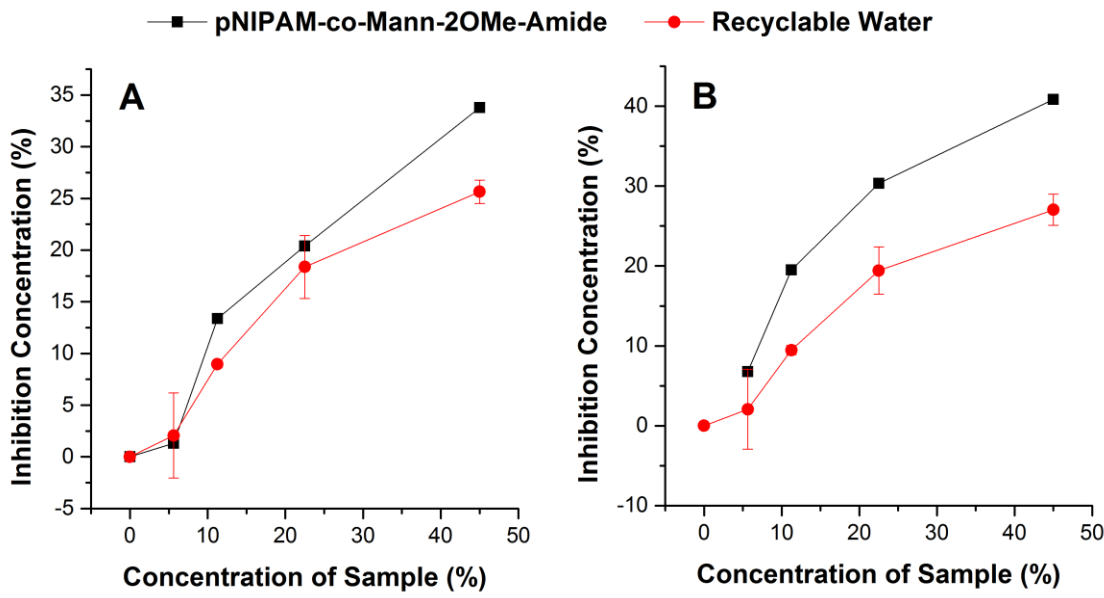
**Figure 4-5.** Microtox toxicity results of the reusability of PAC treated MFT at a sample concentration of 45 % ( $n = 1$ ). MFT toxicity after 14 treatments is shown at 5 minutes (A) and 15 minutes (B) exposure at pH 8.

#### **4.3.4 Microtox Data of pNIPAM-co-Mann-2OMe-Amide Microgel Treated Recyclable Water**



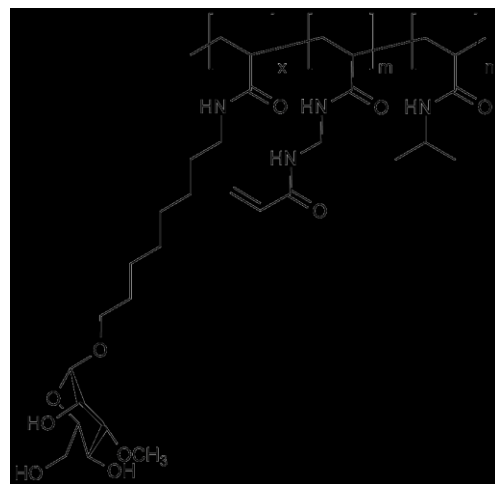
pNIPAM-co-Mann-2OMe-Amide (0.0256 g) treated 10 mL of recyclable water according to General Procedure 6. The toxicity of both the treated water and untreated waste water was analyzed by Microtox bioassay basic test (

Figure 4-6). Based on the Microtox data shown in Figure 4-6 the waste water treated with the carbohydrate-microgel showed an increase in toxicity compared to the untreated waste water. This increase in toxicity could be due to residual NIPAM present after cleaning the carbohydrate-microgel, which is known to be toxic.



**Figure 4-6.** Microtox toxicity results of pNIPAM-co-Mann-2O-Me-Amide Microgel treated recyclable water and untreated recyclable water ( $n = 3$ ) after 5 minutes (A) and 15 minutes (B) of exposure. pH was unmeasured and unaltered.

#### 4.3.5 Microtox Data of pNIPAM-co-Mann-3OMe-Amide Microgel Treated Recyclable Water



pNIPAM-co-Mann-3OMe-Amide (0.0270 g) treated 10 mL of waste water (old) according to General Procedure E. The toxicity of both the treated water and untreated waste water was analyzed by Microtox bioassay (Figure 4-7). Based on the Microtox data shown in the waste water treated with the carbohydrate-microgel shows an increase in toxicity compared to the untreated waste water. Similar to toxicity results of pNIPAM-co-Mann-2OMe-Amide treated waste water this increase in toxicity could be due to residual NIPAM present after cleaning the carbohydrate-microgel, which is known to be toxic.

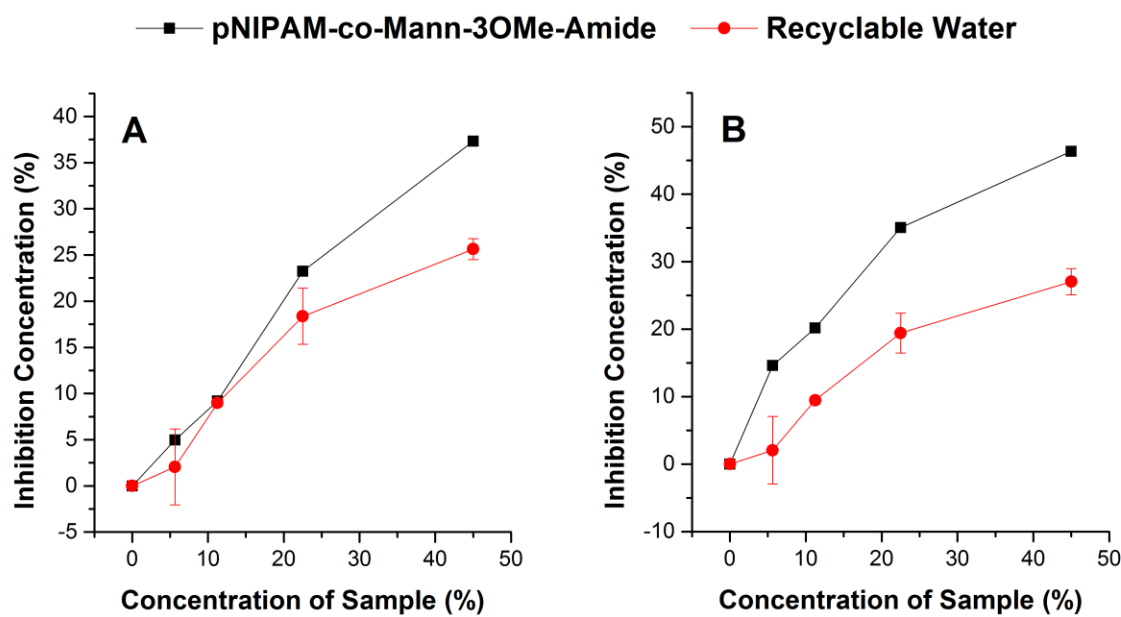
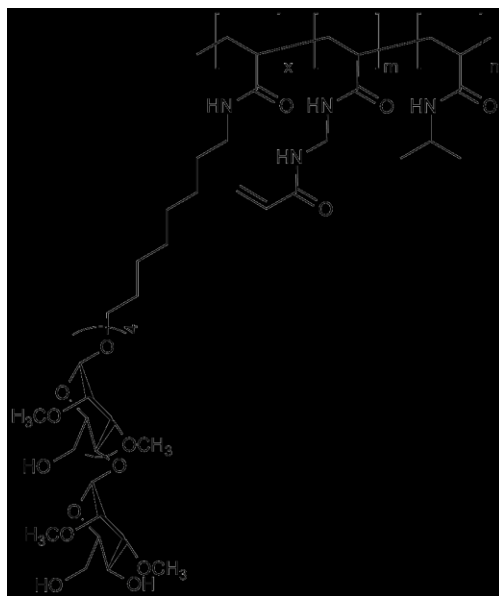


**Figure 4-7.** Microtox toxicity results of pNIPAM-co-Mann-3OMe-Amide Microgel treated recyclable water and untreated recyclable water after 5 minutes (A) and 15 minutes (B) of exposure. pH was unmeasured and unaltered.

#### 4.3.6 Microtox Data of pNIPAM-co-Penta-Mann-2,3OMe-Amide Microgel Treated Recyclable Water



pNIPAM-co-Penta-Mann-2,3OMe-Amide (0.0250 g) treated 10 mL of recyclable water according to General Procedure E. The toxicity of both the treated water and untreated waste water was analyzed by Microtox bioassay (Figure 1-1). Based on the Microtox data the waste water treated with the carbohydrate-microgel showed a decrease in overall toxicity compared to the untreated waste water.

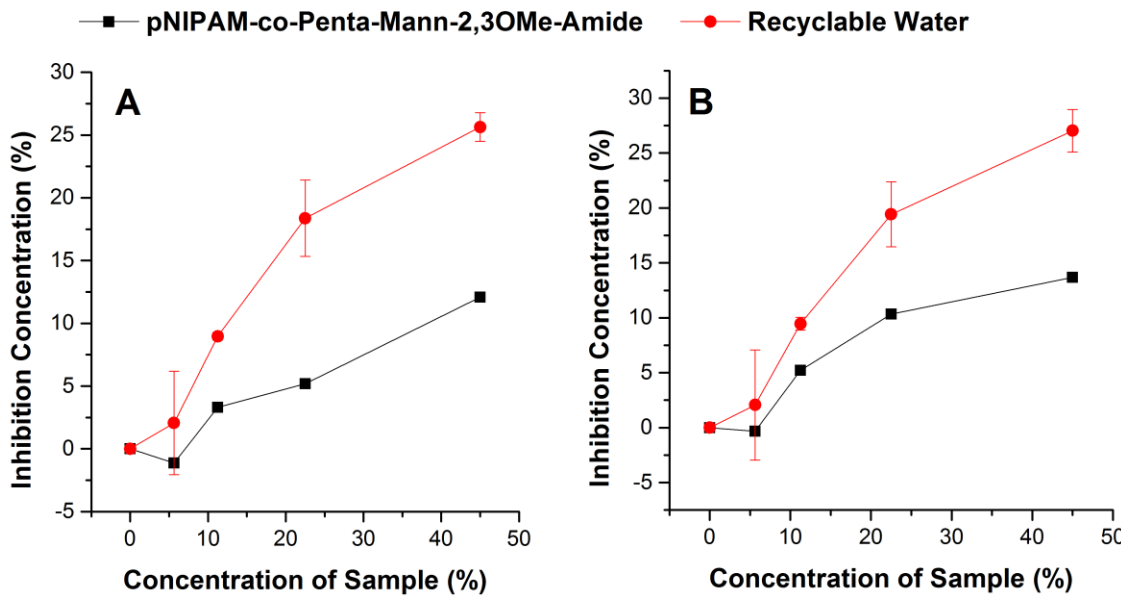


**Figure 4-8.** Microtox toxicity results of pNIPAM-co-Penta-Mann-2,3OMe-Amide Microgel treated recyclable water and untreated recyclable water ( $n = 3$ ) after 5 minutes (A) and 15 minutes (B) of exposure. pH was unmeasured and unaltered.

The benefit of using an oligosaccharide is clearly shown in Figure 4-8 by reducing the overall toxicity of the recyclable water suggestive it may be mimicking the PMPs ability to form stable complexes with bulky organics. However, the synthesis of the penta-mann-2,3OMe-amide is in low yield (~ 0.0400 g) and time intensive (~ 4 months).

pNIPAM-co-Penta-Mann-2,3OMe-Amide (0.0250 g) treated 10 mL of MFT according to General Procedure E. The toxicity of both the treated and untreated MFT was analyzed by Microtox bioassay (Figure 4-9). Based on the Microtox data, the treated MFT with the penta-mann-2,3OMe-amide-modified microgel showed a minor decrease in overall toxicity compared to the untreated MFT and MFT further processed (shaken and centrifuged). Compared to pNIPAM-co-penta-mann-2,3OMe-amide treated recyclable water, the impact of pNIPAM-co-penta-mann-2,3OMe-amide on MFT water significant

improvement; however not compared to MFT that is further processed by being shaken overnight and centrifuged.

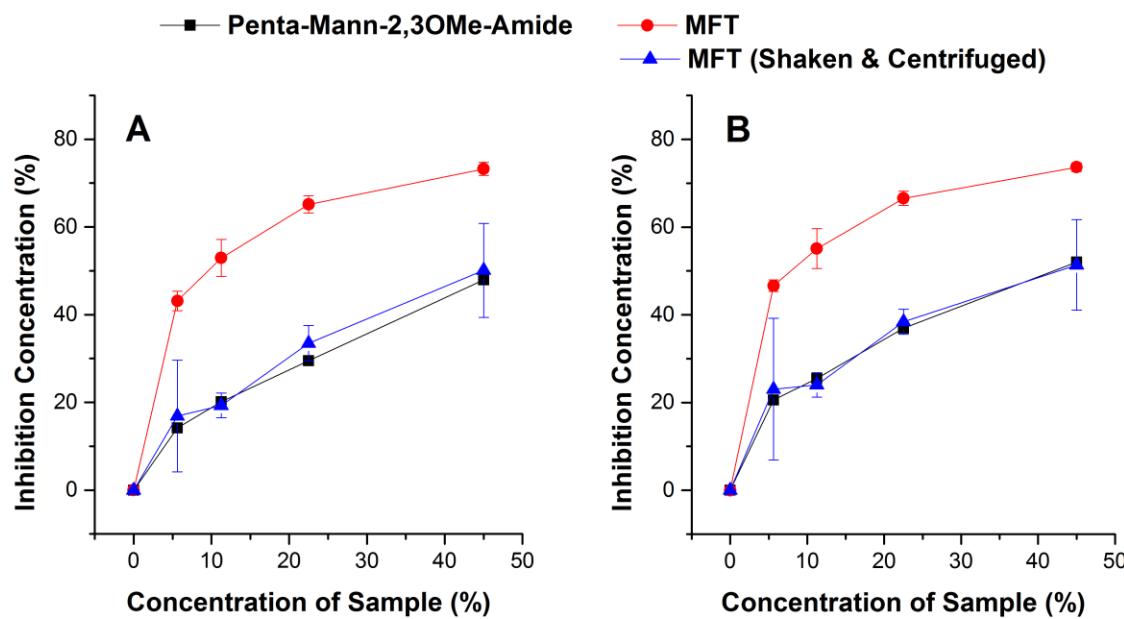
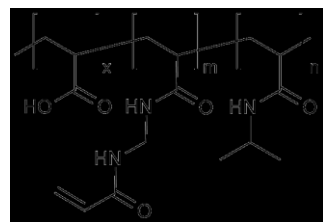


**Figure 4-9.** Microtox toxicity results of pNIPAM-co-Penta-Mann-2,3OMe-Amide Microgel ( $n = 1$ ) treated MFT compared to untreated MFT ( $n = 3$ ) and MFT (centrifuged and shaken,  $n = 3$ ) after 5 minutes (A) and 15 minutes (B) of exposure, pH = 8.

Overall the toxicity results for the polymerized carbohydrate-microgels do not show promising results for the treatment of MFT; however, pNIPAM-co-penta-mann-2,3OMe-amide could be used for the treatment of the recyclable tailings pond water despite its limitations. It is also possible that the treatment volume (10 mL) is too high for these sorbents. Further testing could not be carried with the sugar microgels due to low yield and limited sugar monomer.

#### 4.3.7 Microtox Data of pNIPAM-co-10 % AAc Microgel Treated MFT



pNIPAM-co-10 % AAc microgel (0.0263 g) treated 5 mL of MFT according to General Procedure E. The toxicity of both the treated water and untreated waste water was analyzed by Microtox bioassay (Figure 4-10). Based on the Microtox data the MFT treated with the pNIPAM-co-10 % AAc showed a decrease in overall toxicity at all concentrations compared to the untreated MFT; however, only a minor decrease compared to untreated MFT that has been further centrifuged and shaken, while PAC treated MFT still shows the best performance.

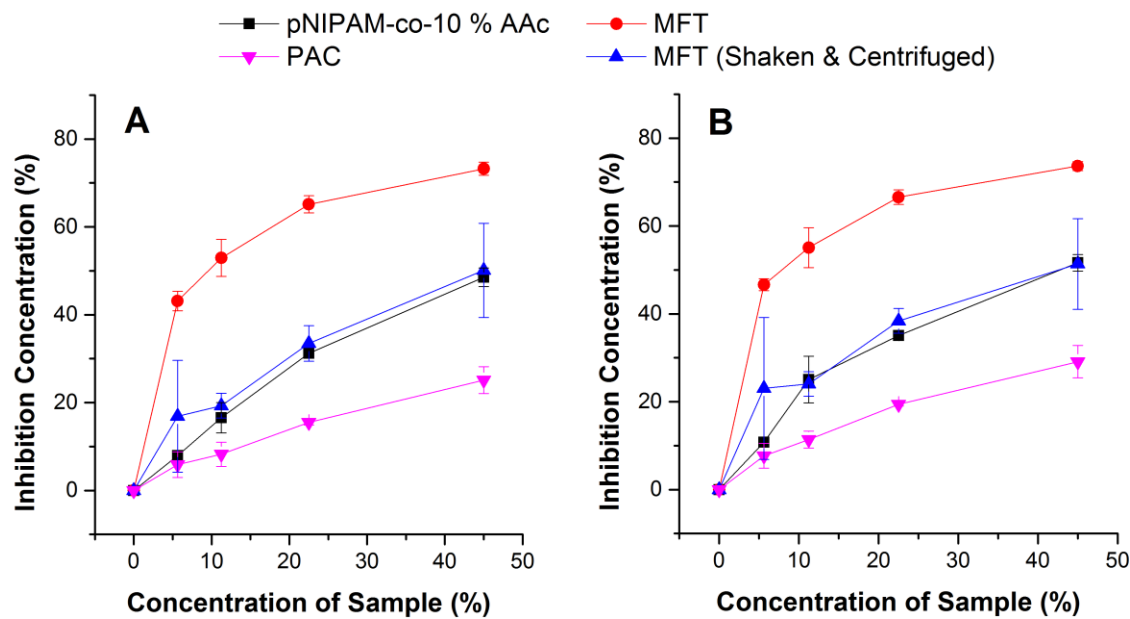


**Figure 4-10.** Microtox toxicity results of pNIPAM-co-10 % AAc Microgel and PAC treated MFT compared to untreated MFT and MFT (centrifuged and shaken) after 5 minutes (A) and 15 minutes (B) of exposure, pH = 8.

The treatment of 5 mL samples of MFT was altered by increasing the mass of pNIPAM-co-10 % AAc by 2 $\times$  (0.0511 g) and 3 $\times$  (0.0776 g), which showed no influence on reducing the overall toxicity based on the Microtox bioassay (Figure 4-11). Previous literature discussing water remediation with Orange II showed improvement when increasing the treatment concentration; however, no improvement occurred.<sup>152,155,156</sup>

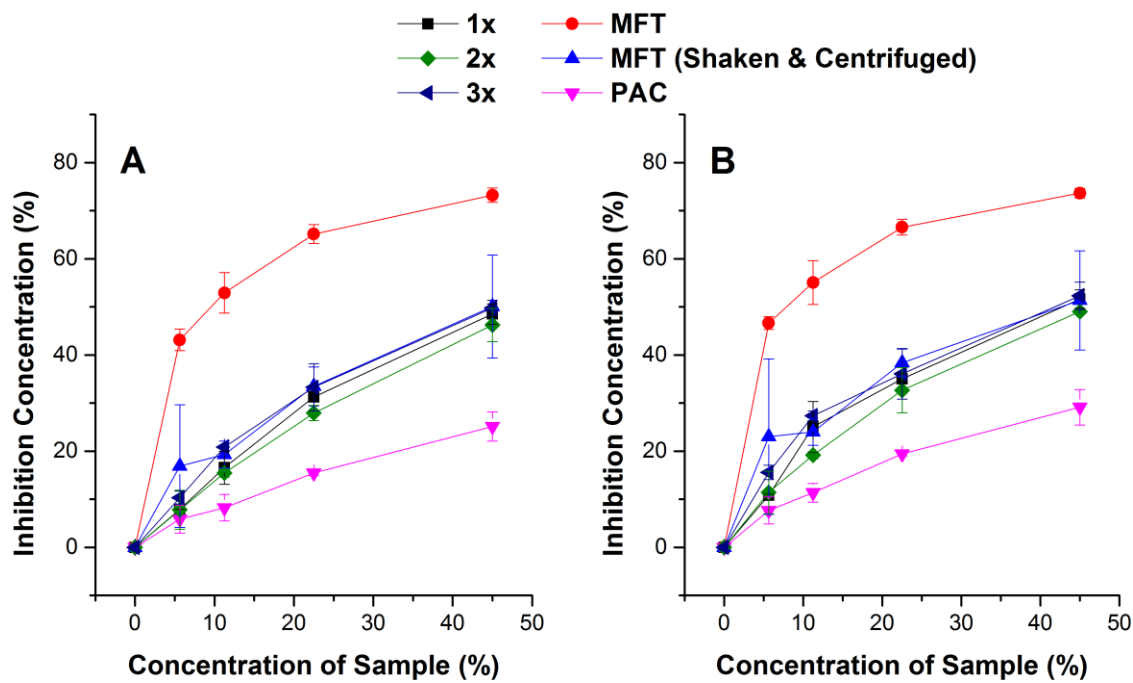
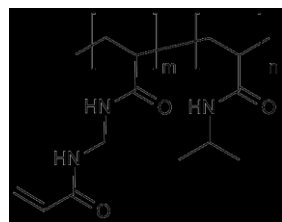


**Figure 4-11** Microtox toxicity results of pNIPAM-co-10 % AAc (1 $\times$ , 2 $\times$ , 3 $\times$ ) and PAC treated MFT compared to untreated MFT and MFT further centrifuged and shaken after 5 minutes (A) and 15 minutes (B) of exposure, pH 8.

#### 4.3.8 Microtox Data of pNIPAM-BIS Microgel Treated MFT



pNIPAM-BIS microgel ( $\sim 0.0260$  g) treated 5 mL of MFT according to General Procedure E. The toxicity of both the treated untreated MFT was analyzed by Microtox bioassay (Figure 4-12). Based on the Microtox data the MFT treated with pNIPAM-BIS showed a large decrease in toxicity at all concentrations compared to the untreated MFT and no change compared to untreated MFT that has been further centrifuged and shaken (Figure 4-12).

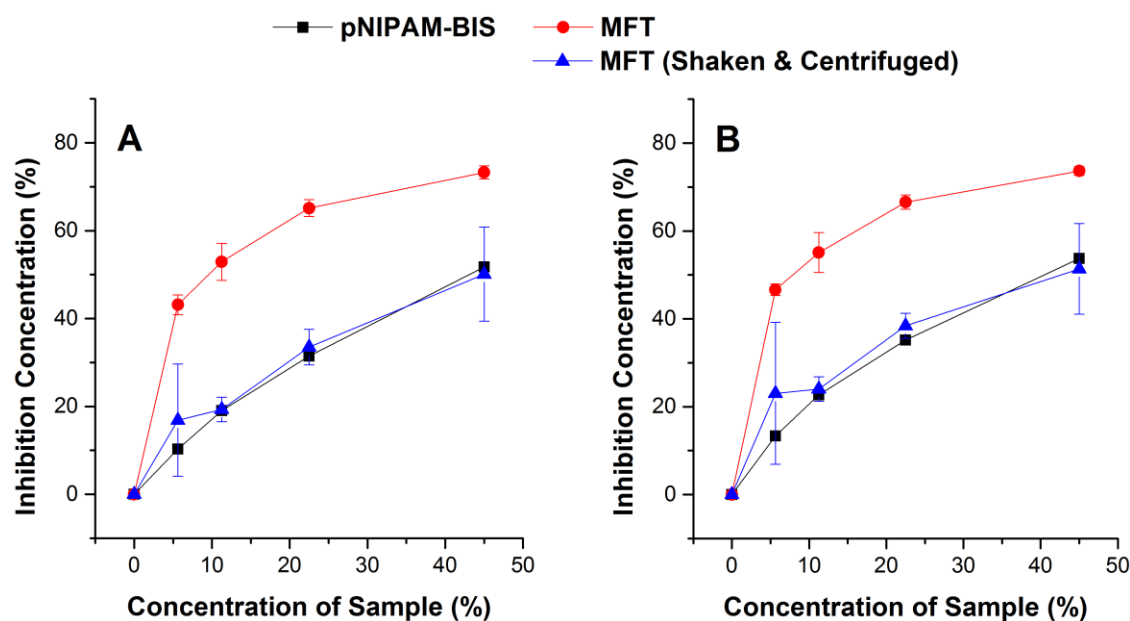
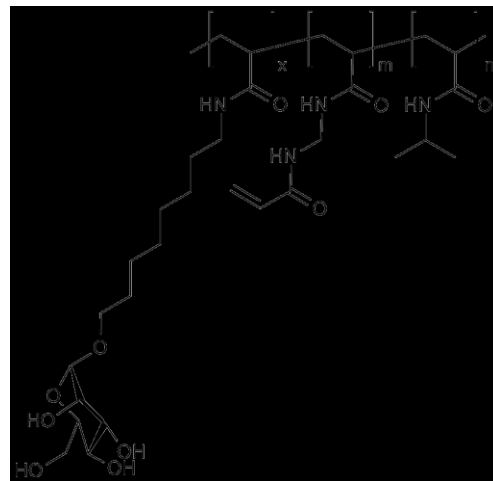


**Figure 4-12.** Microtox toxicity results of pNIPAM-BIS microgel ( $n = 1$ ) treated MFT compared to untreated MFT ( $n = 3$ ) and MFT further centrifuged and shaken ( $n = 3$ ) after 5 minutes (A) and 15 minutes (B) of exposure, pH 8.

#### **4.3.9 Microtox Data of pNIPAM-co-50 % AAc-Mann-Octylamine Microgel Treated MFT**



pNIPAM-co-50 % AAc-mann-octylamine microgel ( $\sim 0.0260$  g) treated 5 mL of MFT according to General Procedure 6. The toxicity of both the treated and untreated MFT and MFT further processed by shaken and centrifugation was analyzed by Microtox bioassay (Figure 4-13). Based on the Microtox data the MFT treated with pNIPAM-co-50 % AAc-mann-octylamine showed a large decrease in toxicity at all concentrations compared to the untreated MFT and no change compared to untreated MFT that has been further centrifuged and shaken. pNIPAM-co-50 % AAc-mann-octylamine treated MFT is uncomparable to PAC treated MFT.

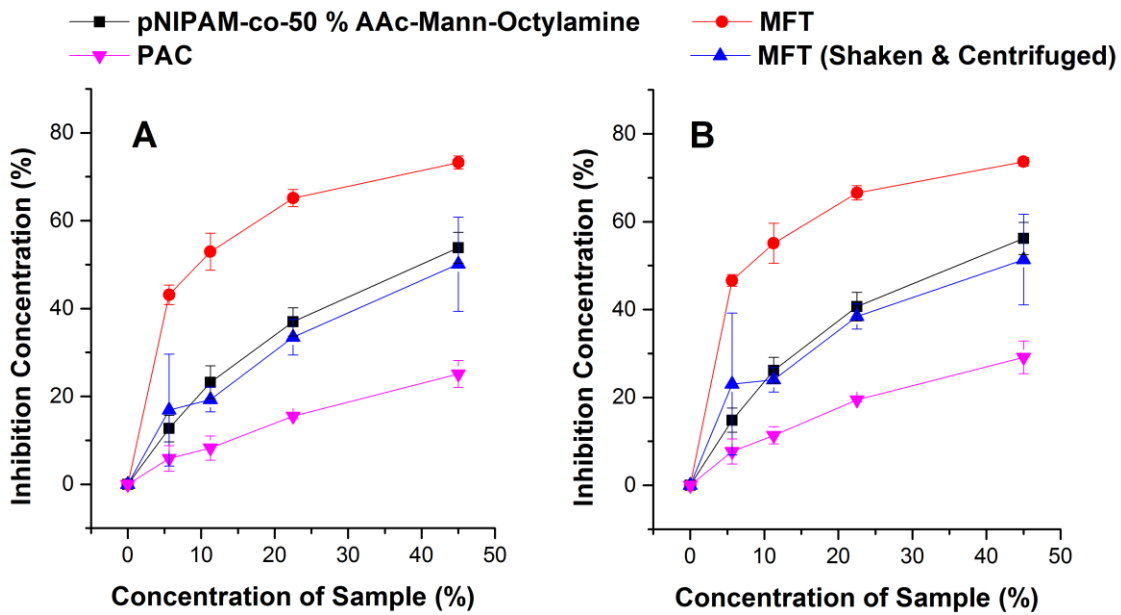
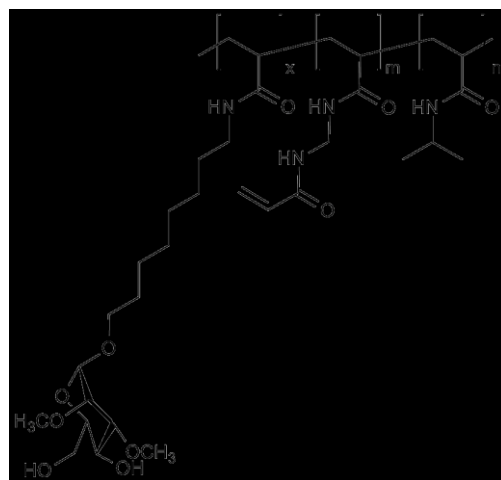


**Figure 4-13.** Microtox toxicity results of pNIPAM-co-50 % AAc-Mann-Octylamine Microgel and PAC ( $n = 3$ ) treated MFT compared to untreated MFT ( $n = 3$ ) and MFT further centrifuged and shaken ( $n = 3$ ) after 5 minutes of exposure (A) and 15 minutes of exposure (B), pH 8.

#### 4.3.10 Microtox Data of pNIPAM-co-50 % AAc-Mann-2,3OMe-Octylamine Microgel

##### Treated MFT



pNIPAM-co-50 % AAc-mann-2,3OMe-octylamine microgel (0.0249 g) treated 4.8 mL of MFT according to General Procedure 6. The toxicity of both the treated and untreated MFT and MFT further processed by shaken and centrifugation was analyzed by Microtox bioassay (Figure 4-14). Based on the Microtox data the MFT treated with pNIPAM-co-50 % AAc-mann-2,3OMe-octylamine showed an increase in overall toxicity at all concentrations compared to the untreated MFT and a larger increase compared to untreated MFT that has been further centrifuged and shaken. pNIPAM-co-50 % AAc-mann-octylamine treated MFT is uncomparable to PAC treated MFT. Overall, pNIPAM-co-50 % AAc-mann-2,3OMe-octylamine treated MFT water more toxic based on the Microtox data. This increase in toxicity could be due to unreacted residual NIPAM present in the microgel, which is known to be toxic.

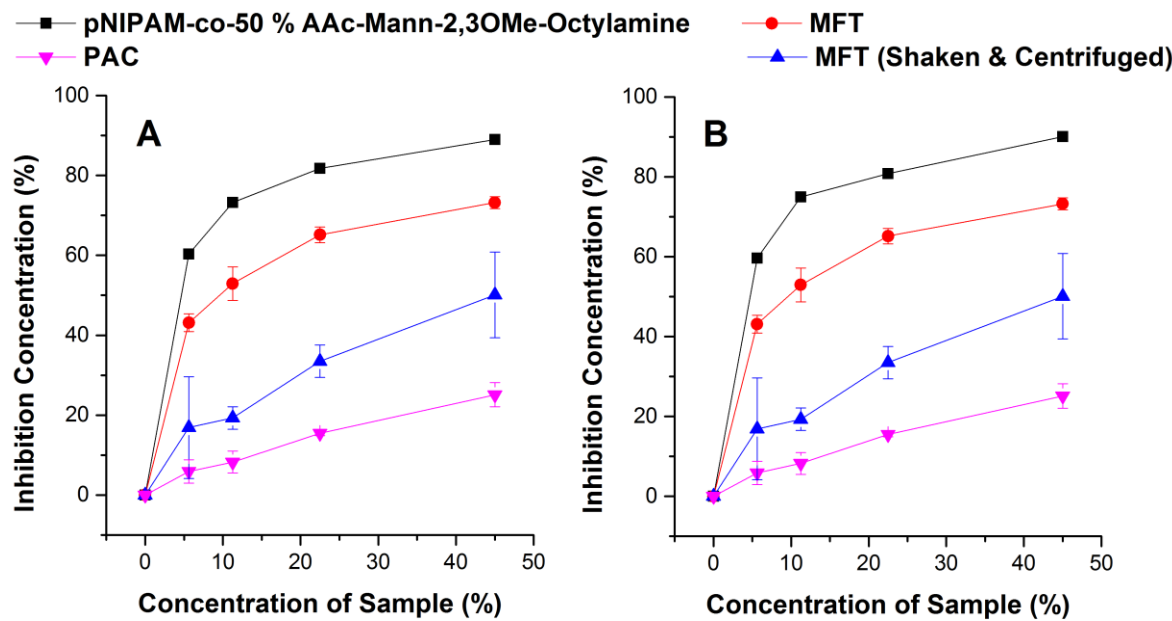


**Figure 4-14.** Microtox toxicity results of pNIPAM-co-50 % AAc-mann-2,3OMe-octylamine microgel ( $n = 1$ ) and PAC ( $n = 3$ ) treated MFT compared to untreated MFT ( $n = 3$ ) and MFT further centrifuged and shaken ( $n = 3$ ) after 5 minutes (A) and 15 minutes of exposure (B), pH 8.

#### 4.3.11 Summary

Based on the Microtox bioassay toxicity data both the carbohydrate-modified microgels synthesized by radical polymerization or EDC coupling does not reduce the overall toxicity. As mentioned earlier, the acute toxicity of tailings pond water is believed to be due to NAs, suggestive the carbohydrate-modified microgels do not show a preference for NAs.

### 4.4 FT-IR Quantification of Naphthenic Acids

The FT-IR method as described above was used to quantify the total concentration of naphthenic acids (or free carboxylics) in treated ( $\sim 0.0260$  g per 5 mL of MFT) and untreated MFT samples. MFT samples were treated with the following: PAC, pNIPAM-50 % AAc-

mann-octylamine microgel, pNIPAM-co-50 % AAc microgel, pNIPAM-co-50 % AAc-mann-2,3-diOMe-octylamine microgel, pNIPAM-co-50 % AAc-glu-6-OMe-octylamine microgel and processed and analyzed by FT-IR, which is shown in Figure 4-15.

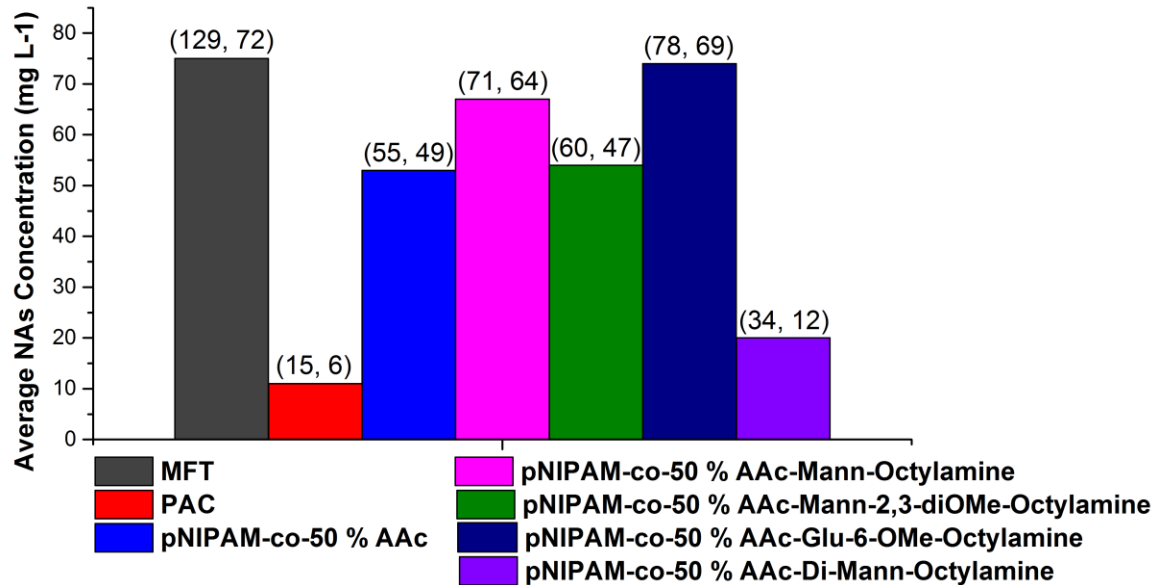


**Figure 4-15.** Data from FT-IR analyses of NAs concentration (average) in MFT ( $n = 3$ ), PAC ( $n = 3$ ), pNIPAM-co-50 % AAc ( $n = 3$ ), pNIPAM-co-50 % AAc-mann-octylamine ( $n = 2$ ), pNIPAM-co-50 % AAc-mann-2,3OMe-octylamine ( $n = 2$ ), pNIPAM-co-50 % AAc-glu-6-OMe-octylamine ( $n = 2$ ), pNIPAM-co-50 % AAc-Di-Mann-Octylamine ( $n = 2$ ). The numbers shown above each bar are the high and low values measured.

Based on the data from the FT-IR analyses (Figure 4-15) PAC treated MFT shows the lowest concentration of NAs ( $11 \pm 7 \text{ mg L}^{-1}$  NAs) compared to untreated MFT ( $75 \pm 3 \text{ mg L}^{-1}$  NAs) matching its performance according to the Microtox data as well. The microgel that performed the best was pNIPAM-co-50 % AAc-di-mann-octylamine ( $20 \text{ mg L}^{-1}$  NAs); however, the synthesis of Di-Mann-Octylamine is more time consuming and costly compared to monosaccharide octylamines. Both pNIPAM-co-50 % AAc ( $53 \pm 3 \text{ mg L}^{-1}$  NAs) and

pNIPAM-co-50 % AAc-mann-2,3OMe-octylamine ( $54 \text{ mg L}^{-1}$  NAs) perform equally the same, but unlike pNIPAM-co-50 % AAc-mann-2,3OMe-octylamine treated MFT, the volume of MFT recovered after treatment with pNIPAM-co-50 % AAc was almost half of the total volume of treated MFT due to the hygroscopicity of the acrylic acid moiety, which is not ideal. The remaining microgels: pNIPAM-co-50 % AAc-mann-octylamine ( $67 \text{ mg L}^{-1}$  NAs) and pNIPAM-co-50 % AAc-glu-6-OMe-octylamine ( $74 \text{ mg L}^{-1}$  NAs) does not as promising potential for removing NAs from MFT.

Overall pNIPAM-co-50 % AAc-di-mann-octylamine shows the best performance, which could be due to the formation of lipophilic interior in the microgel (similar to  $\beta$ -CD) an ideal cavity for naphthyl moieties. It is also possible the performance could be improved by increasing the amount of carbohydrate-modified microgel to MFT. Although the performance of pNIPAM-co-50 % AAc-di-mann-octylamine is promising, pNIPAM-co-50 % AAc-mann-2,3OMe-octylamine is also a promising candidate due to mann-2,3OMe-octylamine being a monosaccharide octylamine, which reduces the time and cost to synthesize. Also, similar to PMPs – two methylated groups at the 2 and 3 positions on the sugar ring could help form a hydrophobic core for trapping organics.

#### **4.4.1 Increasing pNIPAM-co-50 % AAc-Mann-2,3OMe-Octylamine Microgel for MFT Treatment**

Based on the performance of pNIPAM-co-50 % AAc-mann-2,3OMe-octylamine further studies were performed by doubling the treatment concentration from  $\sim 0.0260 \text{ mg}$  of carbohydrate-modified microgel per 5 mL of MFT to  $0.0520 \text{ mg}$  of carbohydrate-modified

microgel per 5 mL of MFT. The treated MFT was analyzed by FT-IR, which is summarized in Figure 4-16.

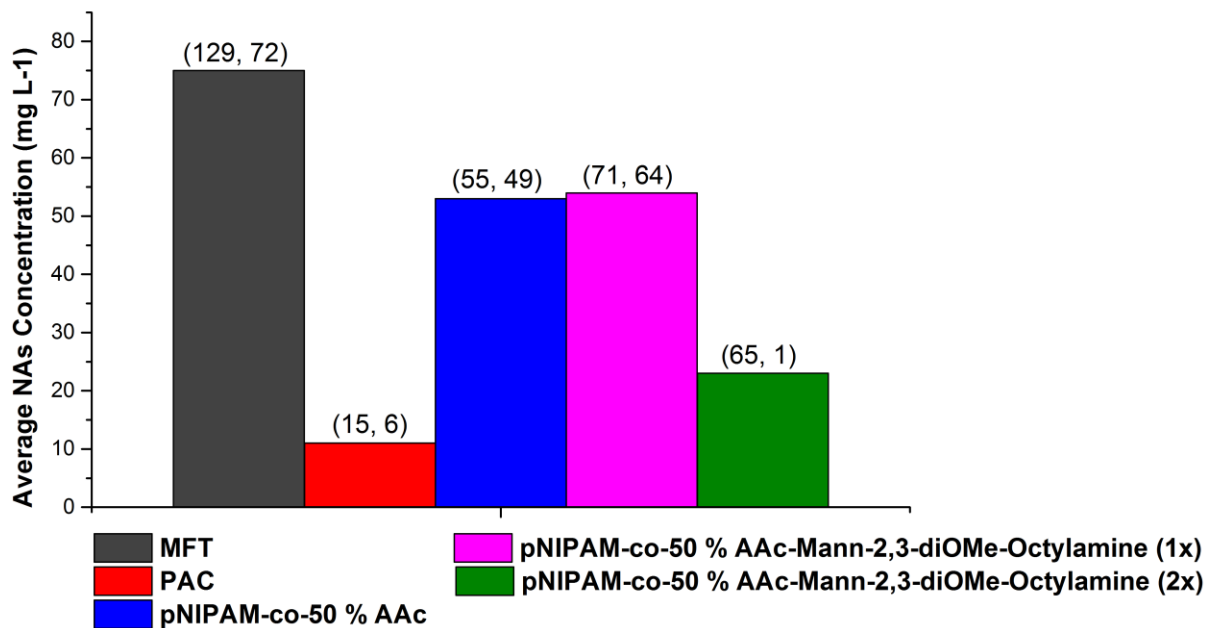


**Figure 4-16.** Data from FT-IR analyses of NAs concentration (average) in MFT ( $n = 3$ ), PAC ( $n = 3$ ), pNIPAM-co-50 % AAc ( $n = 3$ ), pNIPAM-co-50 % AAc-mann-2,3OMe-octylamine ( $1\times$ ,  $n = 2$ ), pNIPAM-co-50 % AAc-mann-2,3OMe-octylamine ( $2\times$ ,  $n = 2$ ). The numbers shown above each bar are the high and low measured values.

Based on the FT-IR data in Figure 4-16, it is difficult to say whether increasing the treatment of pNIPAM-co-50 % AAc-mann-2,3OMe-octylamine by  $2\times$  is effective. The average NAs concentration for  $2\times$  treatment with pNIPAM-co-50 % AAc-mann-2,3OMe-octylamine is  $20 \pm 30 \text{ mg L}^{-1}$  NAs, compared to  $1\times$  treatment with pNIPAM-co-50 % AAc-mann-2,3OMe-octylamine of  $54 \pm 9 \text{ mg L}^{-1}$  NAs. Although it has been reported that the limit of detection for 50 mL samples of tailings pond water using this FT-IR method was 1

$\text{mg L}^{-1}$ . By decreasing the sample size this could increase the amount of error in measurements of samples with low concentrations of NAs.<sup>79</sup>

## Conclusion

The direct polymerization of pNIPAM cross-linked with sugars is a plausible option to synthesize carbohydrate-microgels; however, EDC coupling pNIPAM-co-AAc microgels with saccharide(s)-octylamines is a much better option based on cost, time and characterization with  $^1\text{H}$  NMR spectra. Based on the NMR spectra acquired, nanoprobe  $^1\text{H}$  NMR spectroscopy is a viable option to characterize water soluble microgels and adjusting the pH to the appropriate alkalinity (or acidity) can improve the resolution of the spectra.

The performance of the carbohydrate-coupled microgels treating MFT compared to the polymerized carbohydrate-microgels is comparable according to Microtox bioassay and show marginal improvements in overall toxicity. The effect of carbohydrate-coupled microgels treated MFT shows a decrease in the NAs (or acid extractable organic fraction). Specifically, according to the FT-IR data, pNIPAM-co-50 % AAc-di-mann-octylamine shows the best performance by decreasing the NAs concentration of MFT ( $75 \pm 3 \text{ mg L}^{-1}$  NAs) to  $20 \text{ mg L}^{-1}$  NAs within the range of the performance of PAC ( $11 \pm 7 \text{ mg L}^{-1}$  NAs). It is possible that pNIPAM-co-50 % AAc-mann-2,3OMe-octylamine could be a promising sorbent by increasing the carbohydrate-coupled microgel for MFT treatment; however, a larger samples size is needed for FT-IR analysis.

Ultimately, PAC shows better performance treating MFT. A large reduction in overall toxicity at all inhibition concentrations according to Microtox bioassay data and a large reduction in NAs concentration according to FT-IR analysis:  $11 \pm 7 \text{ mg L}^{-1}$  NAs down from  $75 \pm 3 \text{ mg L}^{-1}$  NAs.

## Future Work

As discussed in Chapter 2 both pNIPAM-based microgels and PMPs both show capabilities of water remediation. A competitive binding assay should be used to confirm pNIPAM-co-AAc binds specifically to Orange II and not towards a polar solvent, which is suggested in this dissertation. PMPs show promising results as a sorbent for NAs; however, they are expensive, produced in low yield and time consuming to synthesize. A method to extract PMPs from a type of Mycobacteria in good yield and in an inexpensive manner would be very beneficial.

Chapter 3 outlines the synthesis and characterization of microgels and carbohydrate-coupled microgels. The use of EDC coupling is a promising area to modify microgels and should be explored in more detail. Specifically, the effect of chain length on the success of coupling with microgels should be investigated further. The characterization of microgels using nanoprobe  $^1\text{H}$  NMR spectroscopy is a promising area based on the spectra shown in this dissertation. A library of microgels characterized using nanoprobe  $^1\text{H}$  NMR spectroscopy should be established, which would be beneficial to the microgel community. Also, using nanoprobe  $^1\text{H}$  NMR spectroscopy as a method to quantify the monomers in microgels by integration is also an important area that should be addressed. The challenge with using nanoprobe  $^1\text{H}$  NMR spectroscopy to quantify the monomers comprising a microgel is the inability to distinguish large broad signals. Optimizing the solvent and pH for running specific types of microgels could be a good initial approach to this issue.

The performance of several carbohydrate-modified microgels was analyzed using Microtox bioassay and FT-IR in Chapter 4. The carbohydrate-coupled microgels that showed

promising results according to FT-IR should be re-analyzed using ESI-MS and a similar method used for the analysis of PMPs.<sup>105</sup> Microgels modified with long-chained alkyl amines should be re-synthesized and their ability to treat MFT should be analyzed by FT-IR. Microtox bioassay analysis should be revisited for the analysis of the promising carbohydrate-coupled microgel treated MFT, which would determine whether the reduction of NAs (or AOF) corresponds to the overall reduction in toxicity. Finally, the recyclability of the carbohydrate-microgels should be investigated in a similar manner that the recyclability of PAC was investigated using Microtox bioassay and, in addition, with FT-IR analysis.

## References

1. Moan, J. L.; Smith, Z. A. *Energy Use Worldwide: A Reference Handbook*; ABC-CLIO: Santa Barbara, 2007.
2. Speight, J. G. *The Chemistry and Technology of Petroleum 5th Ed.*; CRC Press Taylor and Francis Group: Boca Raton, 2014. 271-381.
3. Speight, J. G. *Natural Gas: A Basic Handbook*; Gulf Publishing Company: Houston, 2007. 9-11.
4. Reddy, P. J. *Clean Coal Technologies for Power Generation*; Taylor & Francis Group: Boca Raton, 2013. 44-45.
5. Ball, M. In *The Hydrogen Economy: Opportunities and Challenges*; Ball, M., Wietschel, M., Eds.; Cambridge University Press: New York, 2009, p 46-86.
6. Clark, W. W.; Cooke, G. *The Green Industrial Revolution: Energy, Engineering and Economics*; Elsevier Oxford, 2015. 65-69.
7. Muradov, N. *Liberating Energy from Carbon: Introduction to Decarbonization*; Springer: New York, 2014.
8. Percy, K. E. *Alberta Oil Sands: Energy, Industry and the Environment*; Elsevier: Oxford, 2012.
9. *Canadian Economic Impacts of New and Existing Oil Sands Development in Alberta (2014-2038)*; Briefing Paper: November 2014; Canadian Energy Research Institute: Calgary, 2014.

10. Ross, M. S.; Pereira, A. D.; Fennell, J.; Davies, M.; Johnson, J.; Sliva, L.; Martin, J. W. *Environ. Sci. Technol.* **2012**, *46*, 12796-12805.
11. Kelly, E. N.; Schindler, D. W.; Hodson, P. V.; Short, J. W.; Radmanovich, R.; Nielsen, C. C. *Proceedings of the National Academy of Sciences* **2010**, *107*, 16178-16183.
12. Gray, M. R. *Upgrading Oilsands Bitumen and Heavy Oil*; The University of Alberta: Edmonton, 2015. 232-234.
13. Speight, J. G. In *Handbook of Alternative Fuel Technologies, 2nd Edition*; CRC Press: Boca Raton, 2015, p 210-213.
14. Speight, J. G. *Oil Sand Production Processes*; Elsevier Oxford, 2013. 47-55.
15. Wang, Z.; Fingas, M.; Yang, C.; Christensen, J. H. In *Environmental Forensics: Contaminant Specific Guide*; Morrison, R. D., Murphy, B. L., Eds.; Elsevier: Burlington, 2006, p 341 - 346.
16. Cottrell, J. H. In *The K.A. Clark Volume*; Carrigy, M. A., Ed.; Research Council of Alberta: Edmonton, 1963, p 193-206.
17. Mossop, G. D. *Science* **1980**, *11*, 145-207.
18. Dusseault, M. B.; Morgenstern, N. R. *Can. Geotech. J.* **1978**, *15*, 216-238.
19. Takamura, K. *Can. J. Chem. Eng.* **1982**, *60*, 538-545.
20. Czarnecki, J.; Radoev, B.; Schramm, L. L.; Slavchev, R. *Adv. Colloid Interface Sci.* **2005**, 53-60.

21. Doan, D. H.; Delage, P.; Nauroy, J. F.; Tang, A. M.; Youssef, S. *Can. Geotech. J.* **2012**, *49*, 1212-1220.
22. Dusseault, M. B. *J. Can. Petrol. Technol.* **1980**, *19*, 85-92.
23. Banerjee, D. K. *Oil Sands, Heavy Oil & Bitumen: From Recovery to Refinery*; PennWell: Tulsa, 2012. 11-14,49-70.
24. Sheppard, M. C. *Oil Sands Scientist: The Letters of Karl A. Clark, 1920-1949*; University of Alberta Press: Edmonton, 1989. 20, 21.
25. Chastko, P. A. *Developing Alberta's Oil Sands: From Karl Clark to Kyoto*; University of Calgary Press: Calgary, 2004. 15.
26. Clark, K. A.; Pastern, D. S. *Ind. Eng. Chem.* **1932**, *24*.
27. Long, J.; Drelich, J.; Xu, Z.; Masliyah, J. H. *Can. J. Chem. Eng.* **2008**, *85*, 726-738.
28. Papavinasam, S. *Corrosion Control in the Oil and Gas Industry*; Elsevier Oxford, 2014. 231-234.
29. Kutz, M. In *Towards Sustainable Clean Energy*; John Wiley & Sons: Hoboken, 2010, p 89-95.
30. Government of Alberta (GOA). Alberta Energy Regulator. *ST98-2014: Alberta's Energy Reserves 2013 and Supply/Demand Outlook 2014 - 2023*; Government of Alberta: Edmonton, 2014. <<https://www.aer.ca/documents/sts/ST98/ST98-2014.pdf>>.
31. Government of Alberta (GOA). Alberta Environment and Sustainable Resource Development. *Lower Athabasca Region: Tailings Management Framework for the Mineable*

*Athabasca Oil Sands*; Government of Alberta: Edmonton, 2015.  
<<http://esrd.alberta.ca/focus/cumulative-effects/cumulative-effects-management/management-frameworks/documents/LARP-TailingsMgtAthabascaOilsands-Mar2015.pdf>>.

32. Government of Alberta (GOA). Environmental Management of Alberta's Oil Sands. Government of Alberta: Edmonton, 2009.

<<http://environment.gov.ab.ca/info/library/8042.pdf>>.

33. Small, C. C.; Cho, S.; Hashisho, Z.; Ulrich, A. C. *J. Petrol. Sci. Eng.* **2015**, *127*, 490–501.

34. Allen, E. W. *J. Environ. Eng. Sci.* **2008**, *7*, 123-138.

35. Lupo, J. F. *Tailings and Mine Waste '08*; Taylor & Francis Group: London, 2008. 177-180.

36. Davidson, D. J.; Gismondi, M. *Challenging Legitimacy at the Precipice of Energy Calamity*; Springer: New York, 2011. 115-118.

37. Price, M. *11 Million Litres a Day: The Tar Sands Leaking Legacy*; Environmental Defence: Toronto, 2008. 8-15.

38. Allen, E. W. *J. Environ. Eng. Sci.* **2008**, *7*, 499-524.

39. Toor, N. S.; Franz, E. D.; Fedorak, P. M.; MacKinnon, M. D.; Liber, K. *Chemosphere* **2013**, *90*, 449-458.

40. Cowie, B. R.; James, B. Aqueous geochemistry and stable isotope ratios as a predictive risk management tool for assessing vertical hydraulic connectivity during oil sands resource development in the Athabasca region. *Geoconvention 2014: Focus* Calgary, 2014.
41. Beier, N.; Sego, D.; Donahue, R.; Biggar, K. *Int. J. Min. Reclam. Env.* **2007**, *21*, 144-155.
42. Kannel, P. R.; Gan, T. Y. *J. Environ. Sci. Health., Part A* **2012**, *47*, 1-21.
43. Holowenko, F. M.; MacKinnon, M. D.; Fedorak, P. M. *Water Res.* **2002**, *36*, 2843-2855.
44. Frank, R. A.; Fischer, K. a. A.; avanagh, R. i. K.; Burnison, B. K.; Arsenault, G.; Headley, J. V.; Peru, K. M.; VanDerKraak, G.; Solomon, K. *Environ. Sci. Technol.* **2009**, *43*, 261-271.
45. Headley, J. V.; McMartin, D. W. *J. Environ. Sci. Heal. A* **2004**, *39*, 1989-2010.
46. Rowland, S. J.; Scarlett, A. G.; Jones, D.; West, C. E.; Frank, R. A. *Environ. Sci. Technol.* **2011**, *45*, 3154-3159.
47. Grewer, D. M.; Young, R. F.; Whittal, R. M.; Fedorak, P. M. *Sci.Total Environ.* **2010**, *408*, 5997-6010.
48. Brient, J. A.; Wessner, P. J.; Doyle, M. N. In *Kirk-Othmer Encyclopedia of Chemical Technology*; John Wiley and Sons: Online, 2000, p 1-10.
49. Frank, R. A.; Roy, J. W.; Bickerton, G.; Rowland, S. J.; Headley, J. V.; Scarlett, A. G.; West, C. E.; Peru, K. M.; Parrott, J. L.; Conly, F. M.; Hewitt, a. L. M. *Environ. Sci. Technol.* **2014**, *48*, 2660-2670.
50. Clemente, J. S.; Fedorak, P. M. *Chemosphere* **2005**, *60*, 585-600.

51. Frank, R. A.; Kavanagh, R.; Burnison, K.; Arsenault, G.; Headley, J. V.; Peru, K. M.; Kraak, G. V. D.; Solomon, K. R. *Chemosphere* **2008**, *72*, 1309-1314.
52. Whitby, C. In *Advances in Applied Microbiology*; Elsevier: Oxford, 2010; Vol. 70, p 93-125.
53. MacKinnon, M.; Boerger, H.; *H. Water Pollut. Res. J. Can.* **1986**, *21*, 496-512.
54. Dokholyan, B. K.; Magomedov, A. K. *Voprosy Ikhtiolozii* **1984**, *23*, 1013-1019.
55. Peters, L. E.; MacKinnonb, M.; Meerc, T. V.; Heuveld, M. R. v. d.; Dixona, D. G. *Chemosphere* **2007**, *67*, 2177-2183.
56. Warith, M. A.; Yong, R. N. *Environ. Technol.* **1994**, *15*, 381-387.
57. Pollet, I.; Bendell-Young, L. I. *Environ. Toxicol. Chem.* **2000**, *19*, 2589-2597.
58. Rogers, V. V.; Wickstrom, M.; Liber, K.; MacKinnon, M. D. *Toxicol. Sci.* **2002**, *66*, 347-355.
59. Schramm, L. L. *Surfactants: Fundamentals and Applications in the Petroleum Industry*; Cambridge University Press: Cambridge, 2000. 1-421.
60. Herman, D. C.; Fedorak, P. M.; MacKinnon, M. D.; Costerton, J. W. *Can. J. Microbiol.* **1994**, *40*, 467-477.
61. Clemente, J.; MacKinnon, M. D.; Fedorak, P. M. *Environ. Sci. Technol.* **2004**, *38*, 1009-1016.
62. Clemente, J. S.; Fedorak, P. M. *J. Chromatogr.* **2004**, *1047*, 117-128.

63. Adhoum, N.; Monser, L. *Separ. Purif. Tech.* **2004**, *38*, 233-239.
64. Yang, Y.; Zhang, X.; Wang, Z. *Water Sci. Technol.* **2002**, *46*, 165-170.
65. Bose, P.; Bose, M. A.; Kumar, S. *Adv. Environ. Res.* **2002**, *7*, 179-195.
66. Considine, D. M.; Considine, G. D. *Van Nostrand's Scientific Encyclopedia*; Springer: New York, 1995. 896.
67. Wong, D. C. L.; Compernolle, R. v.; Nowlin, J. G.; O'Neal, D. L.; Johnson, G. M. *Chemosphere* **1996**, *32*, 1669-1679.
68. Mohamed, M. H.; Wilson, L. D.; Headley, J. V.; Peru, K. M. *Process. Saf. Environ.* **2008**, *86*, 237-243.
69. Iranmanesh, S.; Harding, T.; Abedi, J.; Seyedeyn-Azad, F.; Layzell, D. B. *J. Environ. Eng. Sci.* **2014**, *49*, 913-922.
70. Hansen, B. R.; Davies, S. R. H. *Chem. Eng. Res. Des.* **1994**, *72*, 176-188.
71. Martin, J. W.; Han, X.; Peru, K. M.; Headley, J. V. *Rapid Commun. Mass Spectrom.* **2008**, *22*, 1919-1924.
72. Zou, L.; Han, B.; Yan, H.; Kasperski, K. L.; Xu, Y.; Hepler, L. G. *J. Colloid Interface Sci.* **1997**, *190*, 472-475.
73. Gaikar, V. G.; Maiti, D. *React. Funct. Polym.* **1996**, *31*, 155-164.
74. Li, X. *Oral Bioavailability: Basic Principles, Advanced Concepts, and Applications*; John Wiley & Sons: Hoboken, 2011. 42.

75. Gadre, A.; Connors, K. A. *J. Pharm. Sci.* **1997**, *86*, 1210-1214.
76. Ma, M.; Li, D. *Chem. Mater.* **1999**, *11*, 872-874.
77. Mohamed, M. H.; Wilson, L. D.; Headley, J. V.; Peru, K. M. *Can. J. Chem.* **2009**, *87*, 1747-1756
78. Mohamed, M. H.; Wilson, L. D.; Headley, J. V.; Perub, K. M. *Phys. Chem. Chem. Phys.* **2011**, *13*, 1112-1122.
79. Scott, A. C.; Zubot, W.; MacKinnon, M. D.; Smith, D. W.; Fedorak, P. M. *Chemosphere* **2008**, *71*, 156-160.
80. El-Din, M. G.; Fu, H.; Wang, N.; Chelme-Ayala, P.; Pérez-Estrada, L.; Drzewicz, P.; Martin, J. W.; Zubot, W.; Smith, D. W. *Sci.Total Environ.* **2011**, *409*, 5119-5125.
81. Brown, L. D.; Ulrich, A. C. *Chemosphere* **2015**, *127*, 276-290.
82. Pereira, A. S.; Islam, M. S.; El-Din, M. G.; Martin, J. W. *Rapid Commun. Mass Spectrom.* **2013**, *27*, 2317-2326.
83. He, Y.; Patterson, S.; Wangc, N.; Hecker, M.; Martin, J. W.; El-Din, M. G.; Giesy, J. P.; Wiseman, S. B. *Water Res.* **2012**, *46*, 6359-6368.
84. Garcia-Garcia, E.; Ge, J. Q.; Oladiran, A.; Benjamin Montgomery; El-Din, M. G.; Perez-Estrad, L. C.; Stafford, J. L.; Martin, J. W.; Belosevic, M. *Water Res.* **2011**, *45*, 5849-5857.
85. Sorrell, T. N. *Organic Chemistry*; University Science Books: Sausalito, 2006. 364-365.
86. Liang, X.; Zhu, X.; Butler, E. C. *J. Hazard. Mater.* **2011**, *190*, 168-176.

87. Kaiser, K. L. E.; Esterby, S. R. *Sci.Total Environ.* **1991**, *109/110*, 499-514.
88. Bataineh, M.; Scott, A. C.; Fedorak, P. M.; Martin, J. W. *Anal. Chem.* **2006**, *78*, 8354-8361.
89. Headley, J.; Peru, K.; Mcmartin, D. W.; Winkler, M. *J. AOAC Int.* **2002**, *85*.
90. Clemente, J. S.; Yen, T.-W.; Fedorak, P. M. *J. Environ. Eng. Sci.* **2003**, *2*, 177-186.
91. Yen, T.-W.; Marsh, W. P.; MacKinnon, M. D.; Fedorak, P. M. *J. Chromatogr. A* **2004**, *1033*, 83-90.
92. Han, X.; MacKinnon, M. D.; Martin, J. W. *Chemosphere* **2009**, *76*, 63-70.
93. Ross, M. S.; Pereira, A. d. S.; Fennell, J.; Davies, M.; Johnson, J.; Sliva, L.; Martin, J. W. *Rapid Commun. Mass Spectrom.* **2008**, *22*, 1919-1924.
94. Jackson, M.; Brennan, P. J. *J. Biol. Chem.* **2009**, *284*, 1949-1953.
95. Bloch, K. *Adv. Enzymol. Relat. Areas Mol. Biol.* **1977**, *45*, 1-84.
96. Mendes, V.; Maranha, A.; Alarico, S.; Empadinhas, N. *Nat. Prod. Rep.* **2012**, *29*, 834-844.
97. Lee, Y. C.; Ballou, C. E. *J. Biol. Chem.* **1964**, *239*, PC3602-PC3603.
98. Stadthagen, G.; Sambou, T.; Guerin, M.; Barilone, N.; Boudou, F.; Korduláková, J.; Charles, P.; Alzari, P. M.; Lemassu, A.; Daffé, M.; Puzo, G.; Gicquel, B.; Rivière, M.; Jackson, M. *J. Biol. Chem.* **2007**, *282*, 27270-27276.
99. Tuffal, G.; Albigot, R.; Rivière, M.; Puzo, G. *Glycobiology* **1998**, *8*, 675-684.

100. Hunter, S. W.; Gaylord, H.; Brennan, P. J. *J. Biol. Chem.* **1986**, *261*, 12345-12351.
101. Tuffal, G.; Ponthus, C.; Picard, C.; Riviére, M.; Puzo, G. *Eur. J. Biochem.* **1995**, *233*, 377-383.
102. Xia, L.; Lowary, T. L. *Biopolymers* **2013**, *99*, 697-712.
103. Pommier, M. T.; Michel, G. *J. Gen. Microbiol.* **1986**, *132*, 2433-2441.
104. Yamada, H.; Cohen, R. E.; Ballou, C. E. *J. Biol. Chem.* **1979**, *254*, 1972-1979.
105. Liu, L.; Bai, Y.; Sun, N.; Xia, L.; Lowary, T. L.; Klassen, J. S. *Chem. Eur. J.* **2012**, *18*, 12059-12067.
106. Yabusaki, K. K.; Cohen, R. E.; Ballou, C. E. *J. Biol. Chem.* **1979**, *254*, 7282-7286.
107. Maggio, J. E. *Proc. Nati. Acad. Sci. USA* **1980**, *77*, 2582-2586.
108. Kiho, T.; Ballou, C. E. *Biochemistry* **1988**, *27*, 5824-5828.
109. Cheon, H.-S.; Wang, Y.; Ma, J.; Kishi, Y. *ChemBioChem* **2007**, *8*, 353-359.
110. Hsu, M. C.; Lee, J.; Kishi, Y. *J. Org. Chem.* **2007**, *72*, 1931-1940.
111. Cheng, H.; Zhang, G. In *Hydrogel Micro and Nanoparticles*; Lyon, L. A., Serpe, M. J., Eds.; Wiley-VCH Verlag GmbH & Co. KGaA: Weinheim, 2012, p 1-32.
112. Hu, L.; Sarker, A. K.; Islam, M. R.; Li, X.; Lu, Z.; Serpe, M. J. *J. Polym. Sci., Part A: Polym. Chem.* **2013**, *51*, 3004-3020.
113. Pelton, R. H.; Chibante, P. *Colloids Surf.* **1986**, *20*, 247-256.

114. Kokufuta, E.; Wang, B.; Yoshida, R.; Khokhlov, A. R.; Hirata, M. *Macromolecules* **1998**, *31*, 6878-6884.
115. Hoare, T.; Pelton, R. *Biomacromolecules* **2008**, *9*, 733-740.
116. Sorrell, C. D.; Serpe, M. J. *Anal. Bioanal. Chem.* **2012**, *402*, 2385-2393.
117. Moniruzzaman, M.; Fernando, G. F.; Talbot, J. D. R. *J. Polym. Sci., Part A: Polym. Chem.* **2004**, *42*, 2886-2896.
118. Fernández-Nieves, A.; Fernández-Barbero, A.; Nieves, F. J. d. l.; Vincent, B. *J. Phys.: Condens. Matter* **2000**, *12*, 3605-3614.
119. Brugger, B.; Richtering, W. *Adv. Mater.* **2007**, *19*, 2973-2978.
120. Bhattachary, S.; Eckert, F.; Boyko, V.; Pich, A. *Small* **2007**, *3*, 650-657.
121. Klinger, D.; Landfester, K. *Polymer* **2012**, *53*, 5209-5231.
122. Saunders, B. R.; Vincentb, B. *Adv. Colloid Interface Sci.* **1999**, *80*, 1-25.
123. Wu, C.; Zhou, S. *Macromolecules* **1995**, *28*, 5388-5390.
124. Wu, C.; Zhou, S. *Phys. Rev. Lett.* **1996**, *77*, 3053-3055.
125. Snowden, M. J.; Chowdhry, B. Z.; Vincentb, B.; Morrisb, G. E. *J. Chem. Soc. Faraday Trans.* **1996**, *92*, 5013-5016.
126. Kim, J.; Nayak, S.; Lyon, L. A. *J. Am. Chem. Soc.* **2005**, *127*, 9588-9592.
127. Hoare, T.; Pelton, R. *Macromolecules* **2004**, *37*, 2544-2550.

128. Höfl, S.; Zitzler, L.; Hellweg, T.; Herminghaus, S.; Mugele, F. *Polymer* **2007**, *48*, 245-254.
129. Karg, M.; Pastoriza-Santos, I.; Rodriguez-González, B.; Klitzing, R. v.; Wellert, S.; Hellweg, T. *Langmuir* **2008**, *24*, 6300-6306.
130. López-León, T.; Ortega-Vinuesa, J. L.; Bastos-González, D.; Elaïssari, A. *J. Phys. Chem. B* **2006**, *110*, 4629-4636.
131. Zhang, Y.; Guan, Y.; Zhou, S. *Biomacromolecules* **2006**, *7*, 3196-3201.
132. Fischer, M. J. E. In *Surface Plasmon Resonance: Methods in Molecular Biology*; Mol, N. J. d., Fischer, M. J. E., Eds.; Human Press New York, 2010; Vol. 627 p55-73.
133. Hermanson, G. T. *Bioconjugate Techniques*; Academic Press: London, 2013. 560-566.
134. Dewick, P. M. *Essentials of Organic Chemistry: For Students of Pharmacy, Medicinal Chemistry and Biological Chemistry*; John Wiley & Sons: Hoboken, 2006.
135. Hu, X.; Tong, Z.; Lyon, L. A. *Langmuir* **2011**, *27*, 4142-4148.
136. Hazot, P.; Chapel, P.; Pichot, C.; Elaisarri, A.; Delair, T. *J. Polym. Sci., Part A: Polym. Chem.* **2002**, *40*, 1808-1817.
137. Okay, O.; Funke, W. *Makromol. Chem.* **1990**, *191*, 1545-1573.
138. Frank, M.; Burchard, W. *Makrornol. Chem., Rapid Commun.* **1991**, *12*, 645-652
139. Pich, A.; Richtering, W. *Adv. Polym. Sci.* **2010**, *234*, 1-37.
140. Pelton, R. *Adv. Colloid Interface Sci.* **2000**, *85*, 1-33.

141. Khan, A. *J. Colloid Interface Sci.* **2007**, *313*, 697-704.
142. Pich, A.; Richtering, W. In *Chemical Design of Responsive Microgels*; Pich, A., Richtering, W., Eds.; Springer: Berlin, 2010, p 1-37.
143. Hoare, T.; McLean, D. *J. Phys. Chem. B.* **2006**, *110*, 20327-20336.
144. Meng, Z.; Smith, M. H.; Lyon, L. A. *Colloid Polym. Sci.* **2009**, *287*, 277-285.
145. Su, S.; Ali, M. M.; Filipe, C. D. M.; Li, Y.; Pelton, R. *Biomacromolecules* **2008**, *9*, 935-941.
146. Kiser, P. F.; Wilson, G.; Needham, D. *Nature* **1998**, *394*, 459-462.
147. Striegler, S.; Dittel, M.; Kanso, R.; Alonso, N. A.; Duin, E. C. *Inorg. Chem.* **2011**, *50*, 8869-8878.
148. Sorrell, C. D.; Carter, M. C. D.; Serpe, M. J. *Adv. Funct. Mater.* **2011**, *21*, 425-433.
149. Schmidt, S.; Zeiser, M.; Hellweg, T.; Duschl, C.; Fery, A.; Möhwald, H. *Adv. Funct. Mater.* **2010**, *20*, 3235-3243.
150. Jeong, B.; Gutowska, A. *Trends in Biotechnol.* **2002**, *7*, 305-311.
151. Morris, G. E.; Vincent, B.; Snowden, M. J. *J. Colloid Interface Sci.* **1997**, *190*, 198-205
152. Parasuraman, D.; Sarker, A. K.; Serpe, M. J. *ChemPhysChem* **2012**, *13*, 2507-2515.
153. Snowden, M. J.; Thomas, D.; Vincent, B. *Analyst* **1993**, *118*, 1367-1369.
154. Parasuraman, D.; Serpe, M. J. *ACS Appl. Mater. Interfaces* **2011**, *3*, 2732-2737.

155. Parasuraman, D.; Serpe, M. J. *ACS Appl. Mater. Interfaces* **2011**, *3*, 4714-4721.
156. Parasuraman, D.; Sarker, A. K. *Colloid Polym. Sci.* **2013**, *291*, 1795-1802.
157. Hunter, R. J. *Zeta Potential in Colloid Science: Principles and Applications*; Academic Press: San Diego, 1981. 2-10.
158. Clogston, J. D.; Patri, A. K. In *Characterization of Nanoparticles Intended for Drug Delivery*; McNeil, S. E., Ed.; Springer: New York, 2011, p 63,64.
159. AAPTEC. *Technical Support Information Bulletin 1104: Dicyclohexylcarbodiimide (DCC)*; AAPTEC: 2011<<http://www.aapptec.com/technical-bulletins-i-180.html>>.
160. Pangborn, A. B.; Giardello, M. A.; Grubbs, R. H.; Rosen, R. K.; Timmers, F. J. *Organometallics* **1996**, *15*, 1518-1520.
161. Jivraj, M. N.; MacKinnon, M.; Fung, B. In *Syncrude Analytical Methods Manual, 4th ed.*; Syncrude Canada Ltd. Research Department: Edmonton, 1995.